Master's thesis

NTNU
Norwegian University of Science and Technology
Faculty of Engineering
Department of Marine Technology

M.A. van der Giessen

Feasibility of mooring system optimization for floating wind turbines in deep water based on static analysis

Master's thesis in Wind Energy Technology
Supervisor: Dr. E. Bachynski-Polić (NTNU)
Co-supervisor: Dr. Ir. P. van der Male (TU Delft)
July 2021

NTNU
Norwegian University of
Science and Technology

M.A. van der Giessen

Feasibility of mooring system optimization for floating wind turbines in deep water based on static analysis

Master's thesis in Wind Energy Technology
Supervisor: Dr. E. Bachynski-Polić (NTNU)
Co-supervisor: Dr. Ir. P. van der Male (TU Delft)
July 2021

Norwegian University of Science and Technology
Faculty of Engineering
Department of Marine Technology

NTNU
Norwegian University of
Science and Technology

Feasibility of mooring system optimization for floating wind turbines in deep water based on static analysis

by

M.A. van der Giessen

This report is submitted as partial fulfilment of the requirements to obtain the degrees of
Master of Science in Offshore Engineering at Delft University of Technology
&
Master of Science in Wind Energy Technology at Norwegian University of Science and Technology,
under the **European Wind Energy Master** programme.

Officially handed in on [June 30, 2021].
To be defended publicly on [July 7, 2021 at 2:00 PM].

Faculty of Mechanical Engineering, Delft University of Technology
Department of Marine Technology, Norwegian University of Science and Technology

Student number:	4539958 (TU Delft), 537167 (NTNU)	
Project duration:	January 14, 2021 – June 30, 2021	
Thesis committee:	Prof. Dr. A. Metrikine,	TU Delft, chair
	Dr. E. Bachynski-Polić,	NTNU, chair, supervisor
	Dr. Ir. P. van der Male,	TU Delft, supervisor

An electronic version of this thesis is available at http://repository.tudelft.nl.

TU Delft · NTNU

Preface

This report is submitted as partial fulfillment of the requirements to obtain the degree of Master of Science in Offshore Engineering at Delft University of Technology (TU Delft) and the degree of Master of Science in Wind Energy Technology at the Norwegian University of Science and Technology (NTNU) under the European Wind Energy Master programme (EWEM).

During the third semester of the EWEM Offshore Engineering track a pre-thesis project on deep water shared mooring at the Department of Marine Technology of the Norwegian University of Science and Technology as preparation for this research was performed. In combination with the courses Multidisciplinary Design Optimization, Integrated Dynamics of Wind Turbine Analysis and an introduction to the WINDMOOR research project I became enthusiastic about the cost competitiveness and efficient optimization of deep water floating wind turbines. This lead to the topic of this report.

Acknowledgements

I would like to express gratitude to my supervisors Dr. Erin Bachynski-Polić (NTNU) and Dr. Pim van der Male (TU Delft) for their supervision, support and feedback. The online meetings to troubleshoot software issues and for the guidance in general have been very useful and educational.

Lastly I would like to thank everyone from the WINDMOOR project for allowing me to use the 12 MW WINDMOOR model and for being able to participate in their meetings and workshops.

Contents

Preface ii

Acknowledgements iii

List of figures v

List of tables vii

Nomenclature ix

1 Introduction 1
- 1.1 Offshore Floating Wind . . . 1
- 1.2 Design Optimization . . . 1
- 1.3 Problem Statement . . . 2
- 1.4 Literature Review . . . 2
  - 1.4.1 Overview . . . 3
- 1.5 Research Objective . . . 3
- 1.6 Report Structure . . . 4

2 Applied Theory 5
- 2.1 Loading and Motion . . . 5
  - 2.1.1 Wind . . . 6
  - 2.1.2 Waves . . . 10
  - 2.1.3 Current . . . 11
  - 2.1.4 Mooring System . . . 12
- 2.2 Design Standards . . . 17
  - 2.2.1 Mooring System Design and Analysis . . . 18
- 2.3 SIMA . . . 20
  - 2.3.1 General . . . 20
  - 2.3.2 Theory . . . 20
  - 2.3.3 Optimization Algorithm . . . 24
  - 2.3.4 Limitations . . . 26
- 2.4 Reference location . . . 26
  - 2.4.1 Wind climate . . . 27
  - 2.4.2 Metocean data . . . 28
  - 2.4.3 FLS condition set . . . 28
- 2.5 WINDMOOR project . . . 29
  - 2.5.1 General . . . 30
  - 2.5.2 The INO WINDMOOR Semi-Submersible . . . 31
  - 2.5.3 The 12 MW WINDMOOR Turbine . . . 32
  - 2.5.4 Performance . . . 33
  - 2.5.5 Modifications . . . 33

3 Methodology 38
- 3.1 Single Turbine System . . . 38
  - 3.1.1 Optimization Problem Statement . . . 38
  - 3.1.2 Optimization Procedure . . . 42
  - 3.1.3 Analysis . . . 43
- 3.2 Shared Mooring Farm Concept . . . 44
  - 3.2.1 Optimization Problem Statement . . . 44
  - 3.2.2 Optimization Procedure . . . 46
  - 3.2.3 Analysis . . . 46

4 Single Turbine System **47**
4.1 Optimization results . . . 47
4.2 Design analysis . . . 53
4.2.1 Cost . . . 53
4.2.2 Decay tests . . . 54
4.2.3 Fatigue Damage Accumulation . . . 56
4.2.4 Fatigue Damage Estimation Model . . . 57

5 Shared Mooring Farm Concept **73**
5.1 Static analysis results . . . 73
5.2 Result analysis . . . 74
5.2.1 Cost . . . 74

6 Conclusion **75**

7 Future Work Recommendations **77**

8 Appendix **78**
8.1 Simplified model . . . 78
8.2 SIMA static simulation parameters . . . 78
8.3 SIMA decay test simulation parameters . . . 79
8.4 SIMA FLS simulation parameters . . . 79
8.5 Analysis . . . 79
8.5.1 Decay test results . . . 79
8.5.2 FLS measurements vs estimation data . . . 80

List of Figures

1 Conventional vs Optimal design process (Figure 1.2 Martins and Ning 2020) . . . 1
3 Degrees of freedom for a floating structure (Figure 1.3 Faltinsen 1999) . . . 5
4 Stream tube used in one-dimensional momentum theory (Figure 1 E. Bachynski 2020a) . . . 6
5 Three component TurbSim visualization (Figure 3 Jonkman 2009) . . . 9
6 Hydrodynamic problem (Faltinsen 1999) . . . 10
7 Current forces on a slender element (Figure 6.22 Faltinsen 1999) . . . 12
8 Catenary mooring system (Ma et al. 2019a) . . . 13
9 Side view of catenary mooring line (Faltinsen 1999) . . . 13
10 Forces acting on a section of a catenary mooring line (Faltinsen 1999) . . . 14
11 Taut leg mooring system (Ma et al. 2019a) . . . 15
14 Polyester mooring line composition (Bridon-Bekaert 2021b) . . . 17
15 Line definition in SIMA (Figure 2.2 SINTEF-Ocean 2020b) . . . 21
16 Deformation of a bar element (Figure 2.5 SINTEF-Ocean 2020a) . . . 21
17 Deformation of a beam element (Figure 2.9 SINTEF-Ocean 2020a) . . . 21
19 Wind rose (LIFES50+ 2015a) . . . 27
20 Wave rose for selected location (LIFES50+ 2015a) . . . 28
21 Visualization of the 12 MW WINDMOOR turbine on the INO-WINDMOOR semi-submersible (Figure 3.1, Inocean, Carlos Eduardo Silva de Souza et al. 2021) . . . 30
22 Local coordinate system (Figure (b) Carlos Eduardo Silva de Souza et al. 2021) . . . 30
23 WINDMOOR 12 MW wind turbine performance curves . . . 33
24 Mooring line schematic . . . 34
25 Visualization of different models . . . 35
26 Wave force transfer functions from WAMIT simulations . . . 37
27 Anchor bearing capacity as a function of weight . . . 39
28 Optimization flowchart single turbine . . . 42
29 Example of time series specified force/moment for decay test (E. Bachynski 2020b) . . . 43
30 Shared mooring farm concept optimization schematic . . . 45
31 Cost function and critical constraints (design 2) . . . 48
32 Path of optimizer for design variables (design 2) . . . 49
33 Tension at the fairlead in ULS condition . . . 50
34 Design tension in each segment . . . 50
35 Mooring line weight . . . 51
36 Surge and pitch positions for ULS condition . . . 51
37 Path of optimizer for design variables (design 3) . . . 53
38 Decay tests design 2 and design 0 . . . 55
39 Added coefficients in surge . . . 57
40 Mooring line tension time series condition 21 (design 2) . . . 61
41 Reduced interval tension time series condition 21 (design 2) . . . 61
42 Surge motion and tension comparison condition 21 (design 2) . . . 62
43 Heave motion and tension comparison condition 21 (design 2) . . . 62
44 Pitch motion and tension comparison condition 21 (design 2) . . . 63
45 Simulated and estimated surge motion condition 21 (design 2) . . . 63
46 PSD for motion surge, and pitch motion, and the wave spectrum condition 21 (design 2) . . . 64
47 Mooring line tension time series condition 5 (design 2) . . . 65
48 Surge motion and tension comparison condition 5 (design 2) . . . 66
49 Heave motion and tension comparison condition 5 (design 2) . . . 66
50 Pitch motion and tension comparison condition 5 (design 2) . . . 67
51 PSD for motion surge, and pitch motion, and the wave spectrum condition 5 (design 2) . . . 68
52 Simulated and estimated surge motion condition 5 (design 2) . . . 68
53 Reduced interval tension time series (condition 7) . . . 69
54 Heave motion and tension comparison (condition 7) . . . 70
55 Simulated and estimated surge motion (condition 7) . . . 71
56 PSD for surge (condition 7) . . . 71
57 JONSWAP spectrum for peak period of 15 seconds . . . 72
58 Static equilibrium of farm concept with fixed turbines . . . 73
59 Static equilibrium without environment . . . 74

List of Tables

1 Degrees of freedom in order . . . 5
2 Partial safety factors for mooring line design tension (DNVGL 2018b) . . . 19
3 Partial safety factors for mooring line design tension (DNVGL 2018a) . . . 19
4 S-N curve parameters for chain and polyester (DNVGL 2018a) . . . 20
5 FLS safety factor for consequence class 2 (DNVGL 2018b) . . . 20
6 Scaled extreme conditions for different return periods . . . 27
7 Extreme wave parameters (LIFES50+ 2015a) . . . 28
8 Marine growth . . . 28
9 Recommended aligned FLS conditions for Design Load Case 1.2 (LIFES50+ 2015a) . . . 29
10 Description of fairlead and anchor positions at 150 meter depth (Table 3.3 Carlos Eduardo Silva de Souza et al. 2021) . . . 31
11 Natural periods for floating wind turbine system (Table 3.5 Carlos Eduardo Silva de Souza et al. 2021) . . . 31
12 Parameters of the INO-WINDMOOR semi-submersible (Table 3.1 Carlos Eduardo Silva de Souza et al. 2021) . . . 31
13 Parameters of the WINDMOOR 12 MW turbine (Table 5.1 Carlos Eduardo Silva de Souza et al. 2021), the parameters in bold do not differ from the IEA 10 MW turbine. . . . 32
14 Parameters of the tower provided by Equinor (Table 5.7 Carlos Eduardo Silva de Souza et al. 2021) 32
15 Hydrostatic stiffness coefficients for single turbine system . . . 33
16 Parameters for 600 meter water depth mooring system . . . 34
17 Conditions used for simplified model verification . . . 35
18 Static forces . . . 35
19 Motion comparison for wave drift force only . . . 36
20 Motion comparison for rated wind speed only . . . 36
21 Motion comparison for rated wind speed and drift forcing . . . 36
22 Mean positions for extreme wind speeds . . . 37
23 ULS condition set . . . 37
24 Chain mooring line properties . . . 38
25 Polyester mooring line properties . . . 38
26 Mooring line material cost . . . 38
27 Design variables single turbine system and initial bounds . . . 40
28 Simulation parameters for the decay tests . . . 44
29 Design variables farm concept and initial bounds . . . 45
30 Design 1 . . . 47
31 Percentage of standard deviation over mean tension (design 1) . . . 47
32 Design 2 . . . 47
33 Percentage of standard deviation over mean tension (design 2) . . . 48
34 Design 3 . . . 52
35 Percentage of standard deviation over mean tension (design 3) . . . 52
36 Change in design variables of design 3 with respect to design 2 . . . 52
37 Mooring system material cost results (design 2) . . . 53
38 Mooring system material cost results (design 3) . . . 54
39 Natural periods (design 2) . . . 55
40 Natural periods (design 0) . . . 55
41 Accumulated fatigue damage in 20 years (design 2) . . . 56
42 1 hour accumulated damage per condition (design 2) . . . 56
43 Linear and linearized quadratic damping coefficients . . . 60
44 Fatigue damage estimation assessment . . . 60
45 Condition 21 . . . 60
46 Comparison condition 21 (design 2) . . . 60
47 Correlation coefficient tension and motion condition 21 (design 2) . . . 63
48 Comparison condition 5 (design 2) . . . 65
49 Condition 5 . . . 65
50 Correlation coefficient polyester tension and motion condition 5 (design 2) . . . 67
51 Condition 7 . . . 69
52 Damage estimation (condition 7) . . . 69

53 Correlation coefficients (condition 7) . . . 70
54 Initial mooring design farm concept . . . 73
55 Static positions farm concept . . . 74
56 Mass moments of inertia and center of gravity (Table 5.3 Carlos Eduardo Silva de Souza et al. 2021) . . . 78
57 Updated mass moments of inertia in nacelle . . . 78
58 Static calculation parameters for optimization . . . 78
59 User specified optimization parameters . . . 78
60 Simulation parameters for decay tests . . . 79
61 Simulation parameters for FLS simulations . . . 79
62 Natural periods for design defined by Table 32 . . . 79
63 Natural periods for design defined by Table 16 . . . 79
64 Accumulated damage at fairlead . . . 80
65 Estimated damage at fairlead . . . 80
66 Accumulated damage at top of polyester segment . . . 81
67 Estimated damage at top of polyester segment . . . 81
68 Accumulated damage at top of bottom chain segment . . . 82
69 Estimated damage at top of bottom chain segment . . . 82

Nomenclature

Abbreviations

ALS Accidental Limit State

BEM Blade Element Momentum

CapEx Capital Expenditure

FD Frequency Domain

FDA Frequency Domain Analysis

FEM Finite Element Method

FLS Fatigue Limit State

FWTs Floating Wind Turbines

JONSWAP Joint North Sea Wave Observation Project

LCOE Levelised Cost Of Energy

PSD Power Spectral Density

TD Time Domain

TDA Time Domain Analysis

ULS Ultimate Limit State

VSVP Variable-Speed-Variable-Pitch

Design parameters

$A_{f,cost}$ Anchor material cost for shared mooring farm concept

$A_{s,cost}$ Anchor material cost for single turbine system

$f(x)_f$ Objective function for shared mooring farm concept

$f(x)_s$ Objective function for single turbine mooring system

$L_{b,chain}$ Length of bottom chain segment

L_{poly} Length of polyester segment

$L_{t,chain}$ Length of top chain segment

$M_{f,cost}$ Mooring line material cost for shared mooring farm concept

$M_{s,cost}$ Mooring line material cost for single turbine system

$T_{d,a}$ Design tension at anchor

W_a Required anchor weight

W_{chain} Weight per meter chain mooring line in air

W_{poly} Weight per meter polyester mooring line in air

Other variables

D_c Accumulated characteristic fatigue damage

D_d Accumulated Design Fatigue Damage

DFF	Design Fatigue Factor
MBL	Minimum Breaking Load
MBS	Minimum Breaking Strength
S_c	Characteristic capacity
S_{MBS}	Holding Capacity
T_d	Design tension
$T_{c,dyn}$	Characteristic dynamic tension
$T_{c,mean}$	Characteristic mean tension
y_{dyn}	Partial safety factor for dynamic tension
y_{env}	Partial safety factor for environmental tension
y_{mean}	Partial safety factor for mean tension
$y_{pretension}$	Partial safety factor for pretension

1 Introduction

1.1 Offshore Floating Wind

The wind energy industry in Europe has been governed by onshore and bottom fixed offshore installations. So far 8 offshore floating wind projects have been commissioned, accounting for only 63 MW of the total 25 GW offshore installations but an additional 11 offshore floating wind projects should be commissioned by the end of 2022 (WindEurope 2020a). The offshore installations as of 2020 only account for 11% of the total wind generated energy in Europe (WindEurope 2020b). The expectation for the upcoming 5 years is that the majority of new installations will be onshore as well (WindEurope 2020b). However, with increasing opposition due to noise and visual pollution, offshore wind will play a significant part in reaching the sustainability goals in Europe and around the world. The majority of the offshore wind energy resource, 60 - 80%, is in water depths beyond 60 meters (WindEurope 2017). The technical total offshore wind energy resource in Europe and in the United States of America is estimated at 4000 GW and 2450 GW respectively (WindEurope 2017).

One of the issues with offshore wind is that the Levelised Cost Of Energy (LCOE) is double the LCOE of onshore on average which makes it less cost competitive (WindEurope 2019). The current LCOE of floating offshore wind is around 190 Euro per MWh (WindEurope 2020a), which is almost triple the LCOE of onshore wind. In order to capture the offshore wind energy resource, a reduction in LCOE for offshore floating wind is required to become economically competitive and feasible. Research in cost reduction of offshore floating wind is therefore necessary. According to floating offshore wind concepts evaluated in the paper *Feasibility of Floating Platform Systems for Wind Turbines* the mooring system contributes 35 - 44% of the total cost of the offshore floating wind turbine system (Musial, Butterfield, and Boone 2004). If the installation costs of the mooring system are excluded and only the material costs of the mooring lines and anchors are evaluated, the contribution reduces to 26 - 39%. This is still a significant contribution and previous research has shown that the mooring system material costs are a promising area for cost reduction. This was found especially for deep water locations, where mooring system costs increase due to a required increase in mooring line length, line strength and anchor strength. Unconventional mooring line configurations or connecting turbines in a farm configuration could lead to an additional reduction in the total costs. In addition, incorporating optimization of the mooring line characteristics in the design process could further increase the cost savings.

1.2 Design Optimization

The application of optimization in the design process adds another layer to the conventional design procedure. The goal of an optimization algorithm is to minimize an objective function while automating the design process. Flow charts for the conventional and the optimal design process are shown in Figure 1.

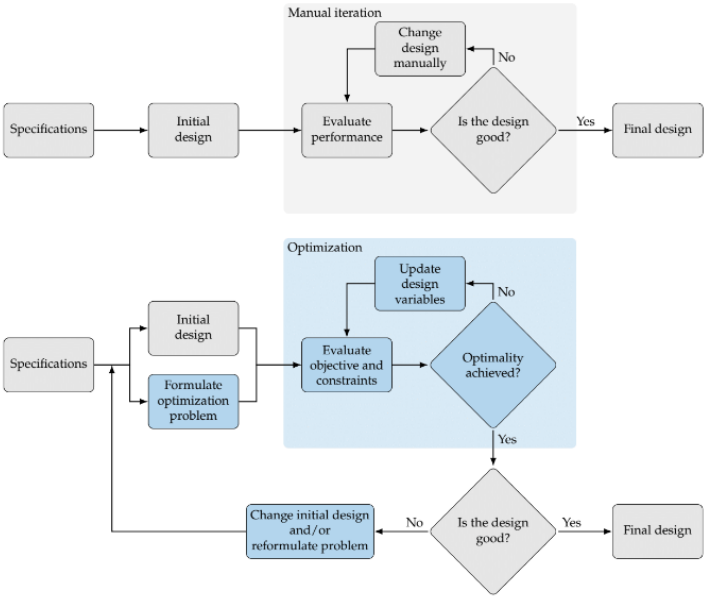

Figure 1: Conventional vs Optimal design process (Figure 1.2 Martins and Ning 2020)

The optimal design process does not terminate until a set level of accuracy is achieved for the objective function. Convergence is obtained for example if the value of the objective function has changed with less than 1% with respect to the previous iteration. The conventional design process terminates when a satisfactory design has been achieved. This design meets the requirements but is likely not the optimal design. An optimal design is defined by the minimum attainable value for the objective function while it satisfies the design constraints. This objective function can be related to any property of the system, for example the total cost of the mooring system, the design of the support structure to minimize loads or minimum pretension in the mooring lines. There are several optimization algorithms that can be implemented but all are defined using a problem statement. The problem statement defines the optimization problem through an objective function, the design variables and the (in)equality constraints. The objective function is formulated using the design parameters. The design variables are the independent variables that are allowed to be varied during the design process. The design space is constrained by bounds for each design variable, a lower and upper value, that it may not exceed. The constraints are the requirements that a design must satisfy and can be written as a function of the design variables. If the constraints are violated the design is not valid and a different design must be evaluated. This process is automated in an optimization algorithm.

Implementing a design optimization algorithm over the conventional design procedure seems preferable. However, an optimization can be computationally intensive and time consuming. This depends on the selected algorithm, the level of detail and the required simulation time for the conditions used. Optimization is therefore not implemented often.

1.3 Problem Statement

Wind turbines need to be deployed in depths beyond 60 meters to capture the majority of the offshore wind energy resource and contribute to achieving the sustainability goals. These depths lead to a preference for floating wind turbines, because conventional bottom-founded support structures become economically infeasible. However, offshore floating wind turbines are currently unattractive due to their high LCOE. Reduction in the production costs can make offshore floating wind more cost competitive. The mooring system has showed potential for cost reduction. Therefore, alternative mooring designs or shared mooring floating wind farms in combination with optimization could significantly reduce the total Capital Expenditure (CapEx) costs. In addition, simplifying the underlying simulations of the optimization could reduce computational intensity and total simulation time.

1.4 Literature Review

A literature study has been performed on deep water mooring, mooring system optimization and shared mooring farm concepts. The most important findings are provided below with a short introduction on the work done.

Connolly and Hall 2019 have developed and provide a shared mooring design algorithm for three concept floating wind farm configurations using four wind turbines. These concepts include shared mooring lines and multiline anchors. The concepts were evaluated at four water depths and compared with respect to line length, line weight, line tensions, displacement and costs savings in comparison to individually mooring four floating wind turbines (FWTs). Cost savings were achieved at depths beyond 400 meters. The anchor and shared mooring lines had a chain catenary profile. They suggest to include wake effects and slow drift forces for future work.
Fontana et al. 2016 evaluated three hexagonal offshore floating wind farm designs and one square offshore floating wind farm design where multiple turbines were connected to one anchor. The analyses were performed in FAST for two co-directional turbulent wind and irregular wave loading directions. The designs allow for easy scaling to a large number of turbines and show a significant reduction in number of anchors. Reductions in anchor tension were achieved but resistance against multi-directional loading is required. This could lead to additional anchor material and installation costs. The mooring line profile was specified as catenary, but no information on the material was provided.
Goldschmidt and Muskulus 2015 investigated the dynamic behavior of three shared chain catenary mooring configurations using a Frequency Domain Analysis (FDA). A row, triangular and rectangular farm design were additionally assessed on cost saving potential. In addition, the natural frequencies of the concepts were determined. It was found that a smaller number of total turbines led to higher cost savings for the selected concepts.
Brommundt et al. 2012 provide a tool for the optimization of the catenary mooring system of a single FWT using a semi-submersible support structure. The optimization was executed in the frequency domain (FD) with a Nelder-Mead simplex algorithm for two sites using MATLAB. It was recommended to include second order

wave forces for more accurate results in future work as they can lead to higher line tensions.
Mirzaei et al. 2013 performed a time domain (TD) mooring pattern optimization using Genetic Algorithms. It was obtained that Genetic Algorithms are a robust optimization algorithm for different engineering applications. The downside of using time domain analysis (TDA) was the increased computation time and cost.

1.4.1 Overview

Research shows that shared mooring farm concepts and optimization can lead to significant cost reductions for the mooring line material and anchors in water depths greater than 400 meters. Catenary chain mooring line characteristics for a selection of shared mooring farm concepts and scalable multiline anchor shared mooring farm concepts have been the focus of research. As specified by the future work recommendations including additional loading sources and wake losses may lead to more accurate results. Besides that, the shared mooring farm concepts, the number of turbines used and mooring line characteristics that have been evaluated are limited and new concepts should be explored. Additionally, it was found that using TDA or FDA leads to a trade off between accuracy, computation time and computation cost.

1.5 Research Objective

To add to existing literature, the goal of this thesis is to investigate the feasibility of static analysis optimization and potential mooring line material and anchor cost savings for a proposed optimized hexagonal six-turbine shared mooring floating wind turbine farm concept while considering nonlinear effects and wake losses at 600 meter depth. Additionally, a sequential quadratic programming optimization algorithm in combination with an efficient static TDA simulation is evaluated using SIMA. The optimization is based on static forcing from the Ultimate Limit State (ULS) condition. The design optimization is limited to the mooring line characteristics. The anchor mooring lines have a semi-taut profile, which has not been used frequently in previous research regarding mooring system optimizations. The anchor mooring line segments in order from fairlead to anchor are made of chain, polyester and chain. It is assumed that the chain segments have the same grade. The shared mooring lines have a catenary profile made of chain. The proposed shared mooring farm concept has been developed as a modification of the hexagonal concept A in *Efficient Multiline Anchor Systems For Floating Offshore Wind Turbines* (Fontana et al. 2016). Concept A and the designed shared mooring farm concept are shown in Figure 2b and Figure 2a, respectively. The lines connecting the semi submersibles are the shared mooring lines. The red dots represent the anchors, the blue triangles represent the semi submersible and the crosses represent the initial position of the wind turbine. The position of the turbine may be adjusted depending on the obtained motion characteristics under turbulent wind and irregular waves.

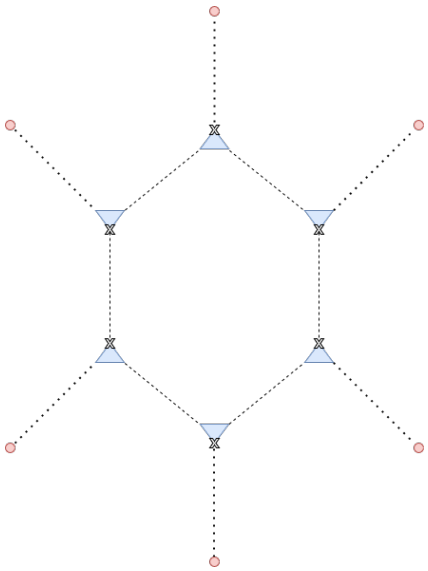

(a) Proposed shared mooring farm concept

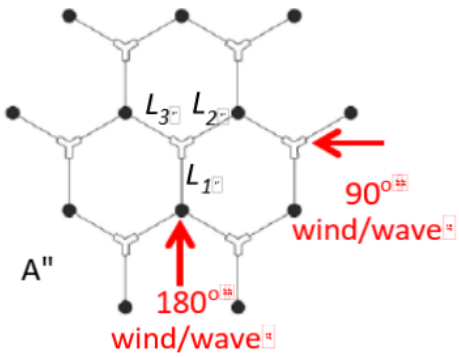

(b) Multiline anchor concept A (Figure 1 (A") Fontana et al. 2016)

The initial hypothesis is that the ULS condition is governing in mooring system design. Additionally, optimization based on the static ULS condition is assumed to sufficiently account for fatigue damage accumulation over the lifetime of the FWT. It is expected that significant cost savings can be achieved using the proposed

optimized farm concept, compared to individually mooring six offshore FWTs using an optimized single turbine mooring system at 600 meters depth. However, the optimized farm concept will likely require an increased anchor mooring line strength and anchor resistance. Additionally, the optimization using a simplified simulation model will likely reduce required computation intensity and time in comparison to a dynamic TDA optimization including a full Fatigue Limit State (FLS) analysis.

1.6 Report Structure

The INO WINDMOOR 12 MW FWT model, used in the WINDMOOR project, has been selected as its semi-submersible suits the designed farm concept and its rated power of 12 MW fits the prospect of the offshore floating wind energy industry. The provided model includes a conventional semi-taut three mooring line station keeping system for 150 meter depth. For the purpose of this thesis, the mooring system is modified to suit a 600 meter depth location. The LIFES50+ medium condition site in the Gulf of Maine has been selected as the reference environmental data location (LIFES50+ 2015d). The bathymetry at this location provides sufficient ground to use the provided environmental conditions for a 600 meter depth location. Applied theory and required modifications to the system are described and analyzed in Section 2.

The methodology for the optimization of the single turbine system is provided in Section 3. Additionally, a preliminary design and optimization procedure of the shared mooring farm concept optimization are provided. The obtained single turbine system is presented, assessed and discussed in Section 4. The shared mooring farm concept optimization results and findings are presented in Section 5.

A conclusion and future work recommendations are provided in Section 6 and Section 7 respectively. Additionally, software related parameters, extensive results and detailed calculations are provided in the Appendix (8).

2 Applied Theory

2.1 Loading and Motion

An offshore structure is loaded by environmental forces from current, waves and wind. These loads can induce wave frequency, high frequency, slow drift and mean drift motion on a floating structure. A rigid floating body has six degrees of freedom, three translational and three angular. The translational degrees of freedom are defined as surge, sway and heave. The angular degrees of freedom are defined as roll, pitch and yaw. The degrees of freedom are visualized in Figure 3 and given in order in Table 1.

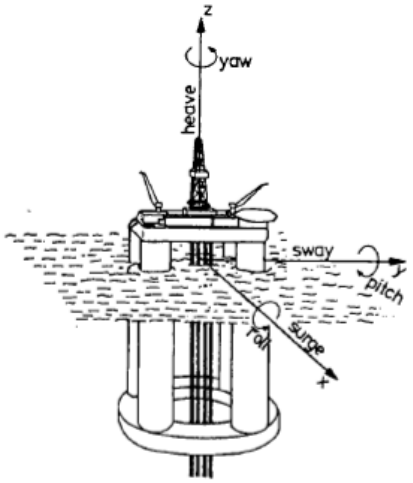

Figure 3: Degrees of freedom for a floating structure (Figure 1.3 Faltinsen 1999)

Table 1: Degrees of freedom in order

	Motion
1	Surge
2	Sway
3	Heave
4	Roll
5	Pitch
6	Yaw

The design of a FWT structure and the operation are constrained by the motion limits in which the system can maintain its function. Therefore it is important to define the motions that limit the operation of the system and which loads induce these motions. For an offshore FWT the energy export is constrained by the integrity of the power cable. Additionally, the system must not capsize and bending loads on the tower should be limited. To ensure the integrity of the power cable and to prevent capsizing, the motion in surge, sway, pitch and roll should be limited. The rigid body motion of a system can be assessed in the TD through TDA or in the FD through a FDA. The TD equation of motion is given in Equation 1. The mass matrix M is a 6 by 6 matrix for the six degrees of freedom, A is the frequency dependent added mass matrix, C_l is the frequency dependent linear damping matrix, C_q is the quadratic damping matrix, K is the stiffness matrix and $F(t)$ is the time dependent external environmental forcing vector. The displacement, velocity and acceleration vectors of the system are given by x, $\dot{x}$ and $\ddot{x}$ respectively.

$$(M + A)\ddot{x}(t) + C_l\dot{x}(t) + C_q\dot{x}(t)x(t) + Kx(t) = F(t) \tag{1}$$

Using FDA is more efficient than TDA as the equation of motion is linearized. The FD equation of motion is given in Equation 2. Displacement, velocity and acceleration are expressed in terms of a sine wave and the damping matrix is linearized. Nonlinear effects are not captured due to the linearization. Nonlinear effects can be present in aerodynamic and hydrodynamic loading, material properties, geometric stiffness and boundary conditions.

$$-\omega^2(M+A)\tilde{x}e^{i\omega t} + C\tilde{x}i\omega e^{i\omega t} + K\tilde{x}e^{i\omega t} = Fe^{i\omega t} \tag{2}$$

2.1.1 Wind

A wind turbine extracts kinetic energy from the wind and converts it into mechanical energy. The rotor transfers its mechanical energy to the generator which consequently converts it into electrical energy. The wind will induce a thrust force and drag force on the tower. In addition to that, the wind can generate wind waves and current.

An expression for the thrust force and the extracted power of a wind turbine is obtained through one-dimensional momentum theory. The theory assumes an ideal wind turbine, meaning the wind turbine does not experience losses when converting wind into electrical energy. A more detailed explanation of an ideal wind turbine is provided by M. Hansen in the book *Aerodynamics of wind turbines* (Hansen 2015). The assumptions for an ideal wind turbine are listed below.

- Homogeneous, incompressible, steady-state flow
- No frictional drag due to the disk
- No airflow through boundaries of the stream tube (no wake rotation)
- Infinite number of blades, uniform thrust acting on disk
- Continuous velocity over disk
- Pressure far from stream tube outlet is equal to ambient pressure

The theory solves the problem shown in Figure 4 through conservation of mass, conservation of momentum and Bernoulli's law. This method also introduces an axial induction factor a, which is an expression for the fractional decrease in wind speed over the stream tube given in Equation 3.

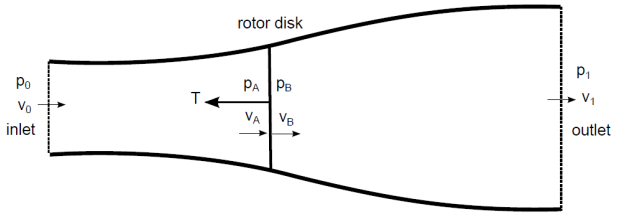

Figure 4: Stream tube used in one-dimensional momentum theory (Figure 1 E. Bachynski 2020a)

$$a = \frac{v_0 - v_A}{v_0} \tag{3}$$

An expression for the velocity at the outlet of the stream tube is given in Equation 4.

$$v_1 = v_0(1-2a) \tag{4}$$

Combining the expression for v_1 with Bernoulli's equation, conservation of mass and momentum leads to the expressions for thrust and extracted power given in Equation 5 and Equation 6 respectively.

$$T = \frac{1}{2} \cdot \rho \cdot A \cdot (v_0^2 - (v_0(1-2a))^2) \tag{5}$$

$$P = \frac{1}{2} \cdot \rho \cdot A \cdot v_0^3 \cdot 4a(1-a)^2 \tag{6}$$

The extracted power is a function of the air density ρ_{air}, the rotor area A, the incoming wind speed v_0 and the power coefficient C_p. The power coefficient should be maximized to maximize power extraction. The theoretical maximum power coefficient is obtained by setting the derivative of the power coefficient with respect to the axial induction factor equal to zero. This results in the theoretical maximum power coefficient of $\frac{16}{27}$, which is called the Betz limit, and a corresponding thrust coefficient of $\frac{8}{9}$.

In reality, a turbine has a finite number of blades and wake rotation does occur. This means that the assumptions used in the one-dimensional momentum theory are not valid. Therefore the maximum power coefficient, the Betz limit, will not be reached and the resulting extracted power is less due to losses from wake rotation for example. By including wake rotation into the theory above an additional coefficient has to be introduced. The angular induction factor a', which is a function of the rotor speed and the imported angular wind velocity. As the volume in the stream tube will be rotating local effects need to be captured and the analysis can not be performed over the stream tube in Figure 4. Therefore the analysis is performed on incremental sections of the stream tube. This leads to incremental expressions for extracted power and thrust. The resulting expression for a' to obtain maximum extracted power is given in Equation 7.

$$a' = \frac{1 - 3a}{4a - 1} \tag{7}$$

This procedure of obtaining the actual thrust force and the extracted power is called the Blade Element Momentum (BEM) method. It combines the one-dimensional momentum theory, wake rotation and the airfoil characteristics of the wind turbine blades. The procedure is described below.

- Guess reasonable values for a and a'
- Determine flow angle ϕ, angle of attack α and calculate the lift and drag coefficients
- Update the values of a and a'
- Check for convergence of the values a and a', if they have not converged repeat the process using the current values for a and a'

The result of this procedure is automatic calculation of thrust, power extraction and loads experienced by the blades. However, additional corrections are required for the assumptions made and physical phenomena that occur. The corrections are briefly described below and should be included in the BEM process. In addition to the corrections provided below, losses due to the hub and losses in the electrical generator can be considered.

- **Prandtl correction:**
  Accounts for the finite number of blades. A finite number of blades results in a reduction in aerodynamic force at the tip. Flow tends to go around the tip, following the pressure gradient, instead of loading it.
- **Glauert correction:**
  Corrects the expression for thrust force depending on the value of the axial induction factor. As the axial induction factor becomes larger than or equal to 0.5, the velocity at the outlet will be negative or zero. A negative or zero wind speed at the outlet makes the one-dimensional momentum theory invalid. Therefore the Glauert correction adjusts the expression for thrust for $a > 0.4$.
- **Dynamic wake:**
  Accounts for the delay in wind speed changes. The Blade Element Momentum theory assumes that the flow in the stream tube will directly reach a new steady state when changes in wind speed occur. In reality, the wake has a delay to adjust to changes in wind speed. Therefore the response of the turbine will lag to the wind speed changes.
- **Dynamic stall:**
  Accounts for the dynamic changes in lift and drag coefficients. The Blade Element Momentum Theory assumes that a specific angle of attack corresponds to a single values for lift and drag coefficients. However, the lift and drag coefficients will change at the same angle of attack based on the fluctuations in relative wind speed.

The tower drag is a function of the wind turbine tower properties and the wind speed. It is calculated using Equation 8.

$$F_{tower} = \frac{1}{2}\rho_{air} D L C_D V_{local} |V_{local}| \tag{8}$$

The tower drag is a function of the local, relative wind speed as a slight reduction in wind speed is experienced as one of the blades passes the tower and as the turbine may be moving. The relative wind speed can not be included in the static analysis, therefore the tower drag is a function of the mean wind speed. The contribution of tower drag is especially important for wind speeds above cut out wind speed. During these conditions the turbine is parked by feathering the blades to actively control and reduce the thrust force. The tower drag force cannot be reduced with control as it depends on the physical tower properties.

The energy contained in the wind environment is concentrated at low frequencies. This means that it will cause a mean displacement and low frequency oscillations in motion and mooring line tension.

In a wind turbine farm configuration the total power production and efficiency is of importance. The reduction in wind speed from the first turbine reduces the energy resource for the following turbine. The first turbine will create a wake by vortex shedding at the tip of the wind turbine blades. These vortices destabilize, mix with surrounding air and form turbulence. Different wake models in combination with BEM can be applied to determine the loads and power production of following turbines in the farm configuration. The available models have their own level of fidelity and corresponding computational cost. Some of the different wake models that are available are listed below.

- N.O. Jensen
- Dynamic Wake Meandering
- Linearized Navier-Stokes
- Parabolized Navier-Stokes
- Small Eddy Simulation

Description of wind environment

The wind environment at a location is defined by historical measurements on wind speed, origin of wind direction and a wind spectrum. The wind speed is defined as the average wind speed over a time period of generally 1 hour. Different averaging time periods can be applied. Additionally, wind gust speeds and extreme conditions are defined in terms of 1, 10, 50 and 100 year return periods.

The wind speed varies over height. The wind speed at any arbitrary height can be obtained using the reference wind speed, corresponding height above the mean water level and the power law velocity profile given in Equation 76 from design standard DNV-OS-J101 (DNVGL 2014).

$$U_{10}(z) = U_{10}(z_0) * (\frac{z}{z_0})^a \tag{9}$$

Here z_0 is the reference height of the measured wind speed, z is the height of interest and a the power law scaling parameter. The power law scaling parameter is generally equal to 0.14 but can vary based on the location. To determine the extreme wind speed for the different return periods a scaling parameter value of 0.11 is used.

An irregular wind speed time series at given height is generated using a wind spectrum, and applied to assess the system on design load cases from the design standards. A TurbSim fluctuating three component wind time series is used in the analysis. The theory provided is based on the *TurbSim User's Guide: Version 1.50* (Jonkman 2009).

TurbSim is a tool to generate stochastic cohorent turbulent full field wind flow time series (NREL 2012). The tool generates three-dimensional velocity vectors within a two-dimensional user specified grid that should cover the rotor, shown in Figure 5.

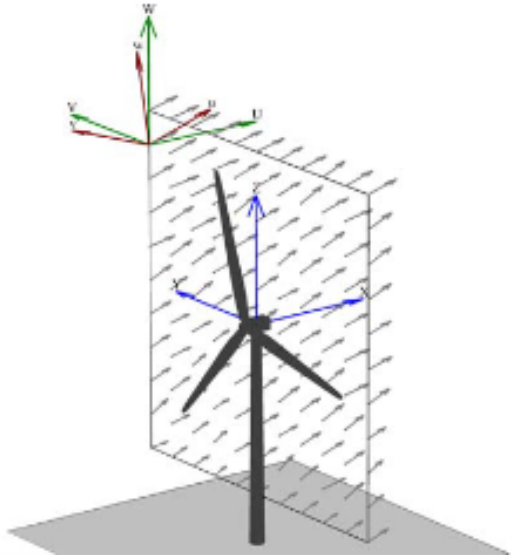

Figure 5: Three component TurbSim visualization (Figure 3 Jonkman 2009)

The generated turbulent wind files are IEC-61400-3 compliant and utilize a normal turbulence model with a Kaimal wind spectrum for fatigue analysis. The Kaimal wind spectrum is given in Equation 10.

$$S_K(f) = \frac{\frac{4\sigma_K^2 L_K}{\bar{u}_{hub}}}{(\frac{1+6fL_K}{\bar{u}_h ub})^{\frac{5}{3}}} \tag{10}$$

Here, K represents the velocity component in the X-direction u, the velocity component in the Y-direction v or the velocity component in the Z-direction w. L is a scale parameter given by Equation 2.1.1.

$$L_k = \begin{cases} 8.10\Lambda_u & \text{if } K = u \\ 2.70\Lambda_u & \text{if } K = v \\ 0.66\Lambda_u & \text{if } K = w \end{cases}$$

Additional relations for the turbulence scale parameter and the standard deviation are provided in Equation 11 and Equation 12, respectively.

$$\Lambda_U = 0.7 \min(60m, h_{hub}) \tag{11}$$

$$\sigma_v = 0.8\sigma_u \tag{12}$$

$$\sigma_w = 0.5\sigma_u \tag{13}$$

The frequency dependent spatial coherence is only specified for the velocity component u and given in Equation 14.

$$Coh_{i,j}(f) = \exp(-a\sqrt{(\frac{fr}{\bar{u}_{hub}})^2 + (0.12\frac{r}{L_c})^2} \tag{14}$$

Here, a is the coherence parameter and equal to 12, L_c is the coherence scale parameter given by Equation 15.

$$L_c = 5.67 \min(60m, h_{hub}) \tag{15}$$

2.1.2 Waves

The wave environment will cause wave frequency oscillations in motion of the system and tension of the mooring lines. In addition, nonlinear effects can cause a mean or slow drift displacement of the system and mean tension in the mooring lines. The hydrodynamic problem that needs to be solved depends on the structure. For a semi-submersible, which is a large volume structure, the hydrodynamic problem is separated in the two problems shown in Figure 6.

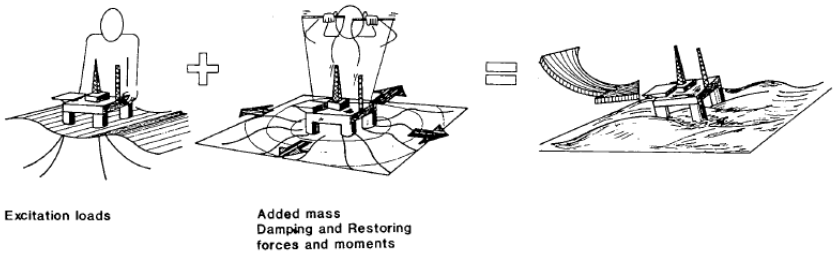

Figure 6: Hydrodynamic problem (Faltinsen 1999)

The first problem is shown on the left in Figure 6 and is called the diffraction problem. In this problem the structure is fixed and loaded by the incoming waves. It is applied to obtain the wave excitation loads, which is a combination of diffraction loads and the Froude Kriloff loads. The Froude Kriloff loads are the loads induced by the waves on the structure. The structure is assumed to be impermeable, which leads to the generation of diffraction waves. The corresponding loads are the diffraction loads. Both are obtained by integrating the wave pressure over the wetted surface of the structure, where the pressure is a function of the velocity potential. The velocity potential is a superposition of the Froude Kriloff velocity potential and the diffraction velocity potential.

The second problem is shown on the right and is called the radiation problem. In this problem, the structure is forced to oscillate at the wave excitation frequency in all degrees of freedom without a wave environment. This leads to the system's motion characteristics in terms of the added mass, damping and restoring coefficients.

The restoring coefficients can be obtained through a hydrostatic analysis. The restoring coefficient in heave is a function of the waterplane area. The restoring coefficients in roll and pitch are functions of the transverse and longitudinal metacentric heights of the structure, respectively.

To determine the loads on slender structures, Morison's equation is applied, for example wave and current loads on mooring lines. It is given in Equation 16. The first part of the equation is the mass force from the wave acceleration and the second part is the drag force from the wave velocity.

$$dF = \rho C_M \frac{\pi D^2}{4} a dz + \frac{\rho}{2} C_D |u| u dz \tag{16}$$

The Morison's equation is an approximation for long wave conditions, meaning the wave length is significantly larger than the diameter of the circular structure. The inertia coefficient C_M and the drag coefficient C_D are dependent on the material properties and the flow at the selected location. In this approximation the diffraction effects are simplified when using Morison's equation. For smaller ratios of wave length over diameter, the diffraction effects become important. Additionally, Morison's equation does not capture the interaction between structures.

Description of wave environment

The wave environment can be defined in terms of sea waves and swell waves. The sea waves are locally generated by the wind, swell waves are waves that have been generated in a distant wind field and have travelled to the specified location. Swell waves generally have longer wave periods than sea waves and are unaffected by the local wind environment. An irregular wave is described in terms of a significant wave height and peak period. The significant wave height is the value that represents the average wave height of the 33% highest wave heights measured in a sea state over a 3 hour period. The time measuring period can be larger or smaller. The peak period is obtained through measurements and is the period that is most likely to occur for the given significant

wave height.

Ocean waves are irregular waves, a superposition of different regular waves with each their own wave height and period. An irregular sea state time series can be obtained by applying linear wave theory and creating different regular waves with a random phases given in Equation 17. This is the wave time series measured at a single point.

$$\zeta = \sum_{j=1}^{N} A_j \sin(\omega_j t + \epsilon_j) \tag{17}$$

A_j is the amplitude of the wave, which is a function of the wave spectrum. The wave spectrum is a function of the peak period and significant wave height. Different wave spectra are available and can be applied, but the most common ones are Pierson - Moskowitz and Joint North Sea Wave Observation Project (JONSWAP).

$$A_j = \sqrt{2S(\omega_j)\Delta\omega} \tag{18}$$

The JONSWAP spectrum is an adaptation of the Pierson - Moskowitz by including an additional fitting factor called the peak enhancement factor. The wave environment is also defined using historically measured data at the desired location in terms of peak period, significant wave height, origin of direction. The extreme conditions are also defined using return periods of 1, 10, 50 and 100 years. The applied JONSWAP spectrum is given in Equation 19.

$$S_\zeta(\omega) = \frac{\alpha g^2}{\omega^5} \exp -\beta(\frac{{\omega_p}^4}{\omega})\gamma^{\exp \frac{(\frac{\omega}{\omega_p}-1)^2}{2\sigma^2}} \tag{19}$$

Here:

- α = spectral parameter
- ω_p = peak frequency in rad/s ($\frac{2\pi}{T_p}$)
- γ = peakedness parameter
- β = form parameter
- σ = spectral parameter
  - σ_a = 0.07 for $\omega \leq \omega_p$
  - σ_b = 0.09 for $\omega \geq \omega_p$

The parameters of the JONSWAP spectrum are dependent on the significant wave height. Assuming that the form parameter is equal to the general value of 1.25, the parameters γ and α are calculated according to Equation 20 and Equation 21.

$$\gamma = \exp[3.484(1 - 0.1975 \cdot (0.036 - 0.0056\frac{T_p}{\sqrt{H_s}})\frac{T_p^4}{H_s^2}] \tag{20}$$

$$\alpha = (\frac{H_s\omega_p^2}{4g})^2 \frac{1}{0.065\gamma^{0.803} + 0.135} \tag{21}$$

2.1.3 Current

Current is a combination of wind-generated current and tidal current. The total current velocity as a function of height is modelled according to DNVGL-OS-J101 (DNVGL 2014) and given in Equation 22. The tidal current velocity is given in Equation 23 and the wind generated current velocity is given in Equation 24.

$$v(z) = v_{tide}(z) + v_{wind}(z) \tag{22}$$

$$v_{tide}(z) = v_{tide}(0) \cdot (\frac{h+z}{h})^{\frac{1}{7}}, \ for \ z \leq 0 \tag{23}$$

$$v_{wind}(z) = v_{wind}(0) \cdot (\frac{h_0+z}{h_0}), \ for \ -h_0 \leq z \leq 0 \tag{24}$$

z is the vertical coordinate from the mean water level, at $z = 0$, h is the water depth and h_0 is a reference value of 50 meter. The loads on circular slender element as visualized in Figure 7 can be calculated using Equation 25 and Equation 26.

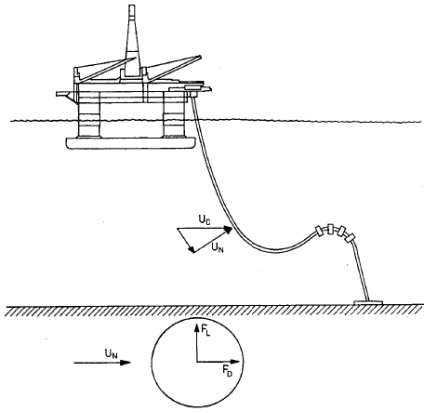

Figure 7: Current forces on a slender element (Figure 6.22 Faltinsen 1999)

$$F_D = \frac{\rho}{2} C_D D U_N^2 \tag{25}$$

$$F_L = \frac{\rho}{2} C_L D U_N^2 \tag{26}$$

The drag and lift coefficients are dependent on the surface roughness of the material, the flow defined by the Reynolds number and the Keulegan-Carpenter number. U_N is the velocity perpendicular to the slender element as shown in Figure 7. The relative velocity between the element and the current should be determined and used when the system is in motion. Current is not applied in the analysis but should be included for more detailed analysis in future work.

Description of current environment

The current environment is defined like the wind environment by a current speed, direction of origin and a velocity profile over height. As mentioned above, the current varies with the water depth and the maximum current velocities are experienced at the mean water level. The extreme current conditions are also defined using a 50 or 100 year return period value for tidal current and wind induced current. The same velocity profile over depth can be applied for the extreme conditions as described by Equation 22, Equation 23 and Equation 24.

2.1.4 Mooring System

The purpose of a mooring system is to provide resistance against the environmental loads described above and keep the floating structure in its desired position. The mooring system originates from floating production storage and offloading units that required to remain in a specific position for oil and gas winning. The motion of the structure was required to be limited to ensure structural integrity of the wells and safe transport of oil or gas. Besides that these units were manned and required that operations could be performed safely.

The design of a mooring system and its type is dependent on the environment, the system and also the operation. A mooring system can be for permanent deployment or temporary. For the purpose of this report, the focus will be on permanent mooring systems. A mooring system generally consists of a connection element at the structure, a steel or synthetic cable and an anchor at the seabed. Depending on the type of operation, a

spread mooring system, mooring lines connected at different points of the structure, or a single point mooring system can be used. A single point mooring system has mooring lines connected to one point or one area of the structure. It is commonly used for operations that would require weathervaning, orienting the structure differently to minimize the loads, and it therefore allows the structure to rotate around this point of connection. Additional active control can be executed using dynamic positioning thrusters. A spread mooring system ensures the system can operate without active control for different conditions and loading directions.

The mooring system line profile can generally be separated into a catenary mooring profile or a taut leg mooring profile. Both will be described below, but within these systems different mooring line materials and anchor types can be used. Each material and anchor type has its own advantages and disadvantages.

Catenary Mooring

The catenary mooring system is characterised by a large footprint and a line profile that has a suspended and resting part shown in Figure 8. The resting part provides the stiffness as its resistance to lift the weight off the seabed will capture the environmental loading. Chain mooring lines and drag embedded anchors are commonly used for catenary mooring systems. The chain provides better resistance against wear and tear from the seabed and the drag embedded anchors are cheap and easy to install. However these anchors can not resist significant vertical forces. If drag embedded anchors are used it must be verified that upward forces beyond the limit do not occur.

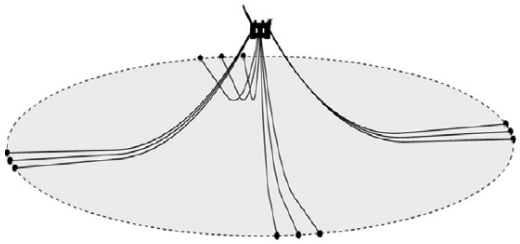

Figure 8: Catenary mooring system (Ma et al. 2019a)

The side view of a static catenary mooring line is shown in Figure 9. The parameter X_B is the resting line length, also the distance from the anchor to the touchdown point, and S is the suspended line length. The forces acting on a section of this line are shown in Figure 10.

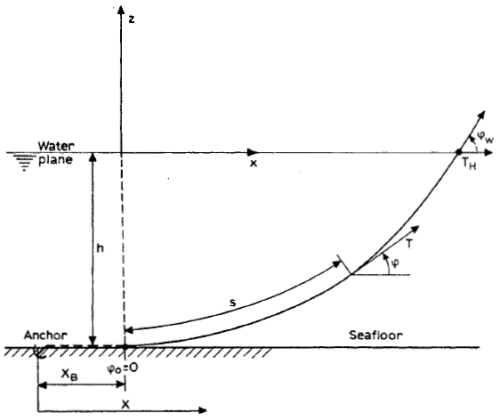

Figure 9: Side view of catenary mooring line (Faltinsen 1999)

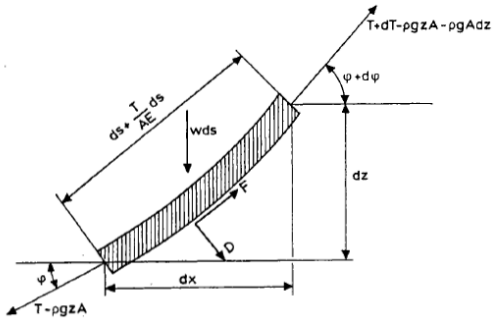

Figure 10: Forces acting on a section of a catenary mooring line (Faltinsen 1999)

For a simple catenary line consisting of one material the equations below are used to determine the static shape of the line under a horizontal pretension F_x. The pretension is commonly a limiting factor in the installation process.

$$S = \frac{F_x}{w} \sinh\left(\frac{w}{F_x}x\right) \tag{27}$$

$$x_{max} = \frac{F_x}{w} \frac{1}{\cosh\left(\frac{hw}{F_x} + 1\right)} \tag{28}$$

$$x_{tot} = S_{tot} - S + x_{max} \tag{29}$$

Equation 27, Equation 28 and Equation 29 are used in an iterative process to determine the suspended line length and the static shape of the line. The tension in the line is determined using Equation 30 and Equation 31.

$$F_{z,max} = F_x \sinh \frac{1}{\cosh\left(\frac{hw}{F_x} + 1\right)} \tag{30}$$

$$F_t = \sqrt{F_x^2 + F_{z,max}^2} \tag{31}$$

The single line catenary mooring system stiffness is obtained using Equation 32.

$$\frac{1}{K_{total}} = \frac{1}{K_{elastic}} + \frac{1}{K_{geometric}} \tag{32}$$

The elastic stiffness is a function of the material stiffness over the length of this segment. The geometric stiffness in surge is defined by the mooring line profile, mooring line material wet weight P, the horizontal force T_H and the water depth h given in Equation 33 Ma et al. 2019b.

$$K_{geometric} = \frac{P}{(arccosh(\frac{Ph}{T_H} + 1)) - (\frac{2}{\sqrt{1+2\frac{T_H}{Ph}}})} \tag{33}$$

Taut Leg Mooring

A taut leg mooring system is characterised by a significantly smaller footprint than the catenary mooring system as shown in Figure 11. The outer circle shown in the picture is the anchor footprint of a catenary mooring system for the same location. As can be seen in Figure 11 the mooring lines are straight and do not rest on the seabed. The anchors used must therefore provide resistance against vertical forces.

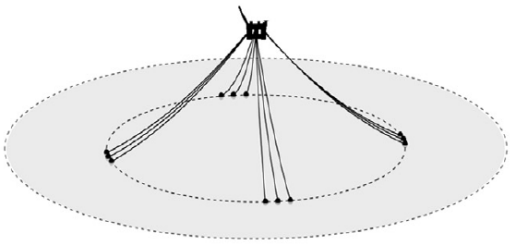

Figure 11: Taut leg mooring system (Ma et al. 2019a)

The line configuration for a taut leg system can be determined using the equations below.

$$x = \frac{T_H}{w}\log(\frac{\sqrt{(T_H^2 + T_Z^2)} + T_Z}{T_H} + \frac{T_H}{EA}l_s \tag{34}$$

$$l_s = \frac{T_Z}{w} \tag{35}$$

$$T_H = \frac{(T_Z^2 - (wh - \frac{1}{2}\frac{w^2}{EA}l_s^2)^2}{2(wh - \frac{1}{2}\frac{w^2}{EA}l_s^2)} \tag{36}$$

Designing a taut leg mooring system is again an iterative process. It starts with an initial guess of the vertical force F_Z followed by using Equation 35, Equation 36 and Equation 34. Finally the tension in the line can be determined using Equation 37. This process is repeated until a force equilibrium and convergence of results has been obtained.

$$T = \sqrt{T_H^2 + T_Z^2} \tag{37}$$

The mooring system surge stiffness for a taut leg profile is defined by two contributions. A geometric stiffness and a material dependent tensional stiffness. The tensional stiffness is the same as the elastic stiffness in the catenary mooring profile. The geometric stiffness is given in Equation 38 and the tensional stiffness is given in Equation 39.

$$C_g = \frac{x_0^2 \cdot C_{33}}{h^2} \tag{38}$$

$$C_l = \frac{EA}{l_0} \tag{39}$$

In Equation 38 C_{33} is the hydrostatic heave stiffness and x_0 is the anchor radius. As the structure is displaced in surge direction by the environmental loading, the horizontal force in the line will increase. Due to the geometry of the mooring system the vertical force increases as well, pulling the structure down. The surge stiffness for one taut leg mooring line is given in Equation 40. The surge stiffness of the total system is obtained by multiplying it with the squared cosine of the angle between the lines.

$$C_{taut} = \frac{1}{\frac{h^2}{x_0^2 C_{33}} + \frac{l_0}{EA}} \tag{40}$$

Mooring Line Material

The general types of mooring line material are chain, steel wire and polyester rope.

Chain

Chain mooring lines are defined in terms of their diameter, chain grade and the type of link. The type of link has a stud fitted in the oval chain link or is studless as shown in Figure 12a and Figure 12b, respectively. The purpose of the stud is to simplify the retrieval of the mooring line upon completion of the offshore project. A studless link is prone to tangling and therefore more commonly used for permanent mooring systems. Besides that the studless mooring line has the same physical properties as a studlink mooring line but a reduced weight (Ma et al. 2019c).

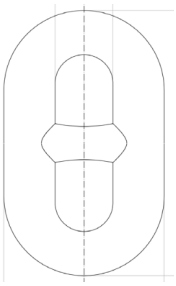

(a) Chain mooring line studlink (Damen 2017)

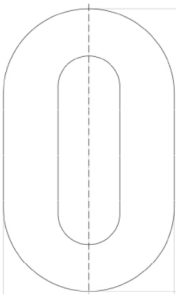

(b) Chain mooring line studless link (Damen 2016)

The chain grade defines the mooring line's minimum breaking load (MBL) as a function its diameter. There are several chain grades available and an increased grade corresponds to a higher MBL.

Steel wire rope

Steel wire rope mooring lines consist of a number of smaller wires combined in one or multiple strands. The number of strands and the design of the core determines the physical properties of the line. Therefore the composition should be selected based on the operation. A visualization of a 6 strand, called the Diamond Blue by Bridon-Bekaert, and a single strand wire rope composition are given in Figure 13a and Figure 13b, respectively.

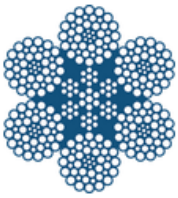

(a) "Diamond blue" wire rope composition (Bridon-Bekaert 2021a)

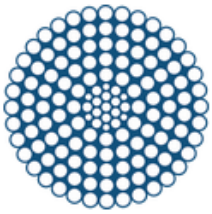

(b) Single strand rope composition (Bridon-Bekaert 2021a)

A steel wire rope mooring line is lighter and more elastic than a chain mooring line of the same diameter (Ma et al. 2019c). It therefore provides more elastic stiffness than geometric stiffness in comparison to a chain mooring line. However, the steel wire rope provides less resistance against wear from the seabed and requires additional corrosion protection to extend the life time.

Polyester rope

A polyester mooring line has significantly better FLS resistance than chain and wire rope. The composition of a polyester mooring line is similar to a wire rope. The polyester mooring line consists of a set of sub-ropes, the sub-ropes consist of smaller polyester wires laid in a strand. The sub-ropes are secured and protected against wear through a jacket and a set of filters. The jacket is the orange ring and the filter is the ring under the jacket as shown in Figure 14.

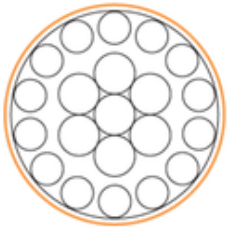

Figure 14: Polyester mooring line composition (Bridon-Bekaert 2021b)

Marine Growth

Marine growth increases the weight and force coefficients of a mooring line segment. The following equations are in accordance with the design standard DNVGL-OS-E301 (DNVGL 2018a). The dry mass of marine growth per meter length is given in Equation 41.

$$M_{growth} = \frac{\pi}{4}[(D_{nom} + 2\Delta T_{growth})^2 - D_{nom}^2]\rho_{growth} \cdot \mu \tag{41}$$

The nominal diameter is the diameter of the mooring line segment. The factor μ is a material dependent scaling factor, which is equal to 2 for chain and equal to 1 for polyester. The added submerged weight of marine growth in kN per meter is given in Equation 42.

$$W_{growth} = M_{growth}[1 - \frac{\rho_{seawater}}{\rho_{growth}}]\frac{9.81}{1000} \tag{42}$$

Additionally, the marine growth increases the drag coefficient of the segment. This is given in Equation 43.

$$C_{D_{growth}} = C_D[\frac{D_{nom} + 2\Delta T_{growth}}{D_{nom}}] \tag{43}$$

Anchors

The selection of the anchor for a mooring system is based on the mooring profile, the soil conditions, the loading direction and magnitude at the anchor and the type of operation. The anchors are generally categorised by the following types:

- Suction pile
- Drag embedded anchor
- Gravity anchor
- Driven pile
- Vertically loaded anchor

A suction pile, vertically loaded anchor and a gravity anchor are commonly used in deep waters. A taut leg mooring line profile leads to vertical loading at the anchor and these types provide the best resistance. A driven pile and gravity anchor are also used in shallower waters for a taut leg mooring profile. A drag embedded anchor provides the least resistance against vertical loading and is therefore mainly used for catenary or semi-taut mooring line profiles.

2.2 Design Standards

There are several organisations that provide technical requirements, design and analysis guidance for offshore structures and operations. According to Audubon 2015, DNV GL, ISO, BSEE, BOEM, API and World Bank Group are providing these standards. Oil and gas operations have been the focus but recently design standards on offshore floating wind have been added. Sirnivas et al. 2014 provides an overview of the regulations, design standards and safety of offshore wind related structures and operations for the United States. Local regulations

are outside the scope of this report. The design standards DNVGL-OS-E301 and DNVGL-ST-0119 are used in the WINDMOOR project and have been evaluated on station keeping and general offshore floating wind requirements. It is noted that there are standards on station keeping and offshore operations from IEC and ISO as well. However, using the exact same design standards leads to a more appropriate comparison of the results obtained in the WINDMOOR project. Therefore DNVGL-OS-E301 and DNVGL-ST-0119 are used. It is specified in this section when information from a different standard is used because of a reference in the standards DNVGL-OS-E301 or DNVGL-ST-0119.

2.2.1 Mooring System Design and Analysis

The mooring system for a floating offshore wind turbine is used to keep the system in a limiting range of motion under dynamic environmental conditions to ensure the integrity of the power cable and maintain power production. DNVGL 2018a states that environmental conditions should be applied in according with the selected site of deployment and the system used. A combination of the most unfavorable conditions should be applied in the same direction loading the system. The design standards DNVGL 2018a and DNVGL 2018b both define two consequence classes. The consequence class defines the systems level of structural safety in terms of the potential risks and consequences of failure (DNVGL 2018b). The standards define two consequence classes.

- Consequence class 1:
  Failure of the mooring system, breaking of one line e.g., does not lead to severe consequences
- Consequence class 2:
  Failure of the mooring system does lead to severe consequences

The severity and the type of consequences depend on the system. For offshore oil and gas production a large leak or loss of life due to an accident can be defined as severe consequences. The risks in the oil and gas industry are more related to safety of personnel and preserving nature as the systems are manned. This does not apply for floating wind turbines as the structure is unmanned and little chemical fluids are transported. The risk of capsizing, sinking, failure of the power cable, uncontrolled drift or collision with nearby structures can be defined as severe consequences for offshore floating wind. The level of redundancy included in the system relates to the potential risk. A higher level of redundancy can reduce the consequences of mooring system failure. Therefore, DNVGL 2018b categorizes a system based on its level of mooring system redundancy. Design of systems without redundancy should be performed using consequence class 2 (DNVGL 2018b). Consequence class 2 is applied for the design and analysis in this report as the base case WINDMOOR model report does not define any redundancy for mooring line failure.

The design standards recommend a mooring system design procedure using partial safety factors. The partial safety factors depend on the loading case, type of load, consequence class and are applied to ensure that the design tension in the mooring lines remains within the required limit. These partial safety factors are also applied to the loads at the anchors. The tension at the anchor is defined as the tension in the last node of the bottom mooring line segment. The design tension in DNVGL-ST-0119 is defined in Equation 44.

$$T_d = y_{mean} \cdot T_{c,mean} + y_{dyn} \cdot T_{c,dyn} \tag{44}$$

The partial safety factors y_{mean} and y_{dyn} are for the mean tension and dynamic tension respectively. The tensions $T_{c,mean}$ and $T_{c,dyn}$ are the characteristic mean and dynamic tension respectively. The characteristic tensions are supposed to be determined using a full dynamic simulation using the ULS conditions. For offshore FWT, the metocean environment defined by the 50 year return period significant wave height, peak period and current is sufficient. For the wind environment this is the 50 year return period 10-minute wind speed or the rated wind speed. The selection of data depends on which combination of environmental conditions induces the largest displacement and rotation of the system. The rated wind speed is included as this could lead to a higher thrust force acting on the system, resulting in larger displacements than the 50 year return period wind speed. The characteristic mean tension is the mean tension from pretension and environmental loads. The characteristic dynamic tension is the standard deviation in the tension caused by the fluctuating part of the environmental loading and requires a full dynamic simulation. The partial safety factors for ULS, a permanent mooring system and consequence class 2 are given in Table 2. No specification is provided if different safety factors should be applied for TDA or FDA.

Table 2: Partial safety factors for mooring line design tension (DNVGL 2018b)

		Consequence class 2 ST-0119
ULS	γ_{mean}	1.5
	γ_{dyn}	2.2

It is interesting to note that the design standard DNVGL-OS-E301 on position mooring provides a different method to determine the design tension. This method uses partial safety factors for the mooring line pretension and the environmental tension. The environmental tension is obtained by subtracting the pretension from the most probable maximum of the mooring line tension. Determining the most probable maximum requires either a 3 hour long dynamic simulation or ten to twenty shorter simulations (DNVGL 2018a). The values of the partial safety factors for a TDA and permanent mooring are given in Table 3.

Table 3: Partial safety factors for mooring line design tension (DNVGL 2018a)

		Consequence class 2 OS-E301
ULS	γ_{pret}	1.2
	γ_{env}	1.9

For both design standards, it is required that the design tension should be smaller than its characteristic capacity. The characteristic capacity is given in Equation 45.

$$S_c = 0.95 \cdot S_{MBS} \tag{45}$$

S_{MBS} is the miminum breaking strength for a mooring line section or the holding capacity for an anchor. The mooring line design requirement for the ULS conditions is given in Equation 46.

$$T_d < S_c \tag{46}$$

The design standards also provide safety factors and analysis procedures for the Accidental Limit State (ALS) but that is not included in the scope of this report. The ALS analysis should be included in future work. However, fatigue analysis is included and the guidelines from the design standards are provided here.

Fatigue is an accumulation of damage in a structural element due to crack growth caused by cyclic environmental loading. The design standards also implement a safety factor based on the consequence class for mooring system FLS analysis and damage calculation. The design fatigue damage is given by Equation 47.

$$D_d = DFF \cdot D_c \tag{47}$$

D_c is the accumulated characteristic fatigue damage in a structural element caused by cyclic loading over the lifetime of the system. DFF is the safety factor for fatigue design damage and D_d is the accumulated design fatigue damage. The characteristic fatigue damage is determined using a coupled wind wave condition set with corresponding probabilities of occurrence. A full dynamic simulation for each condition should be run and accumulated damage using the Miner's sum is calculated. The characteristic damage D_c is the sum of the accumulated damage from each condition d_i given in Equation 48. The Miner's sum is given in Equation 49.

$$D_c = \sum_{i=1}^{i=n} D_i \tag{48}$$

$$d_i = \sum_{i=1}^{i=n} \frac{n_i(s)}{N_c(s)} \tag{49}$$

$n_i(s)$ is the number of counted cycles for a certain stress range. The number of cycles and the stress range can be obtained through a cycle counting algorithm. $N_c(s)$ is the number of cycles required for failure at this stress range level and given in Equation 50. n is the number of conditions that is used.

$$N_c(s) = a_d \cdot S^{-m} \tag{50}$$

S is the stress range using a double amplitude in MPa, a_d is the specific material parameter of the S-N curve and m is the slope parameter of the S-N curve (DNVGL 2018a). The parameters are given in Table 4.

Table 4: S-N curve parameters for chain and polyester (DNVGL 2018a)

	$a_d[-]$	m [-]
Stud chain	$1.2{\cdot}10^{11}$	3
Studless chain	$6.0{\cdot}10^{10}$	3
Polyester rope	0.259	13.46

The method described above can be applied for polyester rope damage calculation if a relative stress range is used. The parameters for the polyester rope S-N curve in Table 4 are therefore for a relative stress range. The relative stress range is defined as the actual stress divided by the MBS stress.

The obtained characteristic damage for each condition is multiplied with the probability of occurrence of and the design life time in hours, which is generally 20 years.

$$D_i = d_i \cdot p_i \cdot N_h \tag{51}$$

All conditions are added and the total characteristic fatigue damage is obtained using Equation 48, which is then multiplied with the FLS safety factor DFF in Equation 47. The safety factor is material and consequence class dependent and given in Table 5. To ensure that failure in the mooring system does not occur each section of the mooring system must be checked for the condition given in Equation 52.

Table 5: FLS safety factor for consequence class 2 (DNVGL 2018b)

	DFF
Chain	10
Polyester	60

$$D_d \leq 1.0 \tag{52}$$

2.3 SIMA

2.3.1 General

SIMA is a user-friendly workbench for engineers to simulate and analyse marine operations (Hermundstad 2021), built by SINTEF Ocean AS and provided through DNVGL. It enables automation of multiple simulations and easy visualization of the post processed results (Hermundstad 2021). Initially built for offshore oil and gas, installation and transport applications, the software now includes an interface for fixed and floating offshore renewable energy concepts (Berthelsen 2021). SIMA implements two solvers, SIMO and RIFLEX. The user can implement a full SIMO model or a RIFLEX model that interacts with SIMO. A RIFLEX model with rigid SIMO bodies was provided for this thesis. RIFLEX interacts with SIMO for the SIMO bodies load models and environmental time series generation.

2.3.2 Theory

RIFLEX

RIFLEX implements a nonlinear Finite Element Method (FEM) analysis for slender structures. The FEM formulation applies a small strain theory approximation (SINTEF-Ocean 2020a). The slender structures, a mooring line for example, are defined as a bar or beam and according to Figure 15.

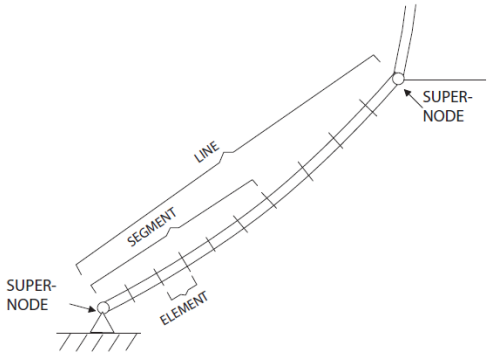

Figure 15: Line definition in SIMA (Figure 2.2 SINTEF-Ocean 2020b)

The deformation of a bar element is shown in Figure 16.

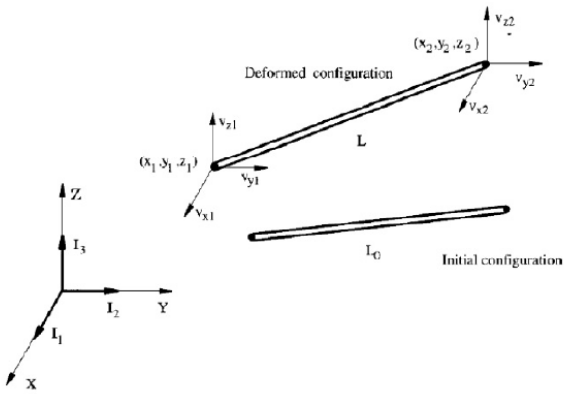

Figure 16: Deformation of a bar element (Figure 2.5 SINTEF-Ocean 2020a)

The bar element has three translational degrees of freedom at the end of each nodes to define the deformation. Additionally, it is assumed that the initial cross section and the deformed cross section are constant over the length. A bar element can therefore only have a axial deformation, elongation or contraction, it can not bend.

The deformation of a beam element is given in Figure 17.

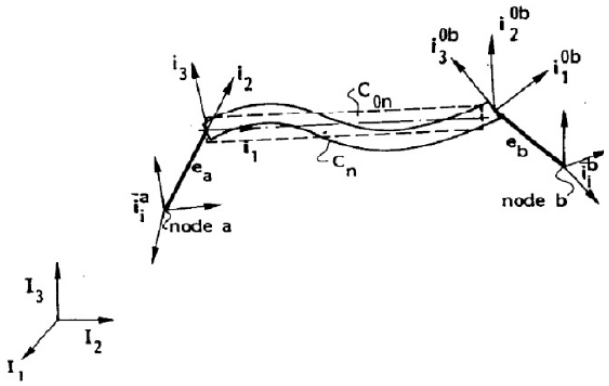

Figure 17: Deformation of a beam element (Figure 2.9 SINTEF-Ocean 2020a)

The end nodes of a beam element have six degrees of freedom, three translational and three angular. A beam element can therefore have axial and lateral deformations.

Static Finite Element Analysis

The static finite element analysis is an iterative process to find the equilibrium configuration of the system, and is defined as the solution of Equation 53.

$$\mathbf{R}^S(r) = \mathbf{R}^E(r) \tag{53}$$

Here, r is the vector containing all the displacements and rotations for the nodes present in the model, $\mathbf{R}^S(r)$ is the vector containing the internal forces at the nodes and $\mathbf{R}^E(r)$ is the vector containing the external forces. Loads and displacements are applied in groups with a specified number of steps and iterations. The number of steps defines the incremental loads and displacements applied, the number of iterations defines the incremental loads and displacements applied within that iteration. At each iteration the force imbalance is determined using Equation 54.

$$\mathbf{R}_k(r) = \mathbf{R}_k^S(r) - \mathbf{R}_k^E(r) \tag{54}$$

Static equilibrium for a load group is obtained when the force imbalance is equal to zero, a value is considered zero for a user specified tolerance. The initial solution to the problem is determined using the displacement vector at iteration k and the previous iteration $k-1$. The difference between the internal reaction forces at the previous iteration and the external forces at the current iteration is multiplied with the Jacobian of the force imbalance with respect to the displacement vector, given in Equation 55.

$$\Delta r_k^0 = -[\frac{R_{k-1}}{\delta r}]^{-1}(\mathbf{R}_{k-1}^S - \mathbf{R}_k^E) \tag{55}$$

The obtained incremental displacement vector is used to determine the solution to the displacement vector of the current iteration, given in Equation 56.

$$r_k^0 = r_{k-1} - \Delta r_k^0 \tag{56}$$

A Newton-Raphson method is applied to increase the convergence of the procedure. This results in a quadratic convergence rate. The solution to the problem at iteration j is given in Equation 57 and Equation 58.

$$\Delta r_k^j = -[\frac{R_{k-1}}{\delta r}]^{-1}\mathbf{R}_k^{j-1} \tag{57}$$

$$r_k^j = r_{j-1} - \Delta r_k^j \tag{58}$$

The static finite element analysis will run through all specified steps. However, the number of iterations within a step is reduced once an iteration satisfies the convergence criterion. The norm of an iteration is the sum of all displacements for a degree of freedom, and given in Equation 59.

$$||r_k|| = \frac{1}{N_t}\sum_{i=1}^{N_t} r_{ki}^2 \tag{59}$$

Here, N_t is the number of degrees of freedom that are active in the analysis. The convergence norm is based on displacements and only translational degrees of freedom are evaluated. The step is terminated once Equation 60 is satisfied. The incremental norm is given in Equation 61.

$$\frac{||\Delta r_k^j||}{||r_k^j||} \leq \epsilon_d \tag{60}$$

$$||\Delta r_k^j|| = ||r_k^j|| - ||r_k^{j-1}|| \tag{61}$$

Here, ϵ_d is the specified displacement tolerance, which is user specified. The static finite element analysis will successfully terminate if the convergence criterion has been satisfied and the maximum number of steps has been reached. If the convergence criterion is not satisfied the analysis terminates with a failure and the number of steps and iterations needs to be adjusted.

The loading sequence applied consists of the following groups.

- Volume forces - (weight and buoyancy)
- Specified displacements - (displacement of mooring system to the final position specified by the end nodes of the mooring lines)
- Body forces - (hydrodynamic forces acting on the semi-submersible)
- Marine growth - (added weight to mooring line elements and adjusted Morison coefficients)
- Boundary change - (fixing or freeing the system)
- Specified forces - (application of loads applied at specified nodes, static thrust force for example)

Dynamic Finite Element Analysis

The dynamic finite element analysis problem is defined by the equilibrium equation given in Equation 62.

$$\boldsymbol{R}^I(\boldsymbol{r},\ddot{\boldsymbol{r}},\boldsymbol{t}) + \boldsymbol{R}^D(\boldsymbol{r},\dot{\boldsymbol{r}},\boldsymbol{t}) + \boldsymbol{R}^S(\boldsymbol{r},\boldsymbol{t}) = \boldsymbol{R}^E(\boldsymbol{r},\dot{\boldsymbol{r}},\boldsymbol{t}) \tag{62}$$

The parameters in Equation 62 are defined below.

- $\boldsymbol{R}^I$ = inertia force vector $\boldsymbol{R}^I(\boldsymbol{r},\ddot{\boldsymbol{r}},\boldsymbol{t}) = [\boldsymbol{M}^S + \boldsymbol{M}^F(\boldsymbol{r}) + \boldsymbol{M}^H(\boldsymbol{r})]\ddot{\boldsymbol{r}}$
  where:
  $\boldsymbol{M}^S$ = structural mass matrix
  $\boldsymbol{M}^F(\boldsymbol{r})$ = mass matrix for internal fluid flow
  $\boldsymbol{M}^H(\boldsymbol{r})$ = mass matrix for added mass contributions
- $\boldsymbol{R}^D$ = damping force vector $\boldsymbol{R}^D(\boldsymbol{r},\dot{\boldsymbol{r}}) = [\boldsymbol{C}^S + \boldsymbol{C}^H(r) + \boldsymbol{C}^D(\boldsymbol{r},\dot{\boldsymbol{r}})]\dot{\boldsymbol{r}}$
  where:
  $\boldsymbol{C}^S$ = structural damping matrix
  $\boldsymbol{C}^H(\boldsymbol{r})$ = hydrodynamic damping matrix
  $\boldsymbol{C}^D(\boldsymbol{r},\dot{\boldsymbol{r}})$ = damping matrix for specified dampers
- $\boldsymbol{R}^S$ = internal structure force vector
- $\boldsymbol{R}^E$ = external force vector
  - Forces on RIFLEX and SIMO bodies
    - Volume forces
    - Specified forces
    - Aerodynamic and hydrodynamic forces
    - Body forces
- $\boldsymbol{r},\dot{\boldsymbol{r}},\ddot{\boldsymbol{r}}$ = displacement, velocity and acceleration vectors

A step by step numerical integration is applied to solve the nonlinear equation Equation 62. The Newmark-beta method is applied with a constant average acceleration method for numerical stability and second order accuracy.

The dynamic finite element analysis solves the incremental equilibrium equation given in Equation 63 at each iteration.

$$(\boldsymbol{R}^I_{t+\Delta t} - \boldsymbol{R}^I_t) + (\boldsymbol{R}^D_{t+\Delta t} - \boldsymbol{R}^D_t) + (\boldsymbol{R}^S_{t+\Delta t} - \boldsymbol{R}^S_t) = (\boldsymbol{R}^E_{t+\Delta t} - \boldsymbol{R}^E_t) \tag{63}$$

This nonlinear incremental equation is linearized by tangential, mass-, damping- and stiffness matrices, given in Equation 64.

$$\mathbf{M}_t \Delta \ddot{\mathbf{r}}_t + \mathbf{C}_t \Delta \dot{\mathbf{r}}_t + \mathbf{K}_t \mathbf{r}_t = \Delta \mathbf{R}^E_{t+\Delta t} - (\mathbf{R}^I_t + \mathbf{R}^D_t + \mathbf{R}^S_t) \tag{64}$$

The right hand side of the equation is dependent on the previous iteration to prevent the accumulation of residual errors. This problem is solved similarly to the static finite element analysis including the same convergence norm.

SIMO

SIMO can be used to analyze the motion and station keeping performance of floating structures and includes the following features (SINTEF-Ocean 2020c):

- Loading due to current, waves and wind
- Nonlinear TDA of low frequency forces and wave frequency forces
- Flexible modelling of multibody systems
- Generation of environmental time series

The static and dynamic analysis are performed in RIFLEX, as a RIFLEX model was provided by the WINDMOOR project. A separate model needs to be made if SIMO is used for static and dynamic analysis. However, SIMO is coupled to RIFLEX to communicate the load models and environmental time series from SIMO and is therefore still used.

Wind and Waves

The wind environment is defined according to Section 2.1.1. Additionally, the turbines performance can be assessed using constant wind speeds and different wind spectra. The irregular wave environment is defined according to Section 2.1.2. However, regular waves and different spectra are offered.

2.3.3 Optimization Algorithm

General

SIMA includes a built in optimization algorithm SimOpt which is based on the gradient based NLQLP algorithm by Prof. Klaus Schittkowski (Schittkowski 2011). It implements the general problem formulation for a constrained optimization:

- The objective function, desired function to minimize
- Design variables, independent parameters allowed to be varied
- Constraints, limitations to valid designs

The optimization problem in SIMA is defined using workflow modules and post processors. A general workflow has to be made in which the design variables and the initial condition for simulation are provided. The simulation of initial condition and initial design should succeed without errors. The results from this initial simulation can be used to calculate the objective function and the constraints in a postprocessor. The results from the post processor are returned to the general workflow as outputs. An optimization workflow is created to define the optimization problem and to print desired results. The optimization workflow requires a general workflow in which the optimization is executed as described above and the outputs objective function and constraints. The optimization workflow also requires that starting values, lower bound, upper bound and step size of the design variables as input. The step size is used for the computation of gradients. In addition to that the user can specify a few NLPQLP related parameters, these are given below.

- Desired final accuracy
- Maximum number of iterations
- Tolerance
- Maximum number of function calls
- Minimum step length

NLPQLP

The NLPQLP optimization algorithm is the implementation of a Sequential Quadratic Programming (SQP) algorithm. SQP is a constrained gradient-based optimization algorithm. The algorithm is used for smooth nonlinear problems that are well-scaled, not too large and all functions must be continuously differentiable (Schittkowski 2011).

The Lagrangian equation is used to simplify the solving of the constrained optimization problem. An unconstrained problem is easier to solve and obtained by implementing the Lagrangian equation in Equation 65 on the constrained problem. $f(x)$ is the objective function, $g_j(x)$ are the constraints and u_j are the Lagrange multipliers.

$$L(x,u) := f(x) - \sum_{j=1}^{m} u_j g_j(x) \tag{65}$$

The combination of the Lagrange equation, an approximation of the Hessian of the Lagrange equation C_k, current design variables x_k and an approximation of the Lagrange multipliers v_k the problem defined by Equation 66 must be solved to obtain the optimal solution d and the corresponding multiplier u_k.

$$\begin{aligned} &\min(\frac{1}{2} d^T C_k d + \nabla f(x_k)^T d \\ &\nabla g_j(x_k)^T d + g_j(x_k) = 0, \ for\ j = 1, ..., m_e \\ &\nabla g_j(x_k)^T d + g_j(x_k) \geq 0, \ for\ j = m_e + 1, ..., m \end{aligned} \tag{66}$$

A new iteration for the design variables x and the Langrange multipliers v is obtained using Equation 67.

$$\begin{bmatrix} x_{k+1} \\ v_{k+1} \end{bmatrix} := \begin{bmatrix} x_k \\ v_k \end{bmatrix} + \alpha_k \begin{bmatrix} d_k \\ u_k - v_k \end{bmatrix} \tag{67}$$

The search direction step length parameter α is within the range of 0 to 1, as the whole problem is normalized. To ensure that the algorithm reaches global convergence and satisfy the Karush-Kuhn-Tucker (KKT) conditions, the step length parameter must satisfy sufficient decrease. This is given in Equation 68

$$\phi_r(\alpha) := \psi_r(\begin{bmatrix} x \\ v \end{bmatrix} + \alpha \begin{bmatrix} d \\ u - v \end{bmatrix}) \tag{68}$$

Here, ψ_r is a penalty which is applied if the algorithm creates design variables that exceed the bounds. The penalty function is given in Equation 69.

$$\phi_r(x,v) := f(x) - \sum_{j \in J} (v_j g_j(x) - \frac{1}{2} r_j g_j(x)^2) - \frac{1}{2} \sum_{j \in K} \frac{v_j^2}{r_j} \tag{69}$$

Here, r_j are the penalty parameters to ensure that the constraint value $g_j(x)$ is smaller than the Lagrange multipliers over the penalty parameter. The penalty function must satisfy Equation 70.

$$\phi_{r_k}^{'}(0) = \nabla \psi_{r_k}(x_k, v_k)^T (\begin{bmatrix} d_k \\ u_k - v_k \end{bmatrix}) \leq 0 \tag{70}$$

To ensure that the algorithm does not select a too small or too large step size, an line search algorithm is implemented to update the step size to satisfy the Armijo condition. The Armijo condition is given in Equation 71.

$$\phi_r(\sigma \beta^i) \leq \phi_r(0) + \sigma \beta^i \mu \phi_r^{'}(0) \tag{71}$$

The algorithm starts with a step size of 1 and checks if the Armijo condition is satisfied. If not, the step size is adjusted and a new value for the next iteration is calculated. This process is repeated until the condition is

satisfied. The algorithm may not satisfy the condition for a user specified number of maximum iterations. In this case a non-monotone line search is activated and the updated step size is used once Equation 72 is satisfied.

$$\phi_{r_k}(\alpha_k) \leq \max_{k-p(k)\leq j\leq k} \phi_{r_j}(0) + \alpha_k \mu \phi_{r_k}^{'(0)} \tag{72}$$

Here, p is the user specified tolerance. Finally, the BFGS quasi-Newton formula, given in Equation 73, is applied to approximate the Hessian matrix (Schittkowski 2011).

$$C_{k+1} := C_k + \frac{q_k q_k^T}{p_k^T q_k} - \frac{C_k p_k p_k^T C_k}{p_k^T C_k p_k} \tag{73}$$

The optimization algorithm is terminated successfully if the convergence criterion in Equation 74, under the assumption that the objective function at x_k is not equal to zero, is satisfied.

$$f(x_k) - f(x_{k-1}) \geq \epsilon |f(x_k)| \tag{74}$$

Here, ϵ is a user specified termination accuracy.

If possible the gradients of the objective function and constraints are computed analytically, if not possible, they are approximated using the forward difference given in Equation 75.

$$\frac{\delta}{\delta x_i} f(x) \approx \frac{1}{\eta_i}(f(x + \Delta X) - f(x)) \tag{75}$$

Here, ΔX step size and η_i is the user specified tolerance. For a forward difference the tolerance is equal to the square root of the computation accuracy.

2.3.4 Limitations

As of now SIMA only allows one operating wind turbine with external controller during simulations. The analysis of an offshore floating wind farm must therefore either be performed using quadratic wind coefficients or static forces. In addition, the NLPQLP optimization algorithm includes an option for parallel computation of the gradients. However, the parameter for the number of parallel computations l is set to 1 in SIMA's included algorithm SimOpt and can not be changed as of now. Computation of the gradients will likely be the most time consuming part of the optimization. Parallel computation of the gradients could significantly reduce total optimization time.

2.4 Reference location

The LIFES50+ project (LIFES50+ 2015c), and the Gulf of Maine location specifically, for the environmental data. The location has a mean water depth of 130 meter (LIFES50+ 2015b), but on the south side of the bathymetry profile shown in Figure 18a the depth increases towards 200 meter. Depths of 600 meter are only achieved outside the Gulf of Maine beyond Georges Bank and Browns bank, shown in Figure 18b. This does make the application of the environmental data from the Gulf of Maine to a 600 meter depth location imaginary. However, for the scope of this report and because of the publicly available reference data it is assumed to be reasonable. The LIFES50+ reports Deliverable 1.1 (LIFES50+ 2015b and Deliverable 7.2 (LIFES50+ 2015a) provide information on how and where the environmental data was obtained.

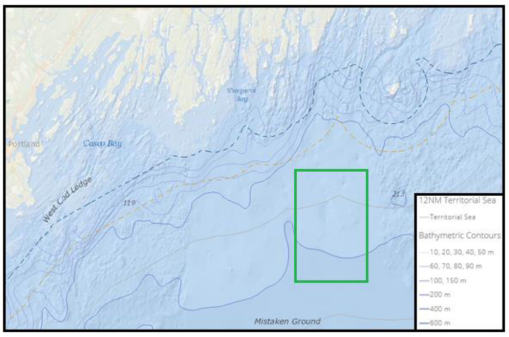

(a) Location medium metocean conditions LIFES50+ (Figure 17 (LIFES50+ 2015b))

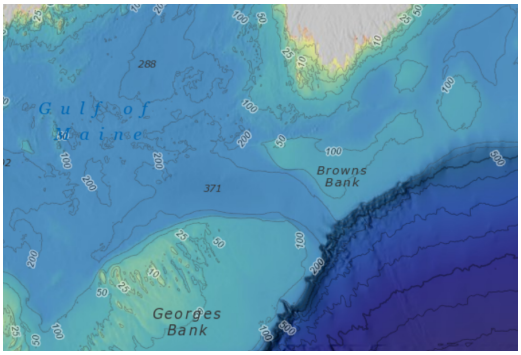

(b) Bathymetry profile near the Gulf of Maine (obtained using Bathymetric Data Viewer by NOAA 2021)

2.4.1 Wind climate

From the aerodynamic loading theory it is obtained that the wind speed time series is required for the analysis of the system. The 10 minute historical average wind speed at hub height provided in the deliverable of 10.46 m/s is for a hub height of 119 meter, however the hub height of the rotor used in this report is 131.7 meter. The hub height is a combination of the freeboard height of the semi-submersible and the height of the turbine itself. The new value of the 10 minute average wind speed at the hub height is obtained using the power law profile from the design standard DNV-OS-J101, given in Equation 76.

$$U_{10}(z) = U_{10}(z_0) * (\frac{z}{z_0})^a \tag{76}$$

Here z_0 is the reference height, in this case 119 meter, and z is the hub height of 131.7 meter. This leads to a wind speed of 10.61 m/s.

The extreme conditions at hub height are obtained using Equation 76 with a parameter a of 0.11, as recommended by DNV-OS-J101. The results are given in Table 6.

Table 6: Scaled extreme conditions for different return periods

Return period	Value	Unit
50 years	44.6	[m/s]
10 years	41.6	[m/s]
5 years	40.2	[m/s]
1 years	37.1	[m/s]

To withstand the extreme conditions it is important to determine the main direction of loading. The wind rose is shown in Figure 19.

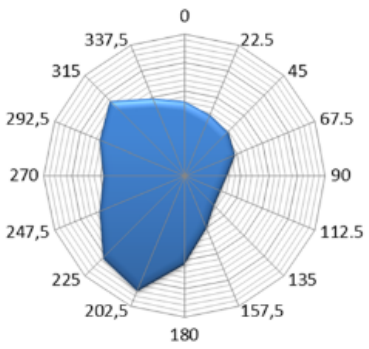

Figure 19: Wind rose (LIFES50+ 2015a)

The directions 202.5, 225 and 315 degrees have the largest number of occurrences. It is assumed that 0 degrees is North and that the wind rose provides the origin of the wind environment. This means that the wind is mainly coming from South - South-West.

2.4.2 Metocean data

The wave climate is defined by a peak period in seconds, a significant wave height in meters and a spectrum. The extreme wave environment is given in Table 7 and used in the ULS analysis. The combination of wave height and peak period that yields the largest response or loads should be used for the ULS condition.

Table 7: Extreme wave parameters (LIFES50+ 2015a)

Return period	Hs [m]	Tp [s]
50 years	10.9	9-16
10 years	9.4	"
5 years	8.9	"
1 years	7.7	"

The wave rose is shown in Figure 20. The same assumptions are made for the wave rose as for the wind rose. Comparing the wind and wave rose yields a difference of approximately 80 degrees in main loading direction. For the ULS analysis it is assumed that the wave and wind environment are alligned.

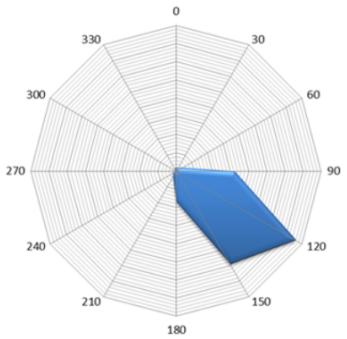

Figure 20: Wave rose for selected location (LIFES50+ 2015a)

Marine Growth

The marine growth thickness is defined as a function of water depth, given in Table 8, with a density of 1325 kg/m^3.

Table 8: Marine growth

water depth [m]	thickness [mm]
+2 to -40	100
below -40	50

2.4.3 FLS condition set

The FLS condition set is a correlated set of wind and wave conditions with probability of occurrence. This set corresponds to Design Load Case 1.2 for the location of Lifes50+. The conditions are applied as alligned, however as described above a misalignment in wind and wave conditions could occur.

Table 9: Recommended aligned FLS conditions for Design Load Case 1.2 (LIFES50+ 2015a)

Vhub [m/s]	Hs [m]	Tp [s]	P [%]
5	1.38	5	3.45
5	1.38	7	6.89
5	1.38	11	3.45
7.1	1.67	5	3.45
7.1	1.67	8	5.99
7.1	1.67	11	11.98
10.3	2.2	5	6.41
10.3	2.2	8	12.83
10.3	2.2	11	6.41
13.9	3.04	7	5.12
13.9	3.04	9.5	10.24
13.9	3.04	12	5.12
17.9	4.29	7.5	2.90
17.9	4.29	10	5.81
17.9	4.29	13	2.90
22.1	6.2	10	0.94
22.1	6.2	12.5	1.88
22.1	6.2	15	0.94
25	8.31	10	0.19
25	8.31	12	0.37
25	8.31	14	0.19

2.5 WINDMOOR project

The WINDMOOR project is a research project investigating the governing loads on the mooring system for a FWT (Carlos Eduardo Silva de Souza et al. 2021). The aim of this project is to improve the knowledge surrounding these loads and properly include them in the future design of mooring systems for floating wind turbines.

The developed and provided base case model consists of the INO WINDMOOR semi-submersible, a semi-taut mooring system for a 150 meter depth location, both designed by Inocean and Equinor, and the WINDMOOR 12 MW wind turbine. A short description of the system and how the base case model has been modified for the purpose of this report are provided in this section.

Figure 21: Visualization of the 12 MW WINDMOOR turbine on the INO-WINDMOOR semi-submersible (Figure 3.1, Inocean, Carlos Eduardo Silva de Souza et al. 2021)

2.5.1 General

The coordinate system of the floating wind turbine system is defined using a right-handed coordinate system for a local coordinate system moving with the semi-submersible to define the relative motions and an earth fixed coordinate system to determine the global motions of the system. The semi-submersible fixed coordinate system is shown in Figure 22. This orientation is also used in SIMA.

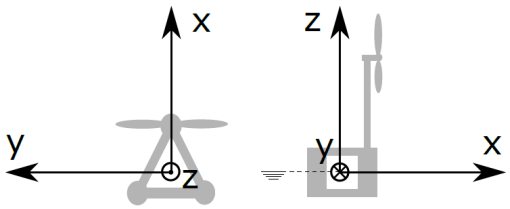

Figure 22: Local coordinate system (Figure (b) Carlos Eduardo Silva de Souza et al. 2021)

The mooring lines are connected to the columns of the semi-submersible at the mean water level, the fairleads, and the anchors of the mooring lines are positioned with 120 degrees spacing in between. The mooring lines for the 150 meter depth location are defined by the global coordinates in Table 10.

Table 10: Description of fairlead and anchor positions at 150 meter depth (Table 3.3 Carlos Eduardo Silva de Souza et al. 2021)

	Fairlead			Anchor		
Mooring line	x [m]	y [m]	z [m]	x [m]	y [m]	z [m]
1	42.7	0	0	700	0	-150
2	-21.4	37	0	-350	606.2	-150
3	-21.4	-37	0	-350	-606.2	-150

The mooring lines have a semi-taut profile consisting of the 4 segments defined below. These are ordered from fairlead to anchor.

- Chain with added mass from marine growth
- Polyester with added mass from marine growth
- Polyester
- Chain

The exact parameters of these segments are not defined in this report but can be found in the *Definition of the INO WINDMOOR 12 MW base case floating wind turbine* report (Carlos Eduardo Silva de Souza et al. 2021). A detailed description of the mooring line system for 600 meter depth that is used as the base case for the optimization is given at the end of this section. The natural periods of the system are given in Table 11.

Table 11: Natural periods for floating wind turbine system (Table 3.5 Carlos Eduardo Silva de Souza et al. 2021)

	Surge	Sway	Heave	Roll	Pitch	Yaw
Natural period [s]	97.3	98.0	16.3	29.5	31.4	88.0

2.5.2 The INO WINDMOOR Semi-Submersible

The semi-submersible is visualized in Figure 21 and for this report it is assumed to be the optimal design. It was obtained by varying the geometric parameters of the structure as the design variables under a set of constraints. The obtained result is defined by the parameters in Table 12. A hydrodynamic analysis was performed in WAMIT, using a linear diffraction-radiation analysis, to obtain added mass, wave damping, first order and second order wave force coefficients. These coefficients are included in the SIMA model. The procedure is provided in detail in the *Definition of the INO WINDMOOR 12 MW base case floating wind turbine* report (Carlos Eduardo Silva de Souza et al. 2021).

Table 12: Parameters of the INO-WINDMOOR semi-submersible (Table 3.1 Carlos Eduardo Silva de Souza et al. 2021)

Parameter	Value
Column diameter	15 [m]
Column height	31 [m]
Pontoon width	10 [m]
Pontoon height	4 [m]
Center to center distance	61 [m]
Deck beam width	3.5 [m]
Deck beam height	3.5 [m]
Total substructure mass	11974.0 [t]
COGx	-5.91 [m]
COGz	-9.7 [m]

The total substructure mass provided in Table 12 includes the ballast that leads to zero vertical displacement for the 150 meter depth mooring system.

2.5.3 The 12 MW WINDMOOR Turbine

The 12 MW WINDMOOR turbine was created by upscaling the 10 MW IEA reference turbine (Bortolotti et al. 2019) in combination with data on the hub and nacelle mass from General Electric's Haliade-X 12 MW wind turbine (GE 2020). The 10 MW IEA reference wind turbine was selected over the DTU 10 MW reference wind turbine as the IEA wind turbine's direct-drive generator is more common for offshore wind than the medium-speed generator from the DTU turbine. Additionally, the increased rotor diameter leads to a reduced specific power. The upscaling procedure was performed using the standard upscaling laws while keeping the same airfoil shape (Carlos Eduardo Silva de Souza et al. 2021). A more detailed description of this procedure is provided in section 5 of the *Definition of the INO WINDMOOR 12 MW base case floating wind turbine* report (Carlos Eduardo Silva de Souza et al. 2021).

The resulting parameters of the WINDMOOR 12 MW turbine and the rotor are given in Table 13.

Table 13: Parameters of the WINDMOOR 12 MW turbine (Table 5.1 Carlos Eduardo Silva de Souza et al. 2021), the parameters in bold do not differ from the IEA 10 MW turbine.

Parameter	Value	Unit
Rated electrical power	12	[MW]
Specific power	324.8	[W/m^2]
Rotor diameter	216.9	[m]
Rotor orientation	Clockwise - upwind	[-]
Number of blades	3	[-]
Hub diameter	5	[m]
Blade length	105.4	[m]
Blade prebend	6.8	[m]
Shaft tilt	6.0	[deg]
Rotor precone	-4.0	[deg]
Hub height	131.7	[m]
Cut-in wind speed	4	[m/s]
Rated wind speed	10.9	[m/s]
Cut-out wind speed	25	[m/s]
Generator efficiency	94.4	[%]
Cut-in rotor speed	5.5	[rpm]
Rated rotor speed	7.8	[m/s]
Maximum tip speed	88.6	[m/s]
Blade mass	63024	[kg]
Hub mass	60000	[kg]
Nacelle mass	600000	[kg]

To complete the description of the 12 MW WINDMOOR and INO-WINDMOOR semi-submersible floating wind turbine system, the parameters of the tower of the wind turbine are given in Table 14. This information and the tower model implemented in the base case model were provided by Equinor (Carlos Eduardo Silva de Souza et al. 2021).

Table 14: Parameters of the tower provided by Equinor (Table 5.7 Carlos Eduardo Silva de Souza et al. 2021)

Parameter	Value	Unit
Diameter at top	5.97	[m]
Diameter at bottom	9.90	[m]
Thickness of wall at top	30.1	[mm]
Thickness of wall at bottom	90.0	[mm]
Length	110.20	[m]
Mass	1161.6	[tonnes]
COGz from base	56.65	[m]

2.5.4 Performance

The model includes a Java-based controller that implements a variable-speed-variable-pitch (VSVP) approach (Carlos Eduardo Silva de Souza et al. 2021). The approach includes peak shaving of the thrust resulting in the thrust as a function of wind speed shown in Figure 23a and the power as a function of wind speed shown in Figure 23b. This results in a desired maximum thrust force of 1700 kN. Adjustments of the peak shaving are still ongoing.

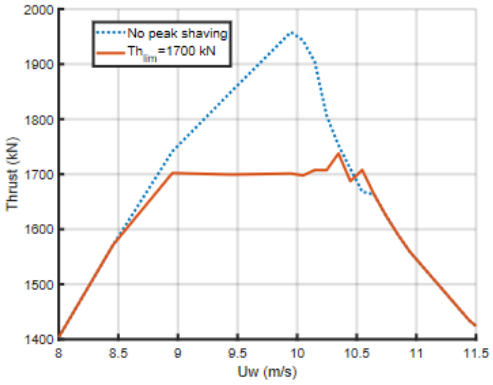

(a) Peak shaving of thrust curve (Figure 5.4 (a) Carlos Eduardo Silva de Souza et al. 2021)

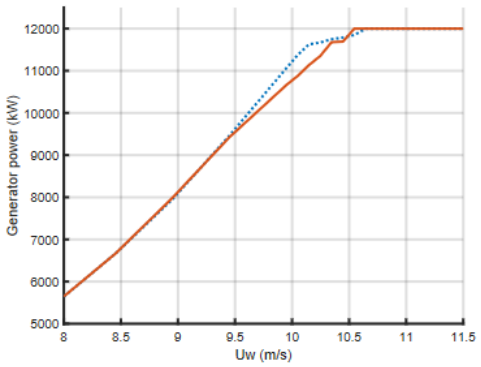

(b) Resulting power curve (Figure 5.4 (b) Carlos Eduardo Silva de Souza et al. 2021)

Figure 23: WINDMOOR 12 MW wind turbine performance curves

The hydrostatic stiffness coefficients of the complete system are given in Table 15.

Table 15: Hydrostatic stiffness coefficients for single turbine system

	Hydrostatic Stiffness
Heave [N/m]	$5.33{\cdot}10^6$
Roll [Nm/rad]	$3.38{\cdot}10^9$
Pitch [Nm/rad]	$3.38{\cdot}10^9$

A detailed description of the java based controller and performance of the semi-submersible, wind turbine and the system as a whole is provided in *Definition of the INO WINDMOOR 12 MW base case floating wind turbine* (Carlos Eduardo Silva de Souza et al. 2021). If specific information on the performance of the system is used the report will be referenced and the information will be provided. But for all additional information the WINDMOOR report should be consulted.

2.5.5 Modifications

The provided model includes a mooring system for 150 meter depth. For the purpose of this report the mooring system has been modified to suit a 600 meter depth location. The obtained mooring line configuration is used as the initial design for the optimization of the single turbine. It is also used for the initial anchor lines of the shared mooring floating wind turbine farm concept. If additional anchor mooring line strength is required the characteristics will be changed.

The limitations of the software used, SIMA, require simplifications of the model for FWT farm analyses. SIMA is only able to perform analyses on one rotor and java-based controller at a time during dynamic simulations. Therefore the analysis of the farm concept must be performed using a simplified model where the rotor and controller have been removed. This simplified model is also used for the single turbine system optimization for consistency and a more appropriate comparison of the obtained results.

The 150 meter depth mooring system has insufficient line length to be used for 600 meter depth and to maintain a semi-taut profile. Therefore the length of the bottom chain segment and the anchor radius have been increased with an arbitrary number, this results in the base case mooring line design for 600 meter depth. The increase in chain length leads to an increase in added mooring line weight and causes a vertical displacement of the system.

Using the hydrostatic heave stiffness of the system given in Table 15 and the resulting heave displacement, the ballast of the semi-submersible is adjusted to obtain a zero vertical displacement in the static condition. If the forces are not in equilibrium, meaning an initial non zero displacement, the system will start to oscillate when freed. This oscillation can lead to divergence in the analysis and cause the analysis to terminate. The initial 600 meter water depth system is defined by the new values for the parameters in Table 16. The mooring line configuration is shown in Figure 24. This mooring design does not satisfy the required constraints but is a valid starting design for the optimization process, as a full dynamic simulation can be performed without errors.

Table 16: Parameters for 600 meter water depth mooring system

Parameter	Value
Top chain segment length	25 [m]
Top chain diameter	0.165 [m]
Polyester segment length	170 [m]
Polyester diameter	0.19 [m]
Bottom chain segment length	850 [m]
Bottom chain diameter	0.165 [m]
Anchor radius	750 [m]
Semi-submersible mass	1.116e7 [kg]

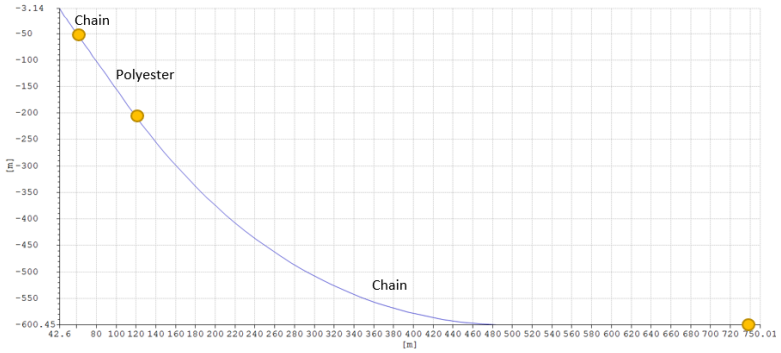

Figure 24: Mooring line schematic

Using the new mooring system, the simplified model is created by applying the steps given below.

- Remove wind turbine blades
  - Add mass of the removed blades to the mass of the hub
  - Add mass moments of inertia of the blades to the mass moments of inertia of the nacelle
- Remove wind turbine and java based controller from the SIMA model

The mass moments of inertia in the nacelle are calculated using the parallel axis theorem. Adding the mass of the blades to the hub leads to a reduction in moment at the tower base. Therefore an additional moment is added to center of gravity of the semi-submersible, which is a function of the vertical force from the blades and the distance between the COGx of the hub and the blades. The calculations are provided in the Appendix (8.1). The resulting motions of three different models are compared to assess the simplified model, using three conditions. The full model calculates motion using the wind-wave environment and the java based controller. The simplified model uses static forces as a substitute for the environment. To identify the impact of applying a static force the full model is also used to compare the motions for the java based controller and the applied static forces. The three models are described below and the conditions are given in Table 17.

- Model 1: Full model using java based controller and constant rated wind speed, regular wave environment in terms of peak period and significant wave height
- Model 2: Full model using applied static wind forces and wave drift force

- Model 3: Simplified model using applied static wind forces and wave drift force

The models are visualized in Figure 25.

Table 17: Conditions used for simplified model verification

	Wind	Wave Drift
Condition 1	X	
Condition 2		X
Condition 3	X	X

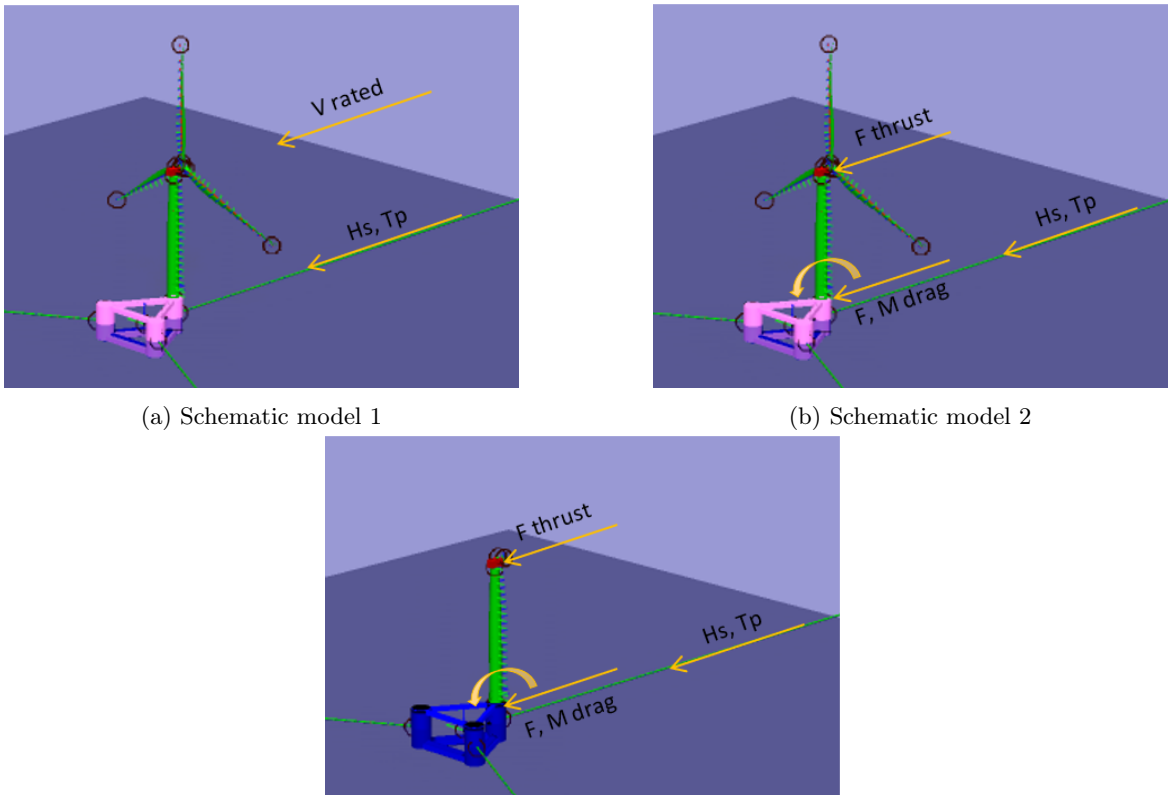

(a) Schematic model 1

(b) Schematic model 2

(c) Schematic model 3

Figure 25: Visualization of different models

The wave forces are provided in SIMA as a function the degree of freedom, the direction, the peak period and the significant wave height. These force functions were obtained using WAMIT. The forces or environment are applied in the negative X direction, resulting in negative surge displacements. The environment used consists of a rated wind speed of 10.6 m/s, a peak period of 15 seconds and a significant wave height of 10.9 meter. The resulting environmental static forces are given in Table 18. The static thrust force is applied at the nacelle, the wave drift force is automatically applied by SIMA, the tower drag force and moment are applied at the bottom of the tower.

Table 18: Static forces

Thrust Force	Wave Drift Force	Tower Drag Force	Tower Drag Moment
1700 kN	12.77 kN	52.13 kN	2.95 MN

The static simulation accuracy for the specified forces module is set at $1e^{-5}$. Using this value and a static wind loading consisting of thrust force, tower drag and tower moments leads to a surge displacement of -72.9 meters. For a smaller value of $1e^{-4}$ the displacement converges to -61.3 meters. For a larger value of $1e^{-6}$ the surge displacement converges to -72.9 meters, but this has an increased simulation time. Therefore the initially set

accuracy is used.

The comparison of the models in terms of mean positions for the conditions is provided in Table 19, Table 20 and Table 21. The mean positions for model 1 are obtained as the mean value of the steady state time series of motion for the desired degree of freedom. A 1400 second simulation is used and a 400 second transient part is removed from the start of the time series.

Table 19: Motion comparison for wave drift force only

Wave Drift Force only		
	Full model	Simplified model
Surge [m]	-7.50	-7.48
Sway [m]	-8.8e-7	-7.7e-7
Heave [m]	0.0045	0.0057
Roll [deg]	-3.1e-5	1.7e-6
Pitch [deg]	4.48	4.43
Yaw [deg]	-2.2e-5	2.6e-6

Table 20: Motion comparison for rated wind speed only

Rated wind speed			
	Full model	Full model (static forces)	Simplified model (static forces)
Surge [m]	-73.16	-72.95	-72.93
Sway [m]	-0.60	-0.09	-0.09
Heave [m]	-0.08	-0.03	-0.03
Roll [deg]	-0.72	-0.19	-0.19
Pitch [deg]	-3.08	-3.43	-3.48
Yaw [deg]	0.39	0.38	0.37

Table 21: Motion comparison for rated wind speed and drift forcing

Full environment			
	Full model	Full model (static forces)	Simplified model (static forces)
Surge [m]	-76.73	-77.99	-77.97
Sway [m]	-0.54	-0.09	-0.09
Heave [m]	-0.08	-0.25	-0.25
Roll [deg]	-0.71	-0.19	-0.19
Pitch [deg]	-2.74	-2.98	-3.02
Yaw [deg]	0.39	0.36	0.35

The application of static forces leads to an overestimation in static surge and pitch positions, which are coupled, when wind and drift forces are applied. The simplified and full model with static forces have similar static positions for all degrees of freedom, showing that the difference is caused by the application of the static forces and the removal of the rotor. Additionally, the coupling between loads applied in the surge degree of freedom and motion in sway and roll is lost. Model 2 and 3 do not have aerodynamic torque as no active rotor is present in these models. The models with static forces therefore significantly underestimate the static positions in sway and roll.

The difference between surge and pitch is caused by the loss of aerodynamic damping. In model 1 the system is in motion for the applied wind and wave conditions, while the static forces are applied incrementally until a static equilibrium has been found in model 2 and 3. In model 1 there is a change in thrust force due to a change in relative wind speed. This affects the mean positions in surge and pitch. Additionally, the local moment at the hub caused by the forces on the blades is lost when applying static forces.

The pitch and surge positions of the simplified model are within 10% and 2% of the full model, respectively. This is assumed sufficient for the scope of this thesis.

ULS Condition

The design standards recommend to use the extreme conditions with a 50 year return period for wind and wave for ULS analysis of offshore floating wind turbines. However, they also state that the must unfavorable combination of wind and wave conditions should be used in ULS analysis. The 50 year wind speed at hub height is 44.6 m/s. The 50 year wave condition is defined by a significant wave height of 10.9 meter and a peak period range of 9 - 15 seconds. The wave force transfer functions for surge and an angle of - 180 degrees, meaning in the negative X-direction, as a function of excitation period are given in Figure 26a and Figure 26b.

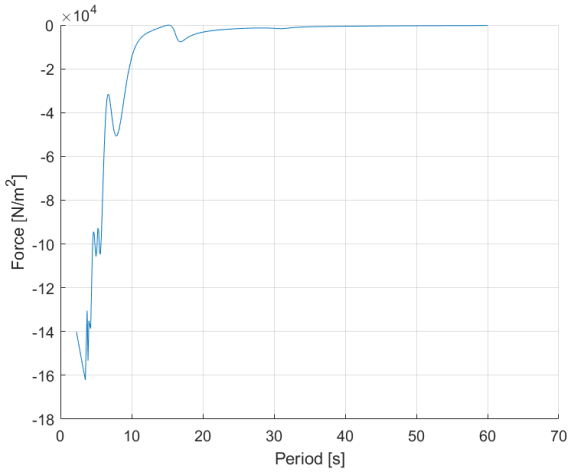

(a) Second order wave drift force transfer function

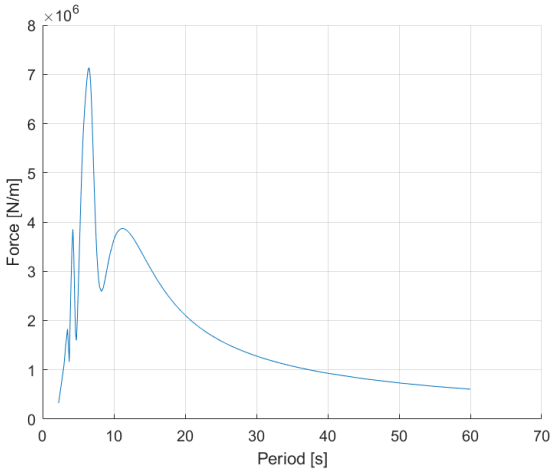

(b) First order wave force transfer function

Figure 26: Wave force transfer functions from WAMIT simulations

The figures show that the largest wave drift force is obtained for the lowest period on the extreme conditions range of 9 seconds. The largest first order wave forces are obtained for a period of 11.25 seconds. As the optimization is performed using static forces and mean displacements the period of 9 seconds is used for the ULS condition.

To determine the ULS wind condition a constant wind speed simulation was performed on the system. A 10.6 m/s wind speed was used on an operating turbine. The 50 year return period wind speed of 44.6 m/s was used on a parked turbine as the wind speed is far above the cut out wind speed of 25 m/s. The mean surge and pitch positions are given in Table 22.

Table 22: Mean positions for extreme wind speeds

	10.6 m/s	44.6 m/s
Surge [m]	-73.2	-42.9
Pitch [deg]	-3.08	3.7

The pitch displacement for 44.6 m/s is slightly less than the static pitch of 4.2 degrees, meaning a rotation of only 0.5 degrees. The rated wind speed condition causes a larger pitch displacement of 7.28 degrees and a larger surge displacement. Therefore, the forces corresponding to the ULS condition given in Table 23 are applied in the optimization.

Table 23: ULS condition set

Wind speed [m/s]	10.6
Peak period [s]	9
Significant wave height [m]	10.9

3 Methodology

3.1 Single Turbine System

The initial mooring system for the single turbine at 600 meter depth is used as the starting point for the optimization. In Section 2.2 it was explained that the mooring system must satisfy requirements set by design standards for position mooring and offshore floating wind turbines. A workflow in SIMA is created to automate the optimization process and guarantee that the mooring system meets the design requirements. The optimization process is defined by the optimization problem statement in terms of the objective function, design variables and constraints. The optimization procedure is the description of the workflow created in SIMA. A specific procedure was created and implemented to account for issues that occurred in initial optimization model. This ensures that the static calculation is more robust and prevents the occurrence of additional errors and termination of the optimization procedure.

3.1.1 Optimization Problem Statement

Objective function

The goal of the single turbine optimization is to minimize the costs of the mooring system at 600 meter depth, limited to the material costs of the mooring lines and the anchors. The information on the mooring line material properties and costs has been provided by the WINDMOOR project. The mooring line properties for chain are given in Table 24. The polyester mooring line properties are given in Table 25.

Table 24: Chain mooring line properties

Grade	MBL [kN]	Dry mass [kg/m]	Axial stiffness [N]
R3	$0.0223 \cdot d^2 \cdot (44 - d \cdot 0.08)$	$0.02 \cdot d^2$	$2 \cdot 2.1 \cdot 10^5 \cdot \frac{\pi}{4} \cdot d^2$
R3S	$0.0274 \cdot d^2 \cdot (44 - d \cdot 0.08)$	”	”
R4	$0.0320 \cdot d^2 \cdot (44 - d \cdot 0.08)$	”	”

Table 25: Polyester mooring line properties

	Equation
Mass [kg/m]	$0.0007 \cdot d^2 - 0.0088 \cdot d + 0.489$
MBL [kN]	$0.2658 \cdot d^2 + 4.9392 \cdot d - 654.74$
Post installation stiffness [MN/m]	$0.0035 \cdot d^2 + 0.063 \cdot d - 8.3976$
Intermediate stiffness [MN/m]	$0.0072 \cdot d^2 + 0.1343 \cdot d - 17.779$
Storm stiffness [MN/m]	$0.0074 \cdot d^2 + 0.1391 \cdot d - 18.424$

The storm stiffness is applied in ULS analysis, the intermediate stiffness in FLS analysis and the post installation stiffness to determine the pretension. The material cost is a function of the mooring line weight and given in Table 26. The values were provided as a range and the upper limit of that range is used.

Table 26: Mooring line material cost

Grade	Material	EUR/kg
R3	Chain	2.0
R3S	Chain	2.1
R4	Chain	2.4
	Polyester	7.5

The variables required to calculate the total mooring line material costs are the diameter of the top chain, polyester, bottom chain segments and their respective lengths. The weight is calculated using the mass functions in Table 24 and in Table 25. The total material cost of the mooring lines for the single turbine system is calculated using Equation 77.

$$M_{s,cost} = 3 \cdot (W_{t,chain} L_{t,chain} + W_{b,chain} L_{b,chain}) \cdot M_{c,cost} + 3 W_{poly} L_{poly} \cdot M_{p,cost} \tag{77}$$

The anchor cost is determined using the information on the drag embedded anchor bearing capacity and cost reference provided in the Carbon Trust Report *Floating Offshore Wind: Market and Technology Review* (James and Ros 2015). The report provides three ranges on anchor weight and corresponding bearing capacity. It is assumed that the upper side of the weight range corresponds to the provided bearing capacity. This is a conservative assumption on the provided data. The data have been used to create the anchor weight and bearing capacity relation shown in Figure 27.

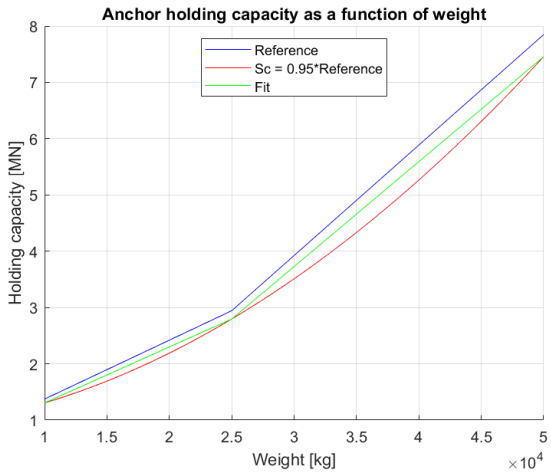

Figure 27: Anchor bearing capacity as a function of weight

The blue graph represents the reference data and the green graph represents 0.95 times the reference data, which is required for the constraint on the design tension at the anchor given in Equation 45 and Equation 46. The red graph represents a second order polynomial fit that has been made based on these reference points as a continuous relation between the anchor weight and the bearing capacity. This relation has been rewritten to determine the required weight of the anchor based on the obtained design tension $T_{d,a}$ given in Equation 78.

$$W_a = \frac{-B + \sqrt{((B)^2 - (4A \cdot ((0.95 \cdot 0.8992) - (T_{d,a}/10^6))))}}{2A} \tag{78}$$

Where:

$$\begin{aligned} A &= 0.95 \cdot 2.2890 \cdot 10^{-9} \\ B &= 0.95 \cdot 2.4525 \cdot 10^{-5} \end{aligned} \tag{79}$$

The obtained weight is used to calculate the cost of the anchor based on the single reference value for a drag embedded anchor of 21000 kg weight and a cost of 70000 British Pounds. It is assumed that the anchor weight and cost have a linear relation. The reference cost is converted to Euros using the average exchange rate from June 2015. The average exchange rate GBP:EUR in June 2015 was 1:1.3893 according to ExchangeRates.org.uk 2021, leading to a cost of 97251 Euros. Inflation has not been included in the price calculation, but could be implemented for a more accurate cost calculation.

$$A_{s,cost} = 3\frac{W_a}{21000}97251 \tag{80}$$

The objective function, the function to minimize, is the addition of the anchor cost function and the mooring line material cost function. This leads to Equation 81.

$$f(x)_s = M_{s,cost} + A_{s,cost} \tag{81}$$

Design variables

The optimization of the mooring system is limited to the mooring line characteristics of a semi-taut profile. The mooring line configuration is forced to have a chain-polyester-chain profile as outlined in Figure 24. The initial

weight in water of the polyester segment is smaller than the buoyancy force. Therefore the polyester segment must be under tension and slack may not occur, leading to a semi-taut profile. In addition, the assumption has been made that the three mooring lines will have the same characteristics to provide resistance for multiple directions of environmental loading. This results in the design variables given in Table 27. The table also provides initial lower and upper bounds. These bounds are used to explore the design space but also limit it. The upper and lower bounds might be adjusted based on if the algorithm tends to move towards the lower or upper bound of a specific design variable. The lower bound for the top chain segment is required to account for wear against the semi-submersible and to provide ALS resistance. The lower bound of the polyester segment is set at an arbitrary value of 10. SIMA requires that all segments have a non-zero length. In addition, it is not expected that the optimizer prefers a zero polyester line length, as polyester has a better resistance against fatigue damage than chain. It will be checked that the optimizer does not tend to go toward the lower limit of the polyester line length. It is noted that the upper and lower bounds are extreme. However, a wide range allows to assess the performance of the optimizer and to explore the design space.

Table 27: Design variables single turbine system and initial bounds

Design variables	Lower bound	Upper bound
Length of top chain segment	20	1000
Diameter of top chain segment	0.0165	0.5
Length of polyester segment	10	1000
Diameter of polyester segment	0.019	0.5
Length of bottom chain segment	200	2000
Diameter of bottom chain segment	0.0165	0.5
Anchor radius	500	4000

Constraints

The system should be able to withstand and survive ULS, ALS and FLS conditions over the lifetime of the system. As ALS is not within the scope of this thesis, the analysis of ALS is not included. The hypothesis for this thesis is that the ULS condition is design driving. The initial constraints are therefore based on the ULS analysis in the design standards, general mooring line constraints and information provided by the WINDMOOR project.

The main purpose of power production should be maintained during all operating and non operating conditions. For offshore FWT power transportation is constrained by the integrity of the power cable. According to the WINDMOOR project, the maximum allowable surge displacement for the system, to maintain integrity of the power cable, is 30 - 35% of the water depth. To be conservative the limit is set at the lower bound of 30%, leading to a maximum allowable displacement of 180 meters for a water depth of 600 meters. The constraint is given in Equation 82. In addition, the industry has a general rule of thumb that the pitch displacement in ULS should be smaller than 10 degrees. This constraint is given in Equation 83. This is to ensure that the rotor nacelle assembly does not excite large moments on the tower and substructure.

Displacement constraints

$$|x_{surge}| \leq 180\ m \tag{82}$$

$$|x_{pitch}| \leq 10\ deg \tag{83}$$

Industry partners in the WINDMOOR project also provided that the pretension of the mooring lines should be smaller than 2 MN for efficient installation.

Pretension constraint

$$\max(T_{fairlead}) < 2\ MN \tag{84}$$

The calculation of the design tension is required for the constraints on MBL for the mooring line segments. As given in Equation 44, the design tension is a function of the characteristic mean tension and the characteristic dynamic tension. The dynamic tension can be obtained through a full 1 hour to 3 hour long dynamic

simulation. As the optimization is based on static analysis, an initial assumption has been made for the characteristic dynamic tension of being equal to or smaller than 10% of the characteristic mean tension. This has been implemented as the dynamic tension is dependent on the characteristics of the mooring system and the environmental conditions. It has been tried to find a direct relation between mean tension and dynamic tension without success. The assumption is checked with the first obtained results from the single turbine optimization. The mean tension in each segment was found to be the largest at the top element of that segment. Therefore the following procedure is applied to determine the constraints for MBL in each segment.

$$T_{dyn} = 0.1 \cdot T_{mean} \tag{85}$$

- Determine mean tension from ULS simulation
- Calculate dynamic tension using Equation 85
- Determine design tension using Equation 44 and safety factors in Table 2
- Determine holding capacity using Equation 45
- Calculate ratio of design tension over holding capacity
- Require that this ratio is smaller than 1 according to Equation 46 (given in Equation 86)

MBL/MBS constraint

$$\frac{T_d}{S_c} \leq 1 \tag{86}$$

Because of the geometric and characteristic similarity of the three mooring lines this only yields 3 constraints. The constraints on MBL are implemented on line 1 as it is in the direct loading direction and will experience the most significant loads. During the ULS condition the other two lines should be checked for slack. Slack should be prevented at all times as it can lead to snap loads under a sudden change of loading magnitude and direction. Because of the loading direction and the mooring system orientation only 1 of the 2 lines on the opposite side needs to be checked for this condition. Slack is obtained when the tension in the mooring line at the fairlead becomes negative, therefore the constraint in Equation 87 is implemented.

Slack constraint

$$\min(T_{fairlead}) > 0 \tag{87}$$

To prevent mooring line failure from excessive wear on the polyester segment it must be checked that the polyester segment does not touch the seabed at all times. The vertical height of the bottom node of the polyester segment is obtained from a short dynamic simulation. The absolute value of the water depth is added and checked according to Equation 88.

Polyester seabed touching constraint

$$Z_{polyester,N_{end}} + |h| > 0 \tag{88}$$

Lastly to ensure that no vertical forces occur at the drag embedded anchor the vertical position of the second to last node is checked similarly to Equation 88. The last node cannot be used as this is set as a fixed boundary condition and will always be resting on the seabed. In addition, preferably the number of nodes would be set as a function of the segment length. This would ensure the same level of accuracy in the FEM analysis for all segments. In addition, this would lead to a more accurate constraint for the anchor uplift. Currently the required line length resting on the seabed according to Equation 89 would change with a change of the bottom chain segment line length. However, implementing more nodes would lead to increased simulation time.

Anchor uplift constraint

$$Z_{b,chain,N_{end-1}} + |h| > 0 \tag{89}$$

3.1.2 Optimization Procedure

The creation of the optimization workflow in SIMA has been a trial and error process. The static calculation in combination with the variation of mooring line parameters lead to a range of problems. The semi-submersible ballast mass is required to change as the added weight from the mooring lines changes. In addition to that the initial number of steps in the static calculation modules did not work for all designs in the optimization procedure. The created workflow should be tested across a broader range of conditions and potentially modified to suit analysis for different loading directions. The optimization workflow is shown in Figure 28.

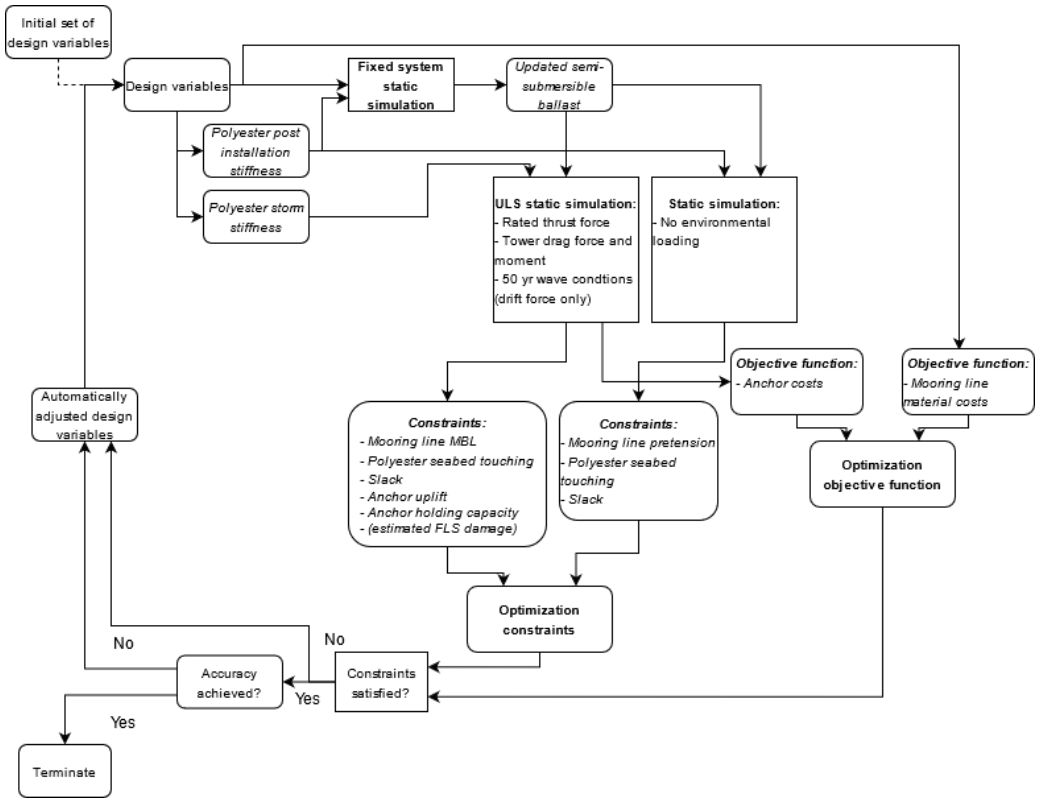

Figure 28: Optimization flowchart single turbine

The fixed system simulation is used to adjust the ballast of the semi-submersible. This simulation does not include environmental forces and the system is fixed at its origin. Each iteration the mooring line tension and angle with the Z-axis at the fairlead are used to determine the initial vertical force of the mooring line design. This force is compared to a reference value and the difference is used to calculate a required change in ballast weight. This weight is added to the original value of semi-submersible ballast and used in the ULS and static simulations. During these simulations the system is freed in the boundary change load group, once it has found the static mooring line equilibrium, followed by application of environmental forces, only in the ULS static simulation. The objective function and constraints are determined in two separate post processors.

Initially 23 constraints are applied:

- Static simulation without environment
  - Pretension (3)
  - Slack (3)
  - Polyester seabed touching (3)
- Static simulation ULS condition
  - Slack (3)
  - Anchor uplift line 1 (1)
  - MBL constraint on fairlead, polyester and bottom chain line 1 (3)

- Anchor MBL constraints (2)
- Polyester seabed touching (3)
- Surge and pitch position (2)

Mooring line 1 is in line with the loading. The mooring line material cost is initially calculated using R3 chain grade, as this grade has the lowest cost per kg and the objective is to minimize material costs. The optimization algorithm automatically updates the design variables based on the information provided in Section 2.3.3. This process is repeated until the desired accuracy has been achieved. The user specified optimization parameters in SIMA are provided in the Appendix (8.2).

3.1.3 Analysis

The design obtained from the optimization is used to test the standard deviation assumption. An irregular wave and wind ULS condition simulation using the full model and the java based controller is performed to determine the mean and dynamic tension in the mooring line segments. These are used to calculate the ratio. The obtained design is not valid if the ratio is larger than the implemented assumption. A larger ratio corresponds to a larger design tension, meaning the MBL constraints are actually not satisfied. If so, an adjustment is made and a larger ratio is applied. The optimization is rerun to check the assumption again until it is valid.

Decay tests are performed to identify the natural frequencies of the system. In addition, the design is tested for accumulated fatigue damage using the conditions in Table 9.

Decay tests

The natural periods for all degrees of freedom are evaluated and compared to the base case model. A separate simulation model was created to perform the decay tests. The wind turbine is in parked condition and the blades are feathered to minimize aerodynamic damping. There is no external environmental loading present in the simulations. The system is displaced in the degree of freedom by an applied force or moment in a similar time series given in Figure 29. The applied force is suddenly removed and the system will return to its equilibrium position. The oscillations in the time series of motion are at the natural frequency. The time series of motion is used to determine the turning points, peaks and troughs, of the motion. The distance between two turning points, two peaks or two troughs, in the time series is measured and defined as the period. The mean value of all periods is defined as the natural period.

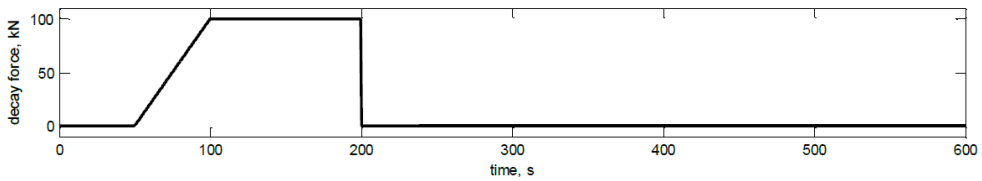

Figure 29: Example of time series specified force/moment for decay test (E. Bachynski 2020b)

The magnitudes and profiles of the forces and moments applied are defined in Table 28 for each degree of freedom. The forces for surge and sway are half the maximum thrust force. The applied force for heave corresponds to a vertical displacement of 1 meter. The moments for roll and pitch are the force applied in surge and sway decay tests multiplied with the hub height. The moment for yaw is generally taken as 10% of the applied moments for roll and pitch. The simulation parameters in SIMA are given in the Appendix (8.3). The simulation time for surge, sway and yaw is increased because of the expected large natural periods. A reasonable number of cycles is required to estimate the natural period accurately.

Table 28: Simulation parameters for the decay tests

Motion	Force/Moment	Simulation length [s]	Ramp duration [s]	Constant duration [s]
Surge	850 kN	3000	100	200
Sway	850 kN	3000	100	200
Heave	5330 kN	1500	50	50
Roll	111950 kNm	1500	50	100
Pitch	111950 kNm	1500	50	100
Yaw	11195 kNm	3000	50	100

Fatigue Damage Accumulation

For each condition in Table 9 a 4000 second TurbSim wind, irregular 3 parameter JONSWAP time series is generated and a transient part of 400 seconds is removed from the start to obtain a 1 hour simulation. The design standards recommend 3 hour simulation for fatigue analysis for a more accurate representation of the environment. However, due to limitations of storage a 1 hour time series was found to be maximum. The simulation parameters used in SIMA are provided in the Appendix (8.4).

The tension time series of mooring line 1 at the top of each segment is converted into a stress time series using the cross sectional area, and the procedure outlined in Section 2.2.1 is implemented using the built in Rainflow counting algorithm from Matlab.

3.2 Shared Mooring Farm Concept

3.2.1 Optimization Problem Statement

Objective function

The goal of the shared mooring farm concept is again to minimize the total cost of the mooring line material and the anchors. The information in Table 24, Table 25 and Table 26 is used in combination with the new design variables of the shared mooring line characteristics. The mooring line material cost is calculated according to the same method in the single turbine optimization. It is given in Equation 90. The anchor cost function for the shared mooring farm concept is given Equation 91.

$$M_{f,cost} = 6(W_{t,chain}L_{t,chain} + W_{b,chain}L_{b,chain}) \cdot M_{c,cost} + 6W_{poly}L_{poly} \cdot M_{p,cost} + 6W_{s,chain}L_{s,chain} \cdot M_{s,cost} \tag{90}$$

$$A_{f,cost} = 6\frac{W_a}{21000}97251 \tag{91}$$

This leads to the objective function for the shared mooring farm concept given in Equation 92.

$$f(x)_f = M_{f,cost} + A_{f,cost} \tag{92}$$

Design variables

The design variables for the shared mooring farm concept optimization are an extension of the design variables for the single turbine optimization. The shared mooring line diameter and turbine spacing are added. However, freely varying the diameter of the shared mooring line within the optimization algorithm in combination with freely varying the anchor mooring line characteristics leads to an imbalance in vertical forces at the fairleads of the semi-submersible. This imbalance leads to too large incremental rotations in roll and pitch of the tower nodes during the static FEM analysis, causing the simulation to fail.

Therefore an additional calculation module is included to adjust the shared mooring line diameter based on the vertical force at the anchor line fairlead. Similar bounds are implemented for design space exploration of the farm concept, given in Table 29. Meyers and Meneveau 2012 suggest a spacing between turbines ranging from 7 to 15 times the rotor diameter.

Table 29: Design variables farm concept and initial bounds

Design variables	Lower bound	Upper bound
Length of top chain segment	20	1000
Diameter of top chain segment	0.0165	0.5
Length of polyester segment	10	1000
Diameter of polyester segment	0.019	0.5
Length of bottom chain segment	200	2000
Diameter of bottom chain segment	0.0165	0.5
Anchor radius	500	4000
Turbine spacing	1518.3	3253.5
Diameter of shared mooring line	0.0165	0.5

Constraints

The proposed constraints in the farm optimization implement the same theory as for the single turbine optimization. However, additional required measurement points are added, increasing the number of constraints. The loading direction, the shared mooring lines numbered in white and the anchor lines number in black are shown in Figure 30.

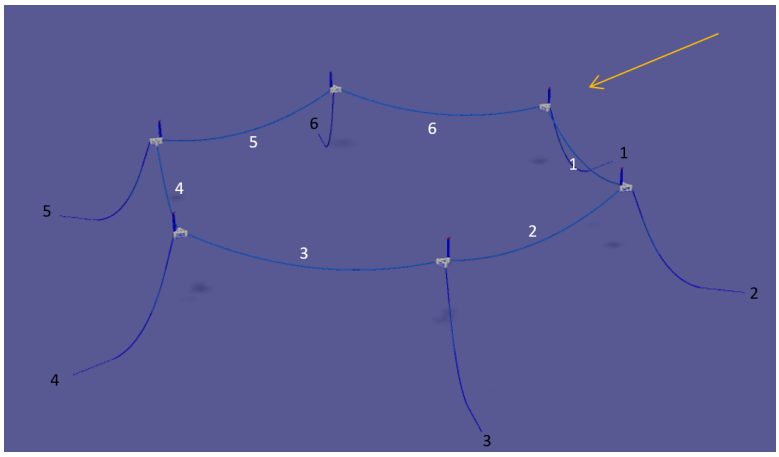

Figure 30: Shared mooring farm concept optimization schematic

The constraints outlined below are applied because of the symmetry of the farm and the loading direction.

Initially 32 constraints are applied:

- Static simulation without environment
  - Pretension anchor lines 1, 2 and 3 (3)
  - Slack anchor lines 1, 2 and 3 (3)
  - Polyester seabed touching anchor lines 1, 2 and 3 (3)
- Static simulation ULS condition
  - Slack anchor lines 3, 4 and 5 (3)
  - Anchor uplift 1, 2 and 6 (3)
  - MBL constraint on fairlead, polyester and bottom chain anchor lines 1, 2 and 6 (3)
  - Anchor MBL constraint lines 1, 2 and 6 (3)
  - Polyester seabed touching anchor lines 3, 4 and 5 (3)
  - Surge and pitch positions all turbines (6)
  - Shared lines MBL constraint at fairlead lines 1 and 3 (2)

3.2.2 Optimization Procedure

The proposed optimization flowchart for the farm concept is obtained by adding the adjustment of the shared mooring line diameter to the flowchart of the single turbine system optimization. To have a static equilibrium without excessive displacements or rotations it is required that the vertical forces from the mooring lines are reasonably in balance. As the number of anchors per turbine is significantly reduced it is assumed that the anchor mooring line characteristics will be governing. Therefore the shared mooring line characteristics are updated based on the vertical force from the anchor line. The simulation with the fixed system is used to determine the initial vertical force from the anchor and shared mooring line based on the axial force and the angle at the fairlead. The initial vertical force from the shared line at the fairlead is given by Equation 93. This force should be equal to the vertical anchor line force which is calculated as described for the single turbine system.

$$F_z = 0.5 \cdot L_{shared} \cdot 0.02d^2 \cdot 9.81 \cdot \sin(\alpha_f) \tag{93}$$

The required shared diameter in meters is then obtained by rewriting Equation 93 into Equation 94. $F_{z,a}$ is the vertical force from the anchor.

$$d = \frac{\sqrt{\frac{F_{z,a}}{0.5 \cdot L_{shared} \cdot 0.02 \cdot 9.81 \cdot \sin(\alpha_f)}}}{1000} \tag{94}$$

The applied static thrust force on the turbines vary as a function of turbine spacing and the applied wake model. The N.O. Jensen wake model implements a momentum balance and assumes a linear wake expansion coefficient. Assuming the first turbine in line operates at a maximum power coefficient, the axial induction factor is equal to $\frac{1}{3}$. The momentum balance in Equation 95, the linear wake expansion in Equation 96 and the axial induction factor of $\frac{1}{3}$ are combined to obtain the wind speed at the second wind turbine in line using Equation 97.

$$\pi r_0^2 V_0^2 + \pi(r^2 - r_0^2)U = \pi r^2 V \tag{95}$$

$$r = \alpha x + r_0 \tag{96}$$

$$V = U \cdot (1 - \frac{2}{3}(\frac{r_0}{r_0 + \alpha x})^2) \tag{97}$$

Here, r_0 is the rotor radius, x the turbine spacing, α the wake expansion coefficient, U the inflow velocity and V_0 the velocity behind the first turbine. According to the report *Wind turbine wake models developed at The Technical University of Denmark: A review* (Göçmen et al. 2016), the wake expansion coefficient is a function of the turbulence intensity equal to $0.4 \cdot TI$. The static thrust force can then be obtained through interpolation with the velocity and the wind turbine's thrust force curve.

3.2.3 Analysis

Due to the limitations of SIMA the full wind turbine model including java based controller can not be used for the analysis of the shared mooring farm concept. To assess the fatigue damage accumulation, using turbulent wind, a relation between thrust force and wind speed is required. The thrust force is given in Equation 98 and generally computed using the BEM theory. A basic approximation of the thrust force as a function of wind speed is made using Equation 99.

$$T = \frac{1}{2} \cdot \rho \cdot A \cdot (v_0^2 - (v_0(1 - 2a))^2) \tag{98}$$

$$C_{T,wind} = \frac{T}{v_0^2} \tag{99}$$

A vector of reference thrust coefficients and corresponding wind speeds needs to be provided. The dynamic analysis automatically interpolates the wind speed with the provided reference values.

4 Single Turbine System

4.1 Optimization results

The design obtained from the first completed optimization is tested using the full model including java based controller and a 4000 second turbulent wind, TurbSim, and irregular waves ULS condition dynamic simulation. The mean and dynamic mooring line tension at the top of each segment, and at the anchor, in anchor line 1 are determined to assess the implemented standard deviation assumption of 10%. The design is defined by Table 30 and the resulting percentages of standard deviation over mean mooring line tension are given in Table 31.

Table 30: Design 1

Design variables	Value
Length of top chain segment	20
Diameter of top chain segment	1249.5
Length of polyester segment	604.05
Diameter of polyester segment	0.1337
Length of bottom chain segment	0.0745
Diameter of bottom chain segment	0.0752
Anchor radius	1625.3
Semi-submersible mass	1.208e7 [kg]

Table 31: Percentage of standard deviation over mean tension (design 1)

Segment	[%]
Fairlead	13.18
Polyester	12.44
Bottom chain	12.61
Anchor	13.73

The desired final accuracy of the optimization was set at 0.1%, requiring the sum of all normalized constraint violations to be smaller than this. The maximum percentage in Table 31 of 13.73% is larger than the applied assumption of 10%. Therefore the obtained design does not satisfy the required constraints. A larger standard deviation than assumed leads to an increased design tension. Consequently, the MBL constraints for the mooring line segments are not satisfied as the holding capacity in Equation 46 does not change with the applied assumption. A larger percentage is required for the optimizer to satisfy the MBL constraints. A more conservative relation of 20% is implemented.

Design 2

Design 2 is the result of a new optimization using an assumption of 20% and the same starting design, defined by Table 16. It is defined by Table 32. The corresponding percentages of standard deviation over mean tension are given in Table 33.

Table 32: Design 2

Design variables	Value
Length of top chain segment	20
Diameter of top chain segment	0.0855
Length of polyester segment	175.04
Diameter of polyester segment	0.1495
Length of bottom chain segment	1461.1
Diameter of bottom chain segment	0.0850
Anchor radius	1410.7
Semi-submersible mass	1.185e7 [kg]

Table 33: Percentage of standard deviation over mean tension (design 2)

Segment	[%]
Fairlead	13.85
Polyester	13.24
Bottom chain	13.45
Anchor	14.37

The obtained design satisfies the standard deviation assumption. It is interesting to note that the ratio has increased for all segments for a more conservative assumption of 20%, in comparison to the design obtained with the 10% assumption. This suggests that the relation is design dependent.

The corresponding cost function and critical constraints of this optimization are shown in Figure 31.

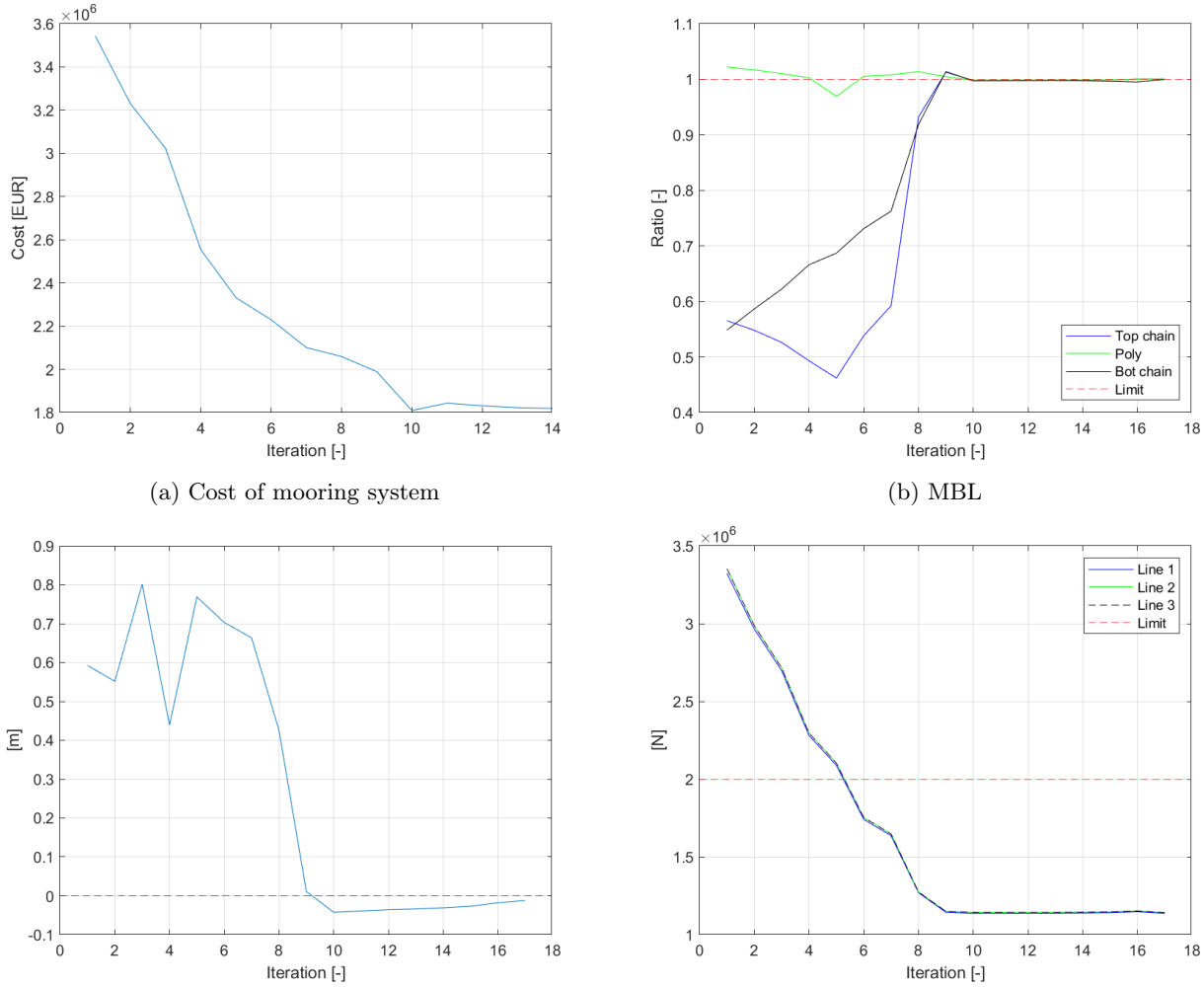

(a) Cost of mooring system

(b) MBL

(c) Anchor uplift

(d) Pretension

Figure 31: Cost function and critical constraints (design 2)

The paths of all design variables during the optimization are provided in Figure 32, to investigate the influence of the variables on the implemented constraints.

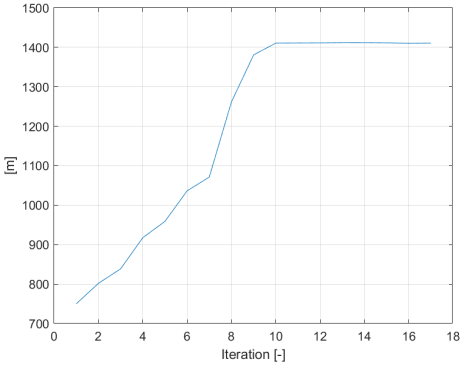

(a) Anchor radius

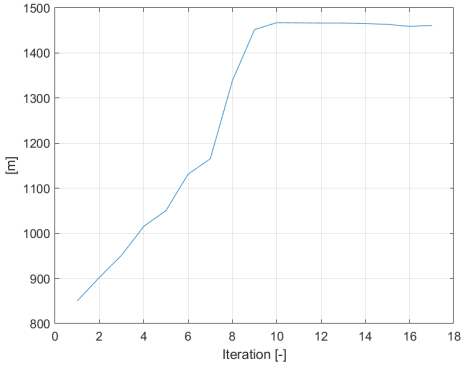

(b) Chain bottom length

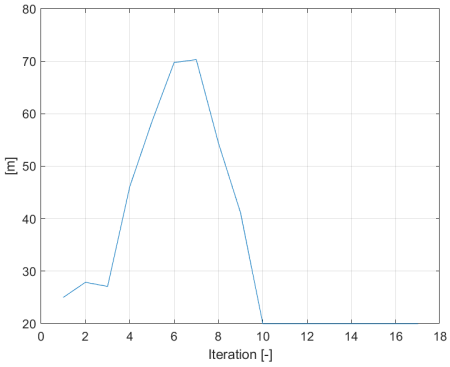

(c) Chain top length

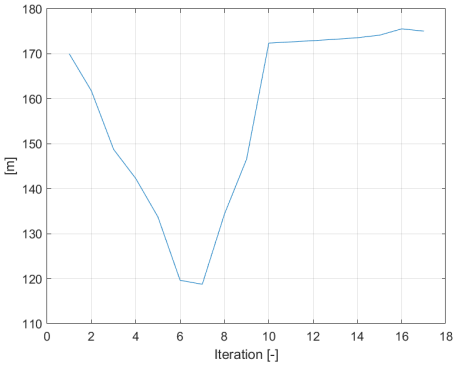

(d) Polyester length

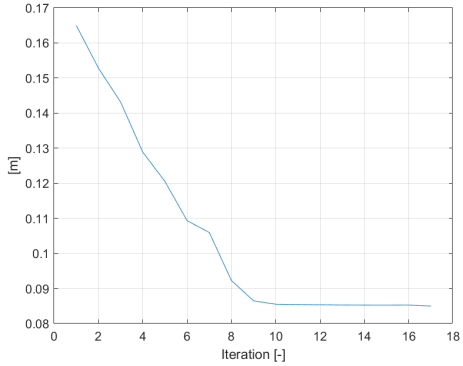

(e) Chain bottom diameter

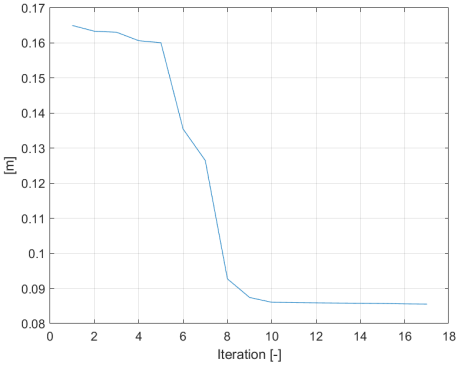

(f) Chain top diameter

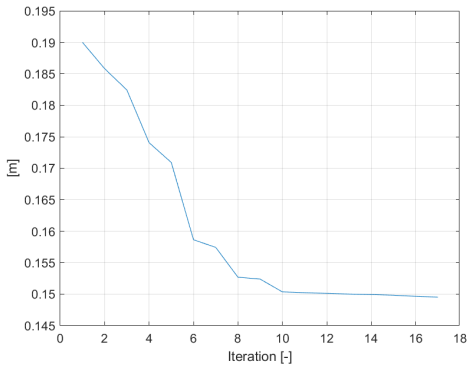

(g) Polyester diameter

Figure 32: Path of optimizer for design variables (design 2)

It is interesting to note that the algorithm initially increases the length of the top chain segment and decreases

the polyester segment length, while the final design has a decreased top chain length and an increased polyester segment length. The anchor radius and length of the bottom chain segment follow a gradual increase. This is paired with a decrease in the MBL constraint for the top chain segment until iteration 5.

The diameters of the polyester and the bottom chain segment follow a gradual decrease like the cost function and the pretension. From iteration 5 to iteration 6 the diameter of the top chain segment is decreased significantly, while the length increases, causing the MBL constraint to change direction and to increase. A reduction in diameter leads to a reduction in MBL, so the design tension must have increased or decreased less than the MBL. The tension at the fairlead is shown in Figure 33.

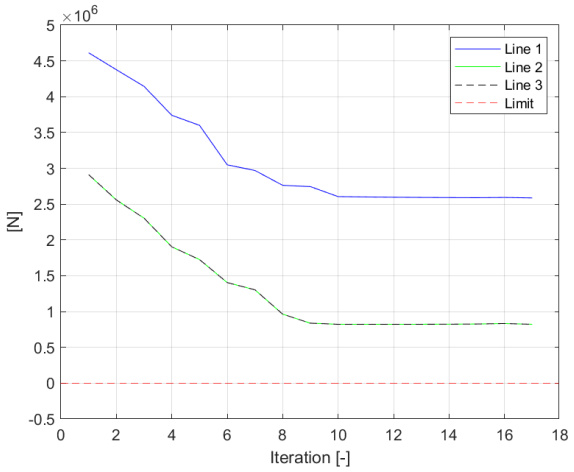

Figure 33: Tension at the fairlead in ULS condition

The tension at the fairlead in ULS condition has decreased by 15.3% and the diameter has decreased by 15.4% between iteration 5 and 6. This corresponds to a decrease in the MBL of the top chain segment of 23.8%. The mooring line tension is dependent on the weight of the other mooring line segments. For example, the diameter of the polyester segment has reduced by 7.2% during this iteration and the design tension has reduced by 11.1%. The bottom chain segment has a reduction of 9.2% in diameter and a reduction of 10.1% in design tension. Implementing a higher chain grade, R3S or R4, would increase the MBL for the same diameter by 23% and 43% respectively. The design tension would remain unchanged as the axial stiffness and the dry mass are independent of the chain grade.

The optimizer focuses on reducing the weight of the mooring line segments by decreasing the diameter of the segments. Additionally, the design tension reduces with the reduction in mooring line segment diameter as shown in Figure 34.

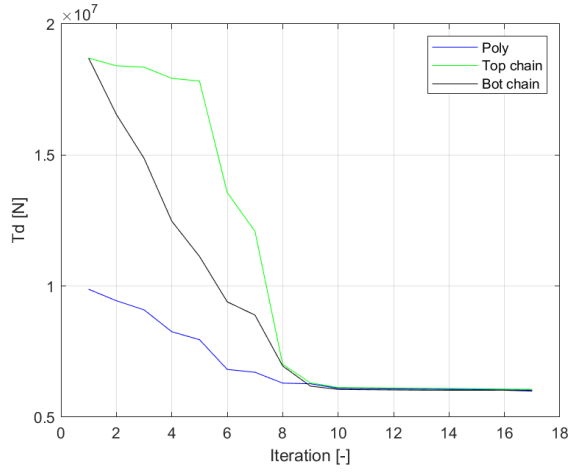

Figure 34: Design tension in each segment

The minimization of mooring line material cost is therefore governed by the weight per meter line length, shown in Figure 35b. Additionally, the bottom chain segment contributes most to the mooring line material cost.

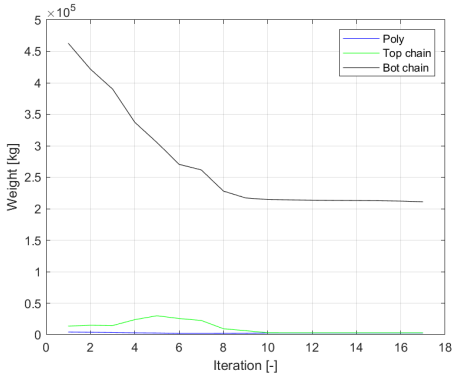

(a) Weight of mooring line segments

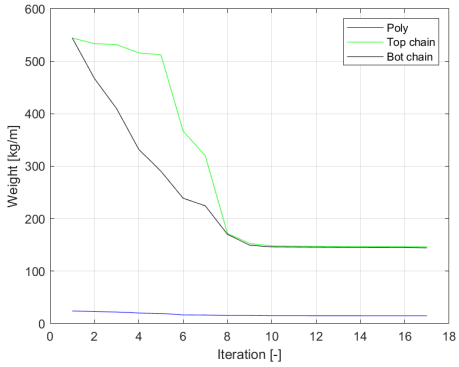

(b) Weight of mooring line segments per meter

Figure 35: Mooring line weight

For a higher chain grade it is likely that the optimizer will further decrease the chain diameter until the lower limit for which it can not satisfy the displacement constraints anymore. Reducing the total mooring line weight and increasing the line line length, while keeping the polyester length similar, reduces the stiffness of the system. The surge and pitch positions in ULS condition are given in Figure 36.

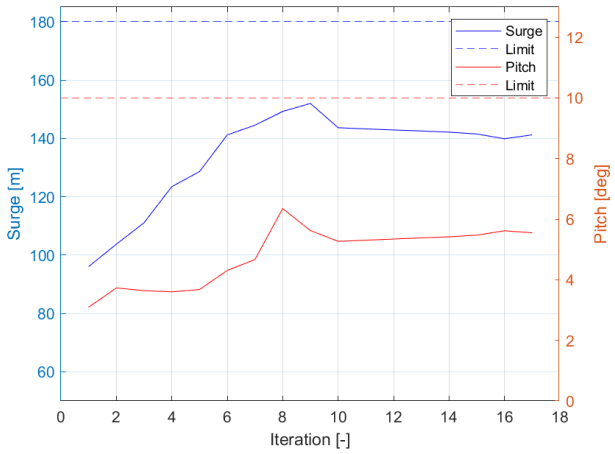

Figure 36: Surge and pitch positions for ULS condition

The pretension in the no environmental loading simulation, slack and position of the last element of the polyester segment in both simulations for line 2 and 3 are approximately equal. Because of the similarity in mooring line composition, for line 2 and 3, and the applied loading direction it is assumed that the corresponding constraints only have to be applied on one line. Besides that, the mooring lines are mirrored with respect to the X-axis so the loading will be distributed equally among these two lines. The required optimization time can therefore be reduced by removing the corresponding constraints of one line, resulting in 18 constraints in total.

Design 3

Design 3 is the result of a new optimization using the same assumption of 20% and the same starting design, defined by Table 16, however the number of constraints has been reduced to 18. This results in the design defined by Table 34. The corresponding percentages of standard deviation over mean tension are given in Table 35.

Table 34: Design 3

Design variables	Value
Length of top chain segment	54.90
Diameter of top chain segment	0.0845
Length of polyester segment	217.14
Diameter of polyester segment	0.1475
Length of bottom chain segment	1409.5
Diameter of bottom chain segment	0.0837
Anchor radius	1441.6
Semi-submersible mass	1.1872e7 [kg]

Table 35: Percentage of standard deviation over mean tension (design 3)

Segment	[%]
Fairlead	16.85
Polyester	14.96
Bottom chain	15.02
Anchor	16.64

The values of the design variables in design 3, in Table 34, are different than design 2, in Table 32. This suggests that the designs obtained may be a local minimum.

The obtained design does satisfy the standard deviation assumption, but the percentages in Table 35 have significantly changed with the percentage of design 2 in Table 33. This enforces the finding that the standard deviation relation is design dependent.

The changes with respect to design 2 are given in Table 36.

Table 36: Change in design variables of design 3 with respect to design 2

Design variables	[%]
Length of top chain segment	174.5
Diameter of top chain segment	-1.17
Length of polyester segment	24.05
Diameter of polyester segment	-1.34
Length of bottom chain segment	-3.53
Diameter of bottom chain segment	-1.53
Anchor radius	2.19

The most significant change occurs for the top chain length and the polyester segment. The path of the optimizer for these variables is given in Figure 37. The diameters of the mooring line segments are similar.

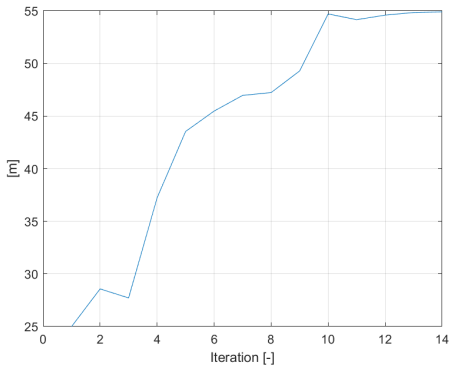

(a) Chain top length

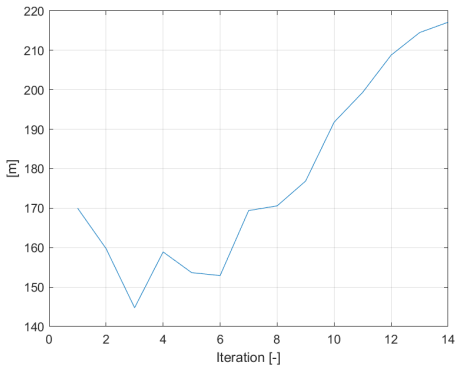

(b) Polyester length

Figure 37: Path of optimizer for design variables (design 3)

The paths are different than for design 2. The sum of constraint violations for design 2 is equal to 4.711 in iteration 0 and equal to 3.718 for design 3. The KKT optimality condition, the norm of the Lagrangian gradient and the BFGS quasi-Newton update parameter are equal for both designs during iteration 0. As stated by Schittkowski 2011, the merit function may become irregular when steep slopes occur in the gradients. The combination of Equation 70 with the parameters above leads to a slightly different sufficient decrease reference value for both designs. Using Equation 69 with a different reference value leads to a different step size α, and consequently a different path. The KKT, norm of Lagrangian gradient and the BFGS quasi-Newton update parameters are different for design 3 and design 2 in the next iteration as different designs are obtained from the same initial design.

Even though, it was expected that the algorithm would convergence to the same mooring system design. This does indicate that the obtained design is a local minimum. Additionally, the assumption that the number of similar constraints can be reduced to obtain the same design does not hold for this optimization problem.

4.2 Design analysis

4.2.1 Cost

The cost of the obtained design is defined as the objective function, the mooring system material costs, and the cost of performing the optimization in terms of required simulation time.

Mooring system material cost

The material cost comparison between the starting mooring system, design 0, and the obtained optimized mooring system, defined by Table 32, is given in Table 37.

Design 2

Table 37: Mooring system material cost results (design 2)

	Mooring lines	Anchors	Total	Reduction
Design 0 [EUR]	2.86e6	6.85e5	3.55e6	
Design 2 [EUR]	1.28e6	5.78e5	1.86e6	48%

The cost reduction is mainly achieved in terms of mooring line material cost. The reduction in anchor material cost is only 15.6%. The cost comparison for design 3, the optimization with 18 constraints, is given in Table 38.

Design 3

Table 38: Mooring system material cost results (design 3)

	Mooring lines	Anchors	Total	Reduction
Design 0 [EUR]	2.86e6	6.85e5	3.55e6	
Design 3 [EUR]	1.23e6	5.88e5	1.82e6	49%

The total cost reduction is 49%, the material cost reduction is 57% and the anchor cost reduction is 14.2%. The cost of design 3 is 2.2% less than design 2. The convergence of the algorithm can be improved by implementing a smaller stopping tolerance and increasing the desired final accuracy. However, this will increase the required optimization time and a smaller stopping tolerance may cause termination round-off errors (Schittkowski 2011).

Optimization cost

The optimization for design 2 required 17 iterations and took 11 hours and 58 minutes in total to complete. On average, one iteration of the workflow, given in Figure 28 with 23 constraints, takes 42 minutes. The approximate simulation time of the separate modules within the workflow is given below.

- Static analysis with fixed turbine: 60 seconds
- Static analysis ULS condition: 510 seconds
- Static analysis no environment: 120 seconds
- Constraints, cost function, other adjustments and creating files: 210 seconds

This leads to a total simulation time of 15 minutes. It may vary based on the design and therefore on how quickly convergence is achieved in the static ULS simulation module. As the number of elements in the mooring line segments does not change across the designs it assumed that the simulation time for each design is similar. The approximate time required to compute gradients is therefore 27 minutes.

The optimization of design 3, with 18 constraints, required 14 iterations and took 8 hours and 12 minutes in total to complete. The corresponding time per iteration is 35 minutes. Additionally, the time required to compute the constraints, cost function and other adjustments is reduced to 140 seconds. This results in 14 minutes to perform the simulations and 21 minutes to compute the gradients. This shows that the required optimization time is governed by the computation of gradients of the objective function and the constraints with respect to the design variables. Each removed constraint reduces the number of gradients to compute by 7.

If the optimization based on the ULS condition was performed using a 1 hour dynamic TD analysis, the simulation of this module would take approximately 40 minutes with the time step parameters from Table 61. This would increase the simulation time of the ULS condition by more than a factor 4. Assuming the time to compute gradients is similar, the total simulation time per iteration would be approximately 74 minutes, for 23 constraints. The full dynamic optimization would then take around 21 hours.

Review cost analysis

The two obtained designs show potential in material cost reduction with respect to the initial mooring system design and simulation time reduction with respect to a full dynamic optimization. Additional optimizations need to be performed to confirm if the achieved designs are local minimums by using different starting mooring system designs and different step sizes. Additionally, the current optimizations need to be reassessed using a smaller stopping tolerance and termination accuracy to determine if the same designs are obtained. Once that has been done a statement can be made on the required constraints. However, for the purpose of this thesis the obtained design is assessed on its dynamics and fatigue damage accumulation before assessing the convergence.

4.2.2 Decay tests

Decay tests for all degrees of freedom for design 2 and design 0 were performed using the parameters in Table 28. The time series of the decay tests are shown in Figure 38. It is interesting to note that under a loading of only half the thrust force the displacement in sway is approximately 100 meter at its peak for design 2. The ULS

loading combination in sway direction with the current orientation of the system may cause a displacement larger than the allowed limit of 180 meter.

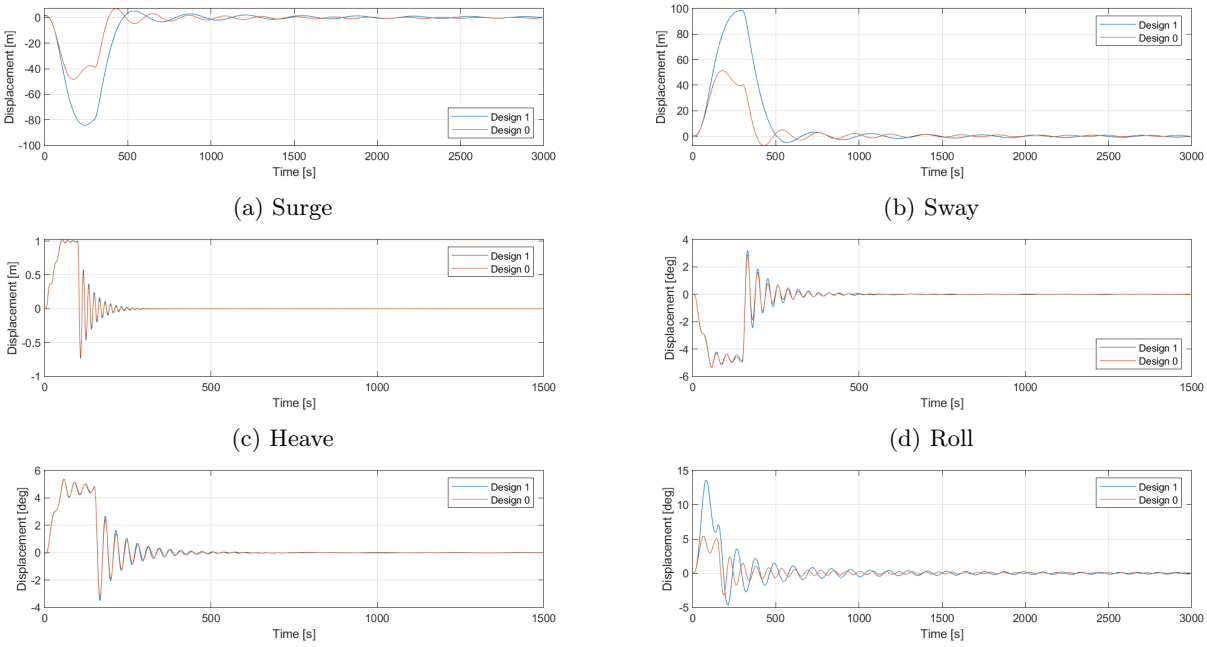

(a) Surge (b) Sway

(c) Heave (d) Roll

(e) Pitch (f) Yaw

Figure 38: Decay tests design 2 and design 0

The corresponding natural periods for each degree of freedom, for design 2, are given in Table 39. The corresponding natural periods for design 0 are given in Table 40.

Table 39: Natural periods (design 2)

	Surge	Sway	Heave	Roll	Pitch	Yaw
Natural period [s]	348	335	15.7	30.6	30.7	112

Table 40: Natural periods (design 0)

	Surge	Sway	Heave	Roll	Pitch	Yaw
Natural period [s]	220	208	15.6	30.5	31.0	78.3

A significant increase in surge, sway and yaw natural periods is experienced in comparison to the natural periods of the system at 150 meter depth, Table 11, for both designs. Additionally, these natural periods for design 2 have increased with respect to design 0, because of a decreased horizontal stiffness. Larger displacements are experienced for the same forcing. The natural periods in heave, pitch and roll are slightly different than the mooring system at 150 meter depth, Table 11. The uncoupled natural period in heave is calculated using Equation 100. The mass of the system has reduced in comparison to the mooring system at 150 meter depth because of the added mooring line weight, consequently reducing the natural heave period of the system as the water plane area has not changed.

$$T_{n3} = 2\pi\sqrt{(\frac{M + A_{33}}{\rho A_{wp}})} \tag{100}$$

The slight difference in heave and roll natural periods between design 2 and 0 is cause by an initial mismatch in the mass of the simplified model and the full model.

4.2.3 Fatigue Damage Accumulation

The accumulated fatigue damage for design 2 in 20 years at the top element of each segment, and at the anchor, is given in Table 41.

Table 41: Accumulated fatigue damage in 20 years (design 2)

	FLS damage
Fairlead	464.6
Polyester	160.5
Bottom chain	389.53
Anchor	167.0

The accumulated damage in all segments exceeds the limit of 1 and failure would occur within 1 year. Optimization of mooring line characteristics to minimize mooring line and anchor material costs solely based on the ULS condition does not account properly for fatigue accumulated damage. The ULS condition is not design driving in mooring system material cost optimization. Using a different chain grade will not affect the accumulated damage as the provided S-N curve by the DNV GL standards is independent of the chain grade.

The accumulated damage for each condition at the fairlead, the top of the polyester segment and the top of the bottom chain segment are given in Table 42. The anchor accumulated damage at the anchor is not provided as it the tension is consistently smaller than at the top of the bottom chain segment. Consequently, the accumulated damage will be smaller than the damage at the top of the bottom chain segment. The most severe condition is highlighted.

Table 42: 1 hour accumulated damage per condition (design 2)

Condition	Fairlead	Polyester	Bottom chain
1	8.216e-6	1.709e-13	7.982e-6
2	8.158e-6	1.153e-13	7.829e-6
3	1.020e-5	2.316e-13	9.638e-6
4	4.748e-5	1.214e-9	4.709e-5
5	4.678e-5	1.004e-9	4.559e-5
6	5.887e-5	2.799e-9	5.684e-5
7	8.556e-5	2.170e-10	8.290e-5
8	1.026e-4	2.997e-10	9.665e-5
9	1.620e-4	2.387e-9	1.499e-4
10	1.296e-4	6.941e-11	1.172e-4
11	1.778e-4	1.642e-10	1.524e-4
12	2.303e-4	4.039e-9	2.059e-4
13	1.844e-4	1.351e-11	1.504e-4
14	4.910e-4	2.326e-8	3.921e-4
15	4.909e-4	6.393e-8	4.247e-4
16	2.162e-3	1.776e-5	1.585e-3
17	2.093e-3	9.469e-6	1.741e-3
18	2.530e-3	5.195e-5	2.160e-3
19	7.179e-3	1.020e-3	4.965e-3
20	**7.446e-3**	1.587e-3	5.903e-3
21	7.129e-3	**3.481e-3**	**5.959e-3**

Fatigue analysis or a fatigue damage accumulation constraint is required to optimize the mooring system using static analysis. The fatigue damage can be assessed through a time consuming full dynamic TD simulation for each condition, or in a FD estimation model. Fatigue damage estimation in the FD is selected as it fits within the aim of this thesis to optimize based on static analysis while reducing simulation time and cost.

Assuming that the mooring line fatigue damage accumulation is governed by surge motion, a one degree of freedom fatigue damage estimation model is created and assessed. It is expected that the calculations in the estimation model result in similar values for the simulated 20 year accumulated fatigue damage.

4.2.4 Fatigue Damage Estimation Model

The fatigue damage estimation model is based on the assumption that the mooring line tension is governed by surge motion. In addition, it is assumed that the motion and loads induced by wind and waves can be separated in frequency. The performance of the model is assessed across two mooring system designs. The designs are defined below.

- Design 2: 20% assumption optimized design, defined by Table 32
- Design 0: starting design of optimization, defined by Table 16

The procedure outlined is applied for all 21 conditions from the reference data set in Table 9. A 1 hour long mooring line tension time series, corresponding to the previously simulated fatigue analysis, is generated at the desired elements. The same wind and wave spectra are applied in combination with the dynamic properties of the design. The equation of motion in the FD is given in Equation 101.

$$-\omega^2(M+A)\tilde{x}e^{i\omega t} + B\tilde{x}i\omega e^{i\omega t} + K\tilde{x}e^{i\omega t} = Fe^{i\omega t} \tag{101}$$

Waves

The cyclic loading F caused by the wave environment is a function of the first order wave forces transfer function. The transfer function was determined using WAMIT during the WINDMOOR project. It is is a function of the peak period and the significant wave height. The time series of a first order wave force is obtained by multiplying the transfer function with the linear wave profile $\zeta(\omega)$. The surge motion in a single degree of freedom system is then obtained by solving Equation 101.

$$x(\omega) = \frac{H_\zeta(\omega)\cdot\zeta(\omega)}{[-\omega^2(M+A(\omega)) + (B+B(\omega))i\omega + K]} \tag{102}$$

The frequency dependent added mass and damping are determined through interpolation between data from WAMIT and the excitation frequency vector, visualized in Figure 39b and Figure 39a respectively. The lower limit or upper limit is applied when the value of the excitation frequency is outside of the available data range.

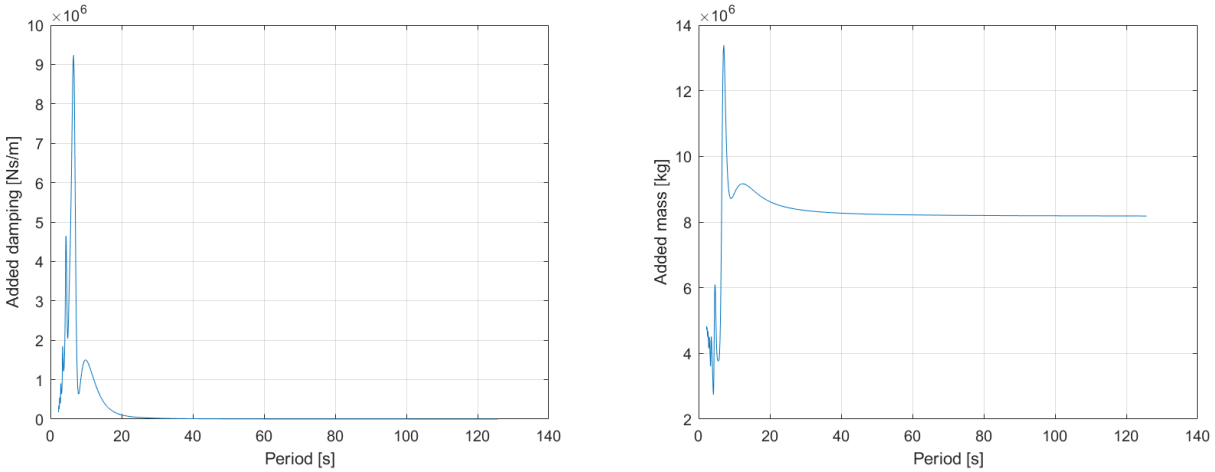

(a) Added damping

(b) Added mass

Figure 39: Added coefficients in surge

The required linear, b_1, and linearized quadratic damping, b_2, coefficients of the system are obtained through the decay test analysis. The procedure outlined applied, and outlined in *Estimation of linear and quadratic roll damping from free-decay tests* (Hoff 2001), is based on potential energy. The potential energy at a peak is defined by Equation 103.

$$V = \frac{1}{2}\omega_0^2\phi(t_n)^2 \tag{103}$$

Here, ω_0 is the natural period in radians per second, determined in the free decay tests and $\phi(t_n)$ is the time dependent amplitude at the peaks, which occur at time t_n. The data points, on a log-linear plot, are used to estimate the decay in potential energy by fitting a piecewise cubic polynomial. A non dimensional loss function $Q(V)$ is introduced and estimated using Equation 104.

$$Q(V) = b_1^* A(V) + b_2^* D(V) \tag{104}$$

The damping coefficients are found by minimizing the error between the data points and the estimate $Q(V)$, resulting in the set of equations given below (Hoff 2001).

$$\begin{aligned} b_1 &= 2\omega_0 b_1^* \\ b_2 &= 2b_2^* \end{aligned} \tag{105}$$

Where:

$$\begin{aligned} b_1^* &= \frac{\sum D(V)^2 \sum A(V)Q(V) - \sum A(V)D(V) \sum D(V)Q(V)}{\sum A(V)^2 \sum D(V)^2 - (\sum A(V)D(V))^2} \\ b_2^* &= \frac{\sum A(V)^2 \sum D(V)Q(V) - \sum A(V)D(V) \sum A(V)Q(V)}{\sum A(V)^2 \sum D(V)^2 - (\sum A(V)D(V))^2} \\ A(V) &= 1 \\ D(V) &= \frac{\sqrt{V}B(V)}{\omega_0} \\ B(V) &= \frac{8\sqrt{2}}{3\pi} \\ Q(V) &= \frac{L(V)}{2\omega_0 V} \\ L(V) &= -\frac{dV}{dt} \end{aligned} \tag{106}$$

The surge stiffness K is estimated in the static ULS simulation. The tension at the fairlead in the static ULS configuration, the pretension and the displacement are used to calculate the stiffness according to Equation 107.

$$K_{line} = \frac{T_{ULS} - T_{pretension}}{\Delta X} \tag{107}$$

This is a linear assumption as only one stiffness value is obtained. The mooring system provides a nonlinear, displacement dependent stiffness in reality. Additionally, the nonlinear material properties of the polyester segment are not captured. The stiffness profile can be obtained through a dynamic simulation at different wind speeds and environmental states.

The surge motion is obtained by multiplying the surge motion transfer function with the wave profile $\zeta(\omega)$. The surge motion spectrum is then obtained using Equation 108, in which $S_\zeta(\omega)$ represents the wave spectrum.

$$S_{x,waves}(\omega) = |\frac{H_\zeta(\omega)}{(-\omega^2(M + A(\omega)) + (B + B(\omega))i\omega + K)}|^2 \cdot S_\zeta(\omega) \tag{108}$$

According to the same procedure, the line tension is obtained by multiplying the surge motion with the mooring line stiffness squared, given in Equation 118. The stiffness in the line segments is determined using the same linear assumption as before, the pretension, the tension in the element in ULS condition and the surge displacement of the system.

$$S_{Fwa,lines}(\omega) = |K_{line}|^2 \cdot S_{x,waves}(\omega) \tag{109}$$

Wind

The same procedure is applied for wind using a unit thrust force instead of the wave force transfer function, and a thrust force spectrum instead of the wave spectrum. The thrust force spectrum is obtained through a dynamic simulation using turbulent wind. A power spectral density function is generated to determine the frequency dependent thrust force based on the thrust force time series. The thrust force spectrum is system dependent and determined using a fixed wind turbine simulation. It only has to be performed once for every mean wind speed. The thrust force spectrum is estimated using a Discrete Fast Fourier Transform (DFFT) of the thrust force time series.

- Convert thrust force time series of length N into DFFT, x_{DFFT}, of length $N-1$
- Generate corresponding frequency vector f, with step df based on time series and time step dt using Equation 110

$$f = [df : N-1]/(N-1) * (1/dt) \tag{110}$$

- Calculate estimated PSD using frequency sampling rate fs and Equation 111

$$\begin{aligned} fs &= \frac{1}{dt} \\ S_{PSD} &= \frac{1}{fs(N-1)} \\ S_{thrust}(f) &= S_{PSD} \cdot |x_{DFFT}|^2 \end{aligned} \tag{111}$$

Here, S_{PSD} is a scaling factor that is required to ensure that the square root of the zeroth order moment is equal to the standard deviation of the fixed turbine thrust force time series. The applied ratio is valid for each wind speed. The spectrum is converted into angular frequency by multiplying the frequency vector and dividing the power vector by 2π.

The surge motion induced by thrust force is determined using Equation 112.

$$S_{x,wind}(\omega) = |\frac{1}{abs(-\omega^2(M+A(\omega)) + (B+B(\omega))i\omega + K)}|^2 \cdot S_{thrust}(\omega) \tag{112}$$

The mooring line tension caused by the wind induced surge motion is obtained using Equation 113.

$$S_{Fwi,lines} = |K_{line}|^2 \cdot S_{x,wind}(\omega) \tag{113}$$

The combined mooring line tension for each segment caused by surge motion is then obtained using Equation 114, based on the assumption of separation in frequency. At each time point a value of the mooring line tension is generated for each frequency with a specific random phase ϵ_j. The random phase is equal for each segment. To create the irregular tension time series, the summation in Equation 115 is used.

$$S_{F,line} = S_{Fwi,line} + S_{Fwa,line} \tag{114}$$

$$F(t) = \sum_{j=1}^{N} \sqrt{S_{F,line}(\omega_j)\Delta\omega 2} \cdot \sin(\omega_j t + \epsilon_j) \tag{115}$$

Here, $\Delta\omega$ is the frequency step between two succeeding frequencies in the excitation frequency vector. The same algorithm for cycle counting and damage calculation is used in the estimation model.

The linear and linearized quadratic damping coefficients for design 2 and design 0 are given in Table 43. The linear damping coefficient is applied in the fatigue damage estimation model.

Table 43: Linear and linearized quadratic damping coefficients

	b1 [kg/s]	b2 [kg/s]
Design 0	5.62e4	5.89e4
Design 2	8.43e4	1.55e4

Results and analysis

The 20 year accumulated damage from simulations and estimation for design 2 and design 0, in the 4 segments, are given in Table 44a and Table 44b, respectively. The accumulated damage for both designs for each condition, simulated and the estimated, and all segments are provided in the Appendix (8.5).

Table 44: Fatigue damage estimation assessment

(a) Design 2

Element	Simulated	Estimated
Fairlead	464.6	64.39
Polyester	160.5	0.057
Bottom chain	389.5	66.18
Anchor	167.0	57.67

(b) Design 0

Element	Simulated	Estimated
Fairlead	16.16	3.705
Polyester	147.7	0.069
Bottom chain	13.47	3.823
Anchor	2.439	2.987

It was expected that the estimation model would calculate similar values for the 20 year accumulated fatigue damage. However, the data in Table 44 shows that the values of simulated and estimated damage in the 4 segments for both designs do not match. The level of underestimation differs for the segments and the designs. The accumulated damgage at the anchor is reasonably estimated for design 0, while underestimated by a factor 2.9 in design 2. Fatigue estimation using the created estimation model based on surge motion only does not estimate the accumulated damage correctly. The most significant underestimation occurs for the polyester segment. The largest difference for both designs occurs in conditions with long wave periods, condition 21 for example. Therefore the performance of the estimation model for this condition is investigated in order to provide feedback for adjustments.

Condition 21 - design 2

Condition 21 is defined by Table 45.

Table 45: Condition 21

Mean wind speed [m/s]	25
Peak period [s]	14
Significant wave height [m]	8.31

The simulated damage, the estimated damage and the factor difference in the elements for condition 21 are given in Table 46.

Table 46: Comparison condition 21 (design 2)

Element	Simulated (S)	Estimated (E)	Factor (S/E)
Fairlead	0.0071	3.830e-6	1.85e3
Polyester	0.0035	3.371e-15	1.04e12
Bottom chain	0.0060	3.953e-6	1.52e3

The factors of $1.85e3$ and $1.04e12$ in Table 46 indicate that the largest difference occurs for the fairlead and the polyester segment respectively. Therefore the estimated and simulated mooring line tension time series at the fairlead and polyester segment are given in Figure 40.

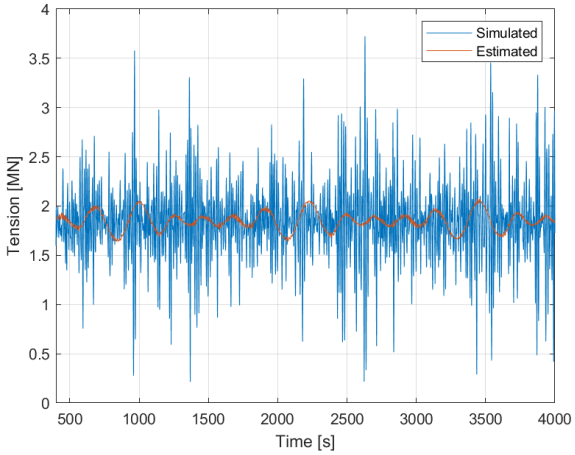

(a) Fairlead

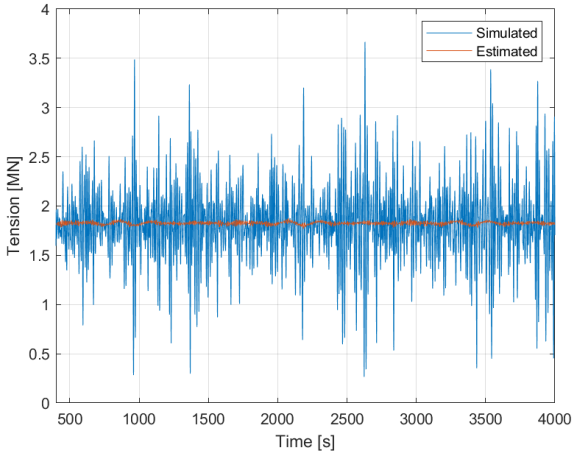

(b) Polyester

Figure 40: Mooring line tension time series condition 21 (design 2)

The estimated tension time series does not capture the high frequency oscillations in mooring line tension. The oscillations in mooring line tension in all segments seems to be in phase with heave and pitch motion. Therefore the tension time series on a smaller interval from 2000 to 2500 seconds are given in Figure 41.

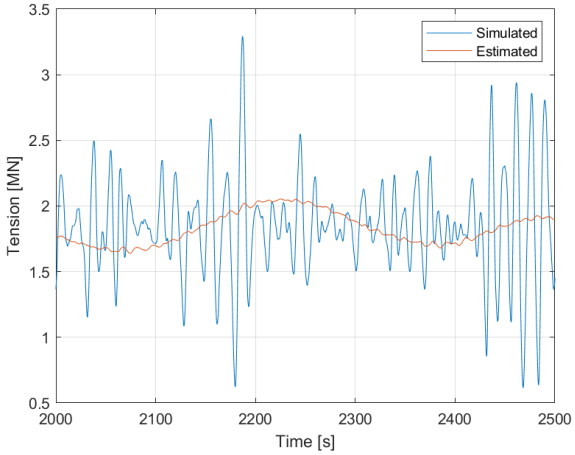

(a) Fairlead tension

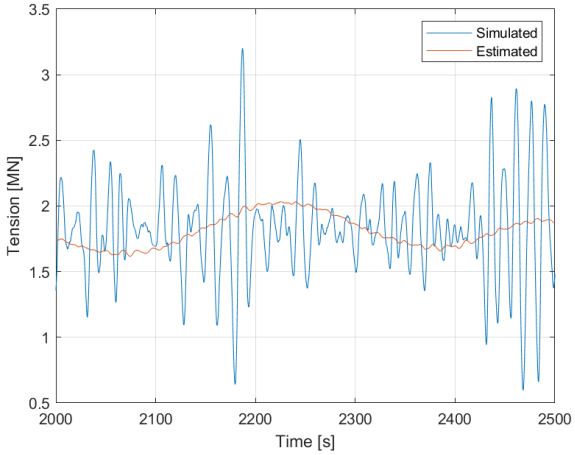

(b) Polyester tension

Figure 41: Reduced interval tension time series condition 21 (design 2)

The simulated mooring line tension in Figure 41a oscillates at an approximate period of 14 seconds, which is the wave excitation peak period. Snap loads seem to occur in both segments. To further investigate the relation between motion and tension, the surge, heave and pitch motion time series on this interval are given in Figure 42, Figure 43 and Figure 44 respectively. Additionally, the normalized and scaled tension at the fairlead and at the top of the polyester segment are provided with a normalized and scaled motion time series. Therefore, negative tensions are present in these figures but do not occur in reality.

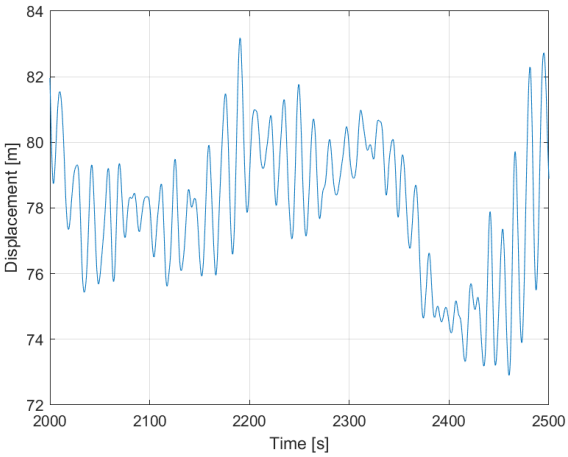

(a) Surge

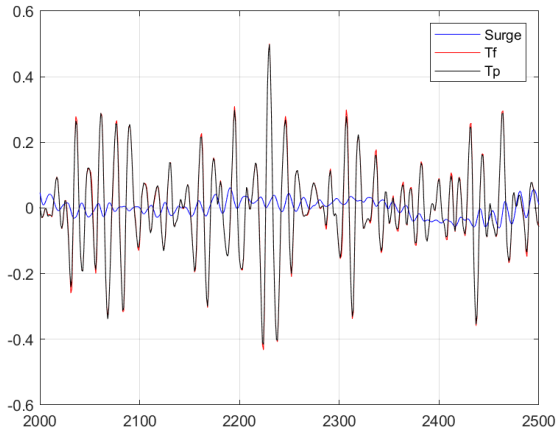

(b) Scaled tensions and surge motion

Figure 42: Surge motion and tension comparison condition 21 (design 2)

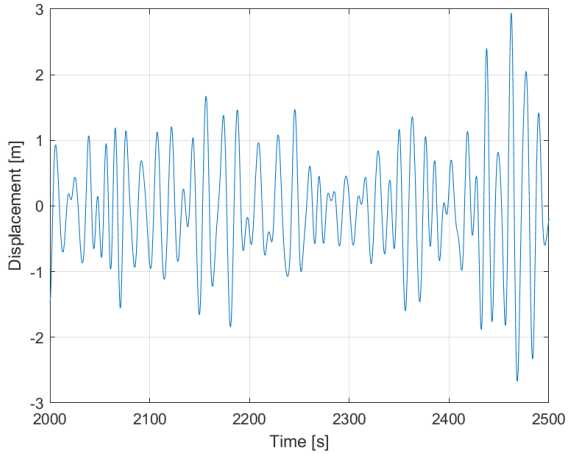

(a) Heave

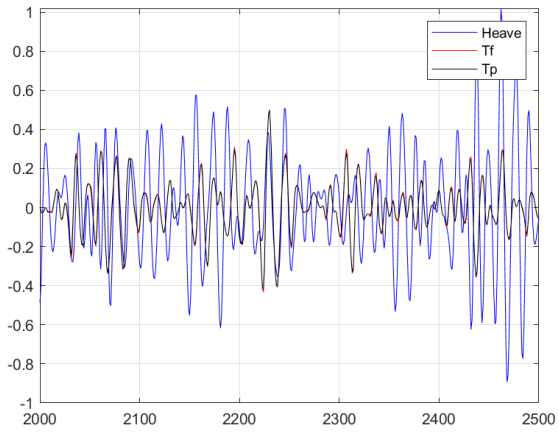

(b) Scaled tensions and heave motion

Figure 43: Heave motion and tension comparison condition 21 (design 2)

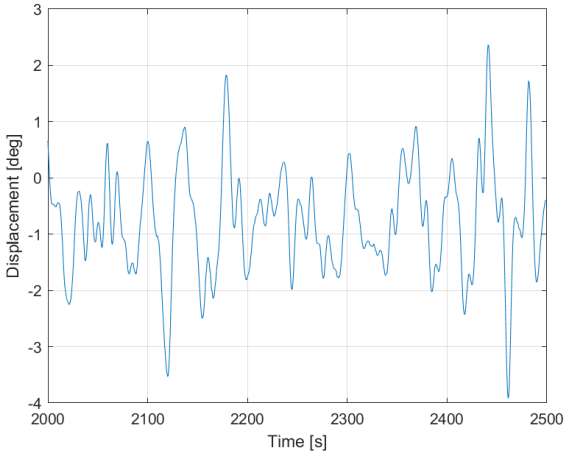

(a) Pitch

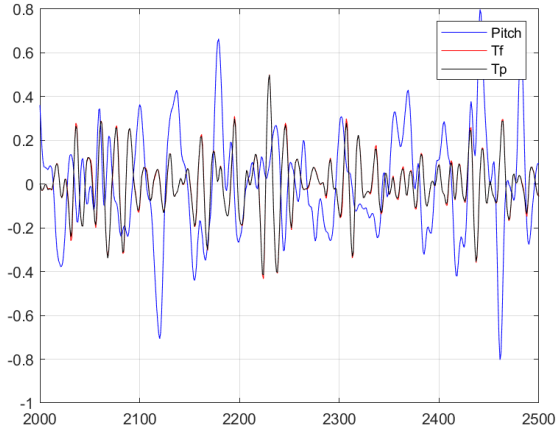

(b) Scaled tensions and pitch motion

Figure 44: Pitch motion and tension comparison condition 21 (design 2)

The qualitative relation between motion and tension is defined by the correlation coefficients between tension and motion, which are given in Table 47. A correlation coefficient of 1 corresponds to exactly in phase, a correlation coeffcient of -1 corresponds to exactly out of phase.

Table 47: Correlation coefficient tension and motion condition 21 (design 2)

	[-]
Surge	-0.15
Heave	0.72
Pitch	-0.40

Heave motion, having a correlation coefficient of 0.72, is most in phase with the mooring line tension in the segments for condition 21. Additionally, pitch has a more significant contribution to the mooring line tension than surge. As surge and pitch are coupled, a 2 degree of freedom estimation model of surge and pitch motion would be more accurate for the estimation of accumulated damage.

The estimated surge motion and the contributions of wind and wave induced surge motion are given in Figure 45.

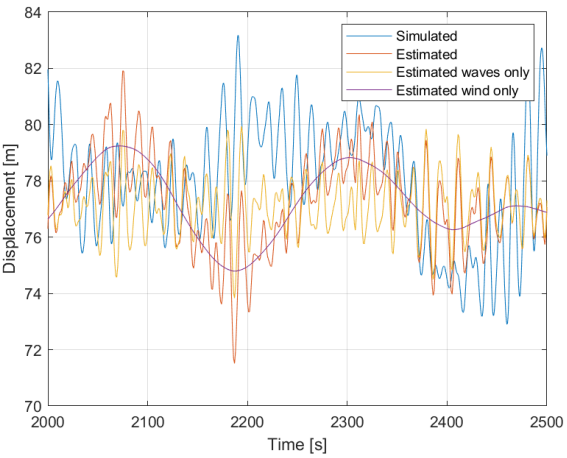

(a) Smaller interval

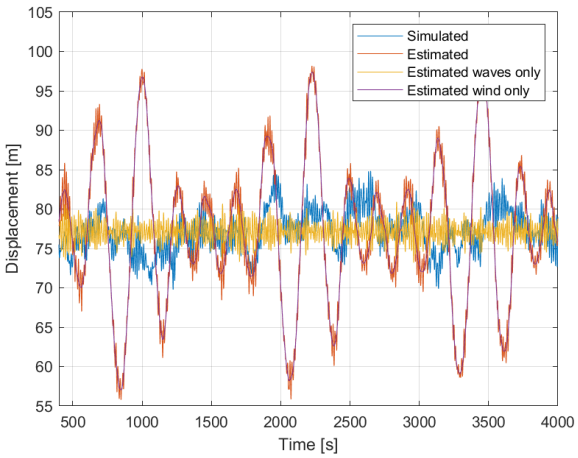

(b) Complete time series

Figure 45: Simulated and estimated surge motion condition 21 (design 2)

The amplitude of wind induced estimated surge motion is inaccurate with the simulated surge motion. The estimation model uses a single stiffness value and linearized damping coefficients. The thrust force spectrum

from the fixed wind turbine simulation does not capture the dynamic interaction between the nacelle and the thrust force. This interaction provides aerodynamic damping from the change in relative wind speed in combination with the characteristics of the controller (Carlos Eduardo S Souza, Hegseth, and E. E. Bachynski 2020). A larger damping value would reduce the amplitude of motion. This was also found in a difference between the standard deviation of thrust force of the fixed wind turbine simulation and the dynamic FLS simulations. For condition 21 the standard deviation of the thrust force of the fixed wind turbine is equal to 140 kN, while dynamic simulation had a standard deviation in thrust force of 170 kN. This connects to the interaction between the nacelle and the incoming wind speed. The relative wind speed leads to fluctuations in thrust force.

The oscillations in wave excited surge motion are captured accurately. The power spectral density functions for surge, heave and pitch including highlighted natural periods are given in Figure 46.

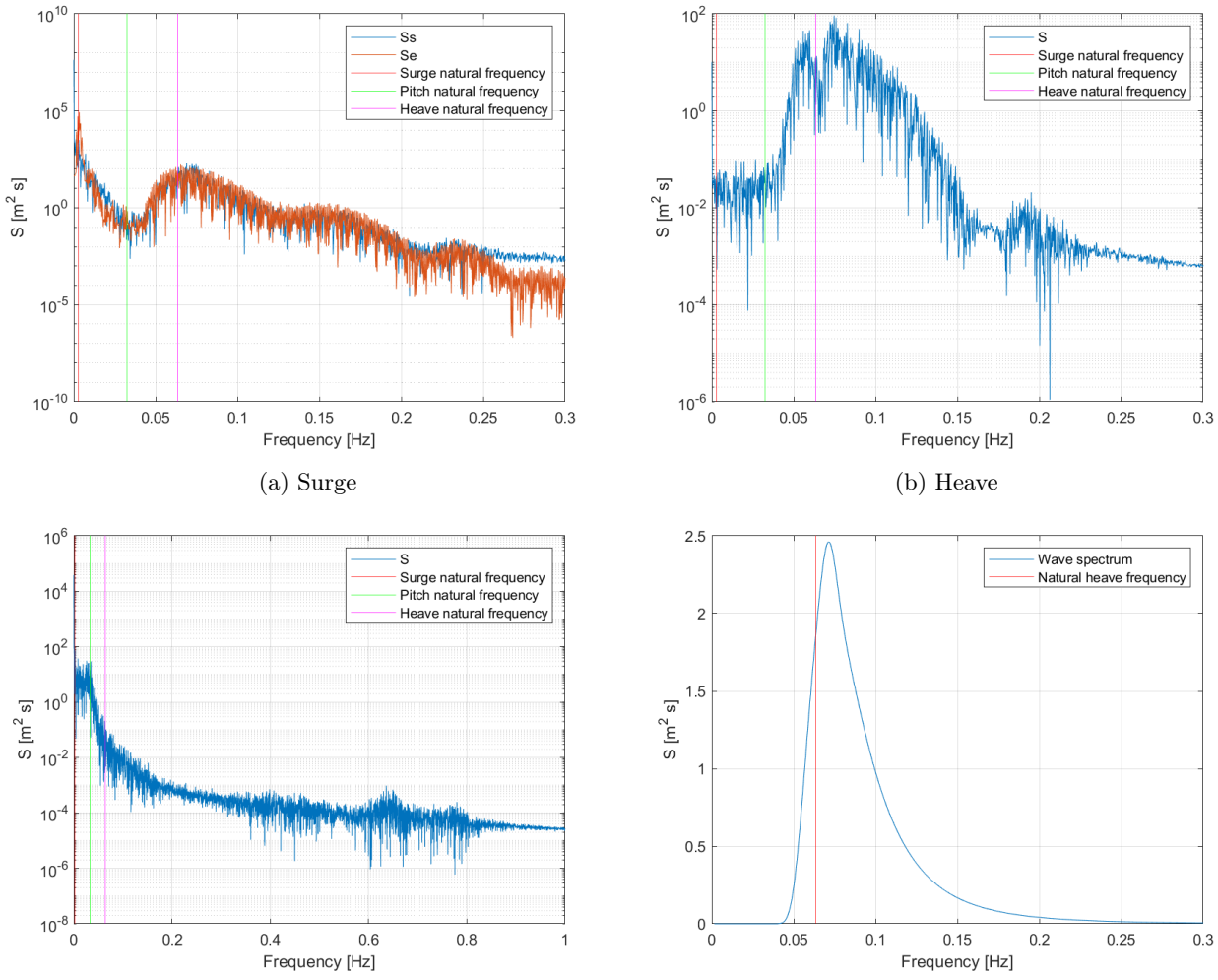

(a) Surge

(b) Heave

(c) Pitch

(d) Wave spectrum

Figure 46: PSD for motion surge, and pitch motion, and the wave spectrum condition 21 (design 2)

The plotted estimated surge motion PSD function Se in Figure 46a shows that the power as a function of excitation frequency is reasonable estimated when compared to the PSD of simulated motion. The power at high frequency oscillations is slightly underestimated and the power at low frequencies is slightly overestimated.

Additionally, heave motion at the fairlead is significantly excited around the natural heave frequency of the system. This is shown in Figure 46b where two peaks in power occur next to the natural heave frequency. Additionally, the JONSWAP wave spectrum in Figure 46d shows that the natural heave frequency is within the linear wave spectrum.

Condition 5 is most accurate in estimation of accumulated damage in the polyester segment, at the fairlead and at the bottom chain segment for design 2. The ratios of simulated damage over estimated damage are closest to 1. The simulated damage, the estimated damage and the factor difference in the elements for condition 5 are given in Table 48.

Table 48: Comparison condition 5 (design 2)

Element	Simulated (S)	Estimated (E)	Factor (S/E)
Fairlead	4.678e-5	4.635e-5	1.01
Polyester	1.004e-9	8.360e-10	1.20
Bottom chain	4.559e-5	4.775e-5	0.95

Condition 5 - design 2

Condition 5 is defined by Table 49.

Table 49: Condition 5

Mean wind speed [m/s]	7.1
Peak period [s]	8
Significant wave height [m]	1.67

The largest difference occurs for the polyester segment. Therefore the mooring line tension time series at the top of the polyester segment is given in Figure 47.

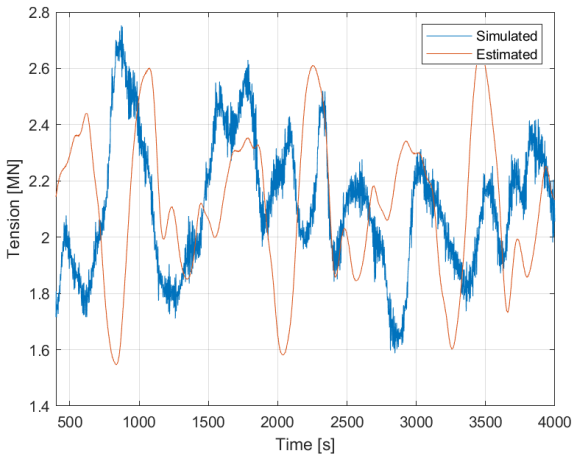

Figure 47: Mooring line tension time series condition 5 (design 2)

The estimated tension time series does not capture the high frequency oscillations in mooring line tension again, but there is a more accurate representation of the low frequency oscillations in tension. The comparisons of tension with respect to motion, on the shorter interval of 2000 to 2500 seconds are given in Figure 48, Figure 49 and Figure 50.

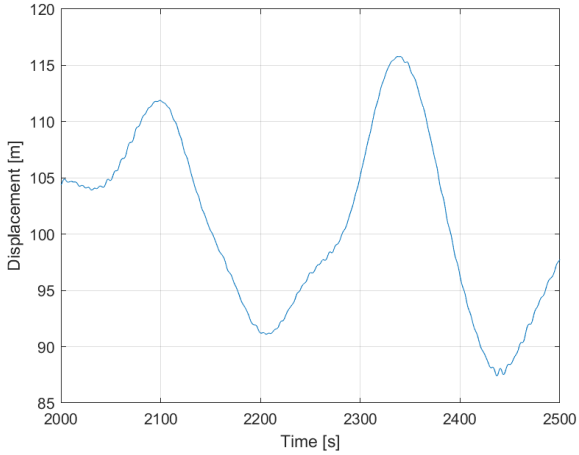

(a) Surge

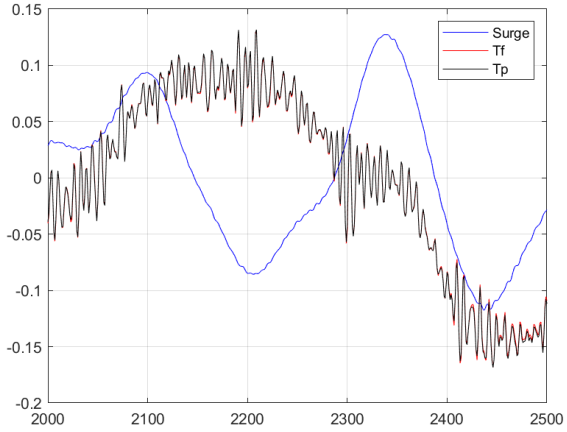

(b) Scaled tensions and surge motion

Figure 48: Surge motion and tension comparison condition 5 (design 2)

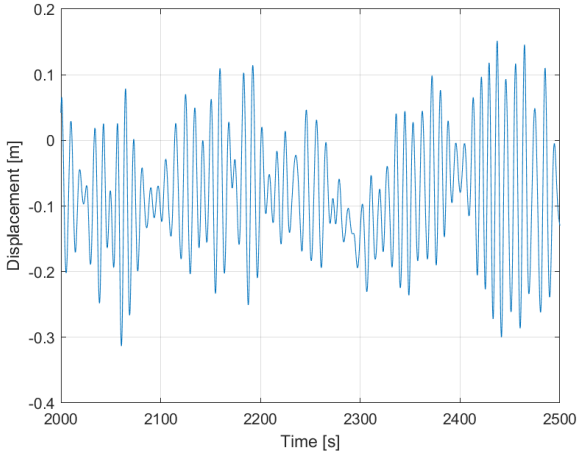

(a) Heave

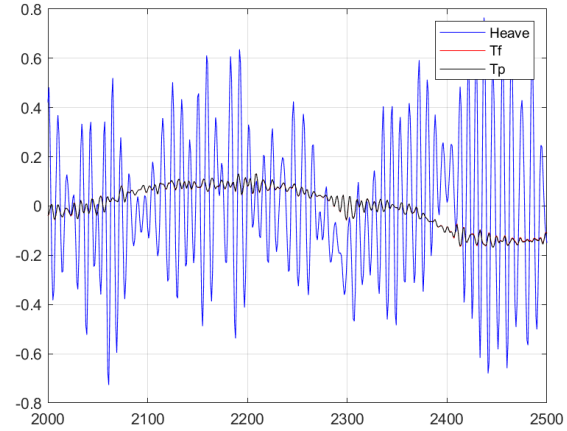

(b) Scaled tensions and heave motion

Figure 49: Heave motion and tension comparison condition 5 (design 2)

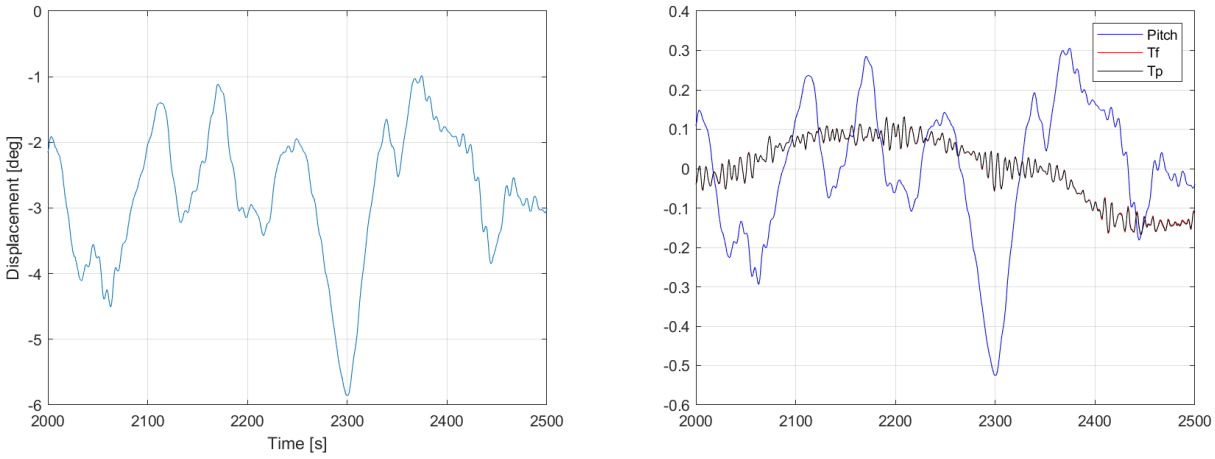

(a) Pitch

(b) Scaled tensions and pitch motion

Figure 50: Pitch motion and tension comparison condition 5 (design 2)

The corresponding correlation coefficients are given in Table 50.

Table 50: Correlation coefficient polyester tension and motion condition 5 (design 2)

	[-]
Surge	0.95
Heave	-0.26
Pitch	-0.76

The numbers in Table 50 indicate that the mooring line tension for this condition is governed by surge and pitch motion. Heave still affects the oscillations in mooring line tension, because of a 0.26 correlation coefficient, but to a much smaller extent than for condition 21. This is because the heave natural period of the system is not excited by the linear wave spectrum, as shown in Figure 51d.

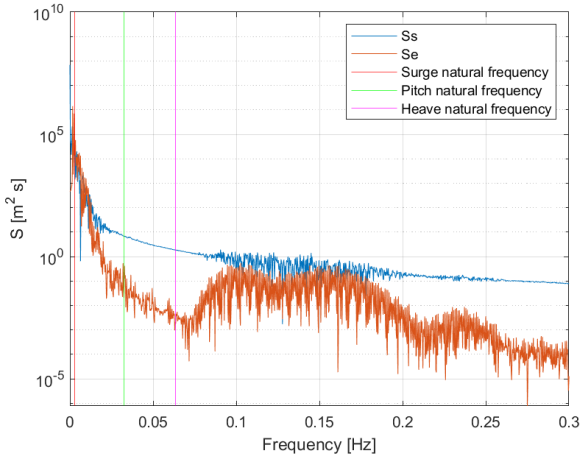

(a) Surge motion PSD

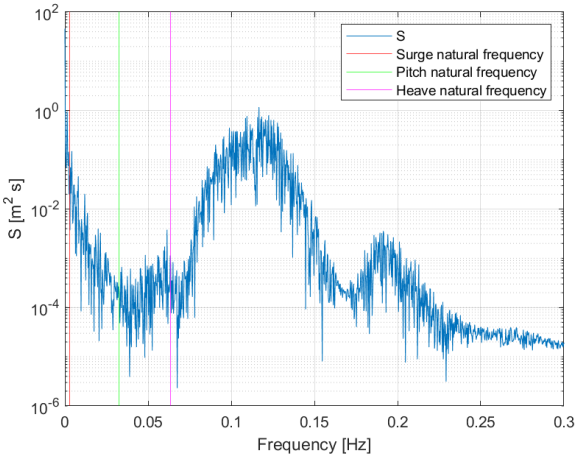

(b) Heave motion PSD

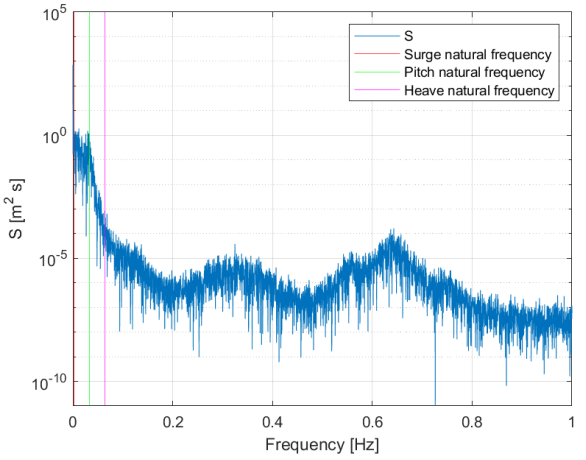

(c) Pitch motion PSD

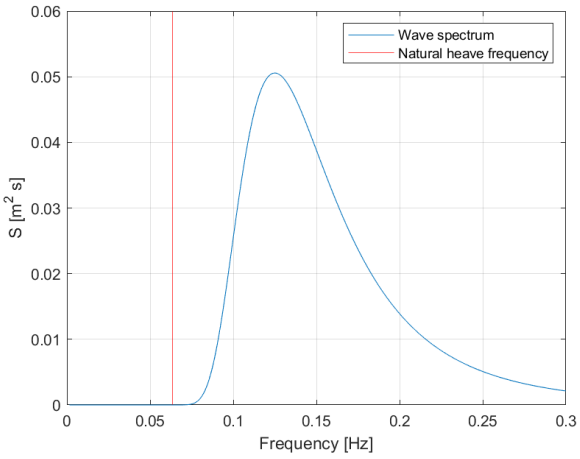

(d) Wave spectrum

Figure 51: PSD for motion surge, and pitch motion, and the wave spectrum condition 5 (design 2)

The estimated surge PSD shows that surge motion is underestimated for higher frequencies. The estimated surge motion is given in Figure 52.

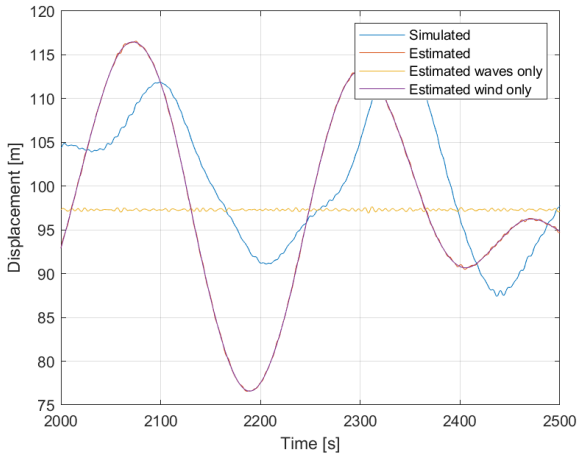

(a) Smaller interval

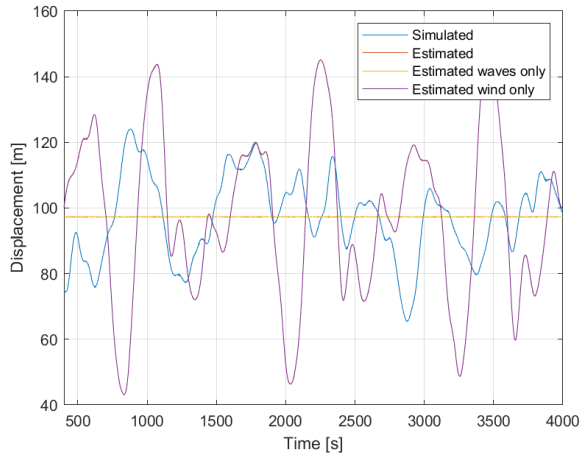

(b) Complete time series

Figure 52: Simulated and estimated surge motion condition 5 (design 2)

Here, the surge motion amplitude is more accurately estimated with the thrust force PSD function while the PSD function estimate is less accurate when compared to condition 21. This indicates that the aerodynamic damping is condition dependent. It is a function of the wind speed and the performance of the controller. Condition 21 has a mean wind speed at the cut out wind speed of the turbine. Therefore there will be a lot of active control to minimize the thrust force. This results in more aerodynamic damping due to the relative wind speed and changes in thrust force.

Condition 7 is highlighted additionally to investigate the influence of a condition with a short wave period on the damage accumulation in design 2 and 0. Condition 7 is defined by Table 51.

Table 51: Condition 7

Mean wind speed [m/s]	10.3
Peak period [s]	5
Significant wave height [m]	2.2

Condition 7 - design 2 and 0

The simulated and accumulated damage for both designs are given in Table 52.

Table 52: Damage estimation (condition 7)

(a) Design 2

Element	Simulated (S)	Estimated (E)	Factor (S/E)
Fairlead	8.556e-5	2.066e-4	0.41
Polyester	2.170e-10	7.823e-8	2.77e-3
Bottom chain	8.290e-5	2.119e-4	0.38

(b) Design 0

Element	Simulated (S)	Estimated (E)	Factor (S/E)
Fairlead	2.892e-6	1.512e-6	1.91
Polyester	4.978e-13	3.202e-12	0.16
Bottom chain	2.698e-6	1.559e-6	1.73

Overestimation of the damage accumulated in the chain segments occurs for design 2 while it is underestimated in design 0. The largest difference between estimation and simulation still occurs for the polyester segment. The polyester tension time series for both designs, simulated and estimated, are given in Figure 53.

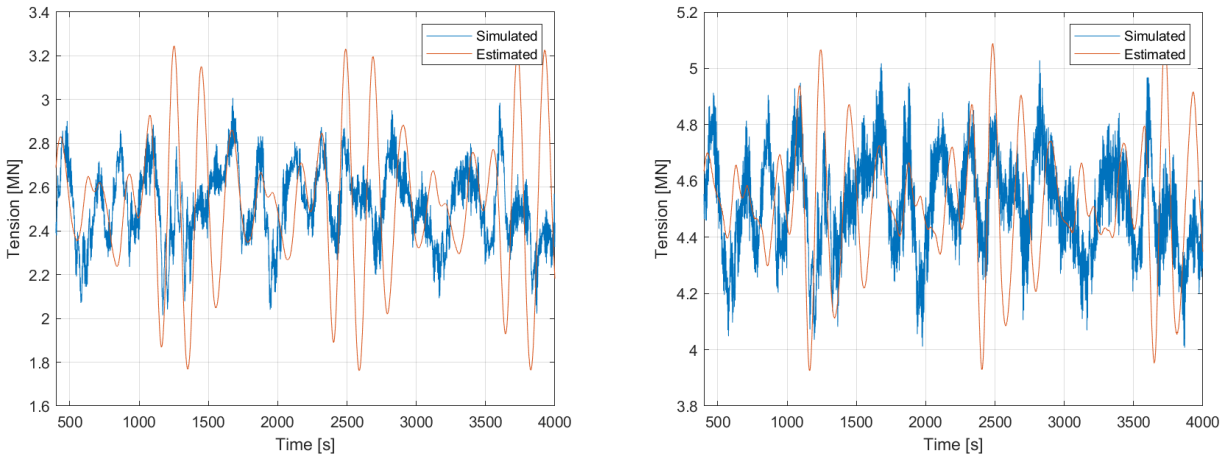

(a) Design 2

(b) Design 0

Figure 53: Reduced interval tension time series (condition 7)

The tension amplitude in both designs is slightly overestimated. As both designs do not capture the high

frequency oscillations in tension, the heave motion shown in Figure 54 must be added to the estimation model.

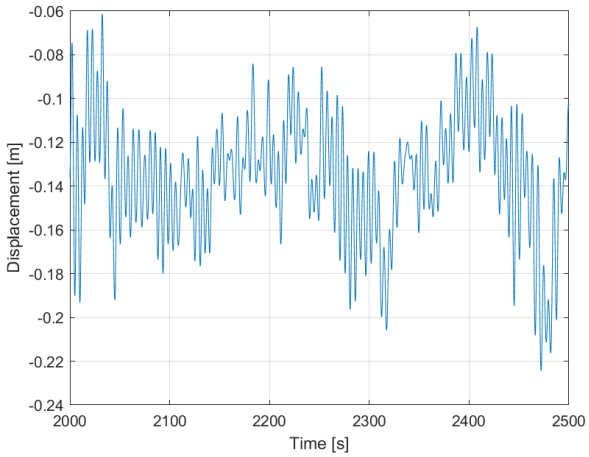

(a) Heave (design 2)

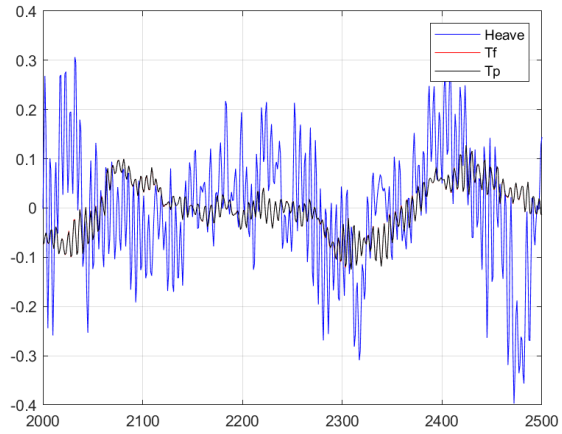

(b) Scaled tensions and heave motion (design 2)

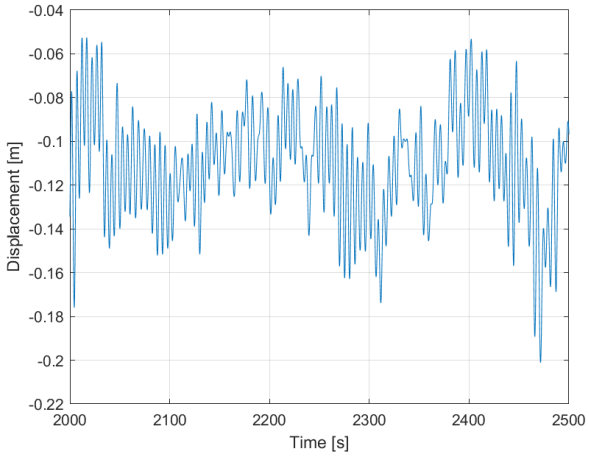

(c) Heave (design 0)

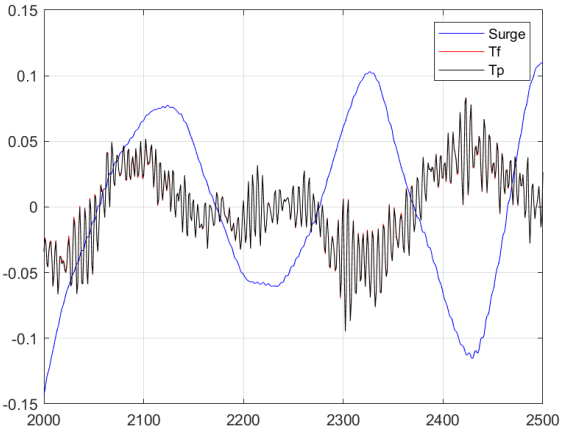

(d) Scaled tensions and heave motion (design 0)

Figure 54: Heave motion and tension comparison (condition 7)

The correlation coefficients for the degrees of freedom are given in Table 53.

(a) Design 2

	[-]
Surge	0.82
Heave	-0.56
Pitch	-0.38

(b) Design 0

	[-]
Surge	0.85
Heave	-0.52
Pitch	-0.28

Table 53: Correlation coefficients (condition 7)

These coefficients confirm that heave must be included. The estimated surge time series are shown in Figure 55.

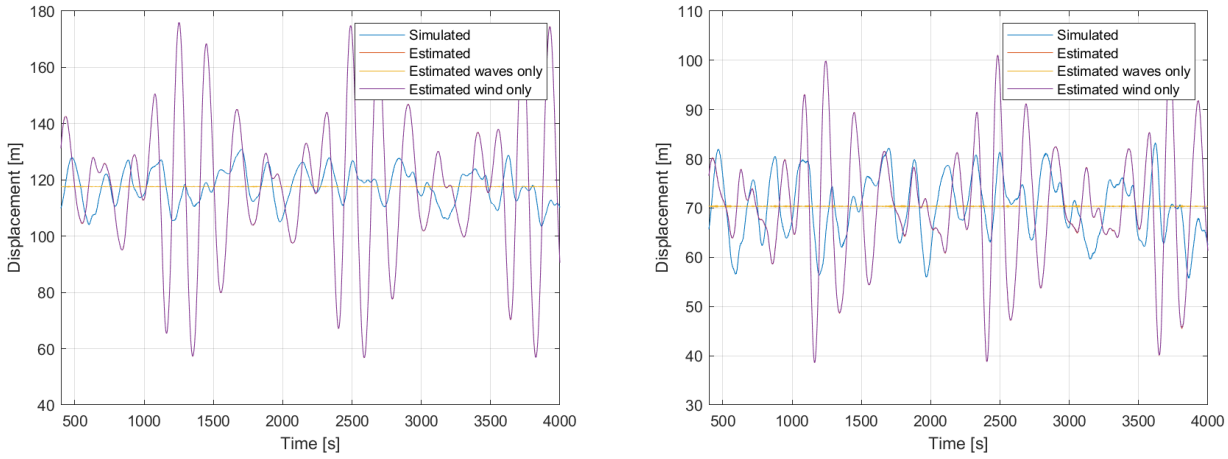

(a) Design 2 (b) Design 0

Figure 55: Simulated and estimated surge motion (condition 7)

The maximum amplitude of surge motion in the estimated time series in design 2 is overestimated by 30% and an by 22% in design 0. Even though the surge motion is overestimated greatly the accumulated damage is. This suggests that the accumulation of fatigue damage in the polyester segment is most severe for heave motion.

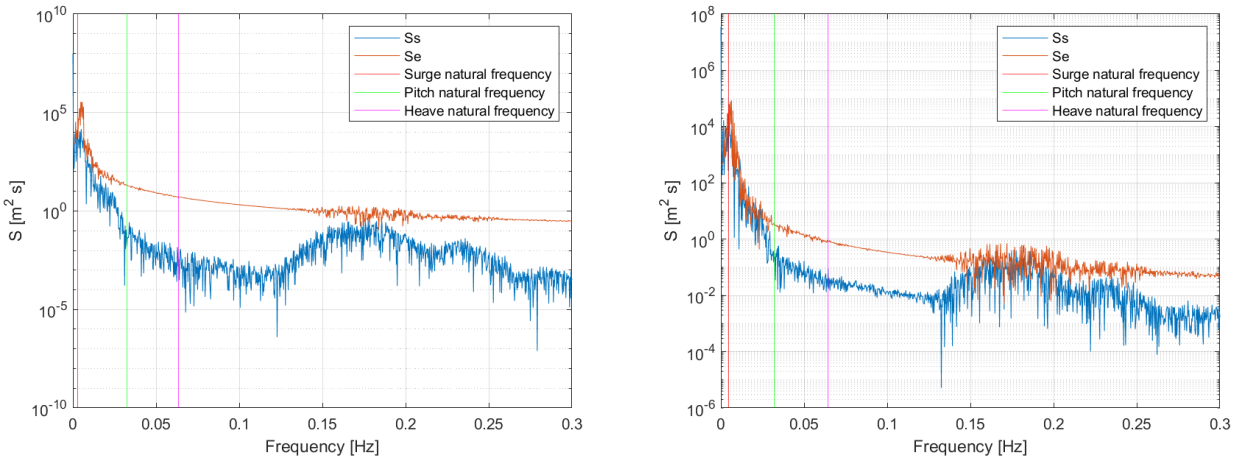

(a) Design 2 (b) Design 0

Figure 56: PSD for surge (condition 7)

The power spectral density functions of simulated and estimated surge motion of design 2 and 0 confirm that the most severe overestimation of the surge motion occurs in design 2 due to the larger difference between the curves.

Review of fatigue damage estimation model

Not including heave and pitch motion in the damage estimation model have been found as the main reasons for underestimation of accumulated damage. Additionally, there is an overestimation of wind induced surge motion due to not considering aerodynamic damping in the thrust force spectrum.

Power spectral density analysis of motion showed that heave motion is excited by the wave frequencies and that surge and pitch motion are mainly excited by low frequency forces. The single degree of freedom fatigue damage estimation model does not capture the corresponding high frequency oscillations in mooring line tension. Therefore, the wave induced heave motion and the wind induced pitch motion should be included in the fatigue damage estimation model. The longest wave periods ranging from 11 to 15 seconds will excite the natural heave period of the system. Therefore, the natural frequency in heave must be smaller than 0.04 Hz to

prevent resonance in heave for the applied condition set, as shown in Figure 57. This corresponds to a natural period in heave larger than 25 seconds. A larger natural heave period can be achieved by reducing the water plane area of the semi-submersible. This is required as the estimation model based a linear wave profile will not estimate the motion correctly at heave resonance. This is required to use the 12 MW WINDMOOR system for the condition set. Otherwise, a different condition set must be used for this system.

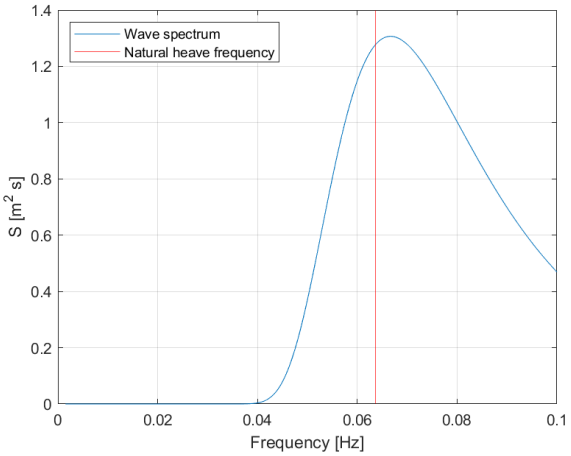

Figure 57: JONSWAP spectrum for peak period of 15 seconds

Additionally, the thrust force spectrum should be adjusted according to the procedure outlined by Carlos Eduardo S Souza, Hegseth, and E. E. Bachynski 2020 to include aerodynamic damping in the model and reduce the overestimation of surge motion.

Assuming that the heave motion is uncoupled from surge motion the mooring line tension spectrum should be improved by adding heave motion using the same method, outlined in Section 4.2.4. The first order wave force transfer function for heave from WAMIT and the equation of motion for heave should be used, given in Equation 116. The stiffness of the system in heave would be equal to the hydrostatic heave stiffness. The other characteristics of the system as a function of frequency are obtained through decay tests and WAMIT data.

$$S_{x3,waves}(\omega) = |\frac{H_{\zeta,x3}(\omega)}{abs(-\omega^2(M + A(\omega)) + (B + B(\omega))i\omega + K)}|^2 \cdot S_{\zeta}(\omega) \tag{116}$$

The estimated line stiffness in heave would be obtained by displacing the system and calculating the stiffness in each element according to Equation 117. This would require an additional simulation model in the workflow and increase the simulation time.

$$K_{line,x3} = \frac{T - T_{pretension}}{\Delta X} \tag{117}$$

$$S_{Fwa,lines,x3}(\omega) = |K_{line,x3}|^2 \cdot S_{x3,waves}(\omega) \tag{118}$$

Currently the stiffness of the system and the stiffness of the lines is recalculated for each condition. The method assumes linear behaviour. If the procedure is implemented in the current SIMA workflow the required stiffness values would be based on the ULS condition only which is in inaccurate representation of the dynamic mooring system and line stiffness. Additionally, the nonlinear properties of the polyester mooring line segment are not captured. The stiffness calculation method works reasonably well for the fairlead and the chain segments. Further improvements are expected when pitch and heave motion are included. However, the polyester segment line stiffness is inaccurate for conditions where heave motion is governing. The stiffness provided by the polyester segment is based on the elastic properties while the chain segments provide stiffness through their weight. The stiffness of the polyester mooring line segment should be a function of the change in tension, the elongation of the segment and the chain mooring line characteristics.

5 Shared Mooring Farm Concept

A completed shared mooring farm concept optimization has not been achieved. The corresponding designed mooring system did not withstand ULS loading condition. The tension in anchor mooring line 1 exceeds the MBL of the chain and polyester segments. Additionally, vertical forces would occur at the anchor. Upon the finding that the ULS condition is was not design driving, the focus has been directed towards the fatigue damage estimation model for the single turbine system. However, findings and analyses of the system are presented.

5.1 Static analysis results

The design implemented is defined by Table 54.

Table 54: Initial mooring design farm concept

Design variables	Value
Length of top chain segment	25
Diameter of top chain segment	0.08
Length of polyester segment	170
Diameter of polyester segment	0.19
Length of bottom chain segment	850
Diameter of bottom chain segment	0.08
Anchor radius	750
Turbine spacing	1520
Diameter of shared mooring line	0.072433

The relation between the shared mooring line diameter and the anchor line was obtained according to Equation 94. The vertical force at the anchor line fairlead of turbine 1 is equal to 0.79 MN and the vertical force from shared mooring line 1 is equal to 0.73 MN. This indicates that the relation is not exact as the angle at the fairlead changes with a change in shared mooring line weight. The static equilibrium with fixed turbines is shown in Figure 58.

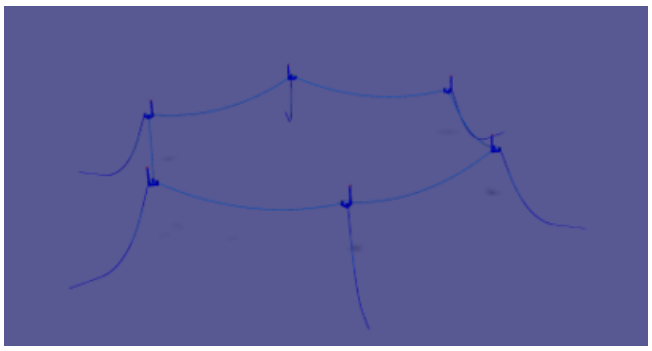

Figure 58: Static equilibrium of farm concept with fixed turbines

Figure 58 shows that the vertical tensions at the fairleads are not in equilibrium. The equilibrium shared mooring farm configuration, when the turbines are freed, is shown in Figure 59.

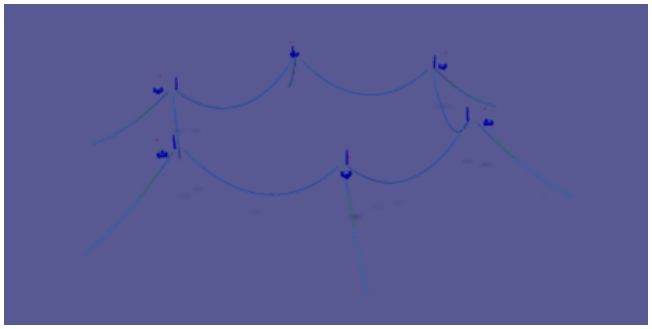

Figure 59: Static equilibrium without environment

The visualization in SIMA does not move the semi-submersibles, but the mooring lines and the tower positions show that the turbines are pulled inwards. This reduces the turbine spacing is to 1410 meters, a reduction of 7%. The vertical force from the anchor in this design configuration is 1.15 MN, the vertical force from the shared mooring lines is 0.73 MN. This is due to the increase in lifted anchor weight. Additionally, all anchors would experience vertical forces in this configuration.

The static pitch position of each turbine is given in Table 55. The turbines follow the same numbering as the anchor lines as shown in Figure 30. Positive pitch is defined according to the right handed coordinate system in Figure 22.

Table 55: Static positions farm concept

(a) Static pitch positions farm concept

Turbine	[deg]
1	3.94
2	0.09
3	2.81
4	1.23
5	2.81
6	0.09

(b) Static roll positions farm concept

Turbine	[deg]
1	0
2	-0.66
3	0.66
4	0
5	-0.66
6	0.66

In static equilibrium without environmental loading the turbines opposite of each other with respect to the X-axis are in phase. This indicates that the position of the turbine and orientation of the rotor, with respect to the anchor line, influences the static positions in pitch and roll.

5.2 Result analysis

5.2.1 Cost

Optimization cost

The approximate simulation times of the farm optimization modules are given below.

- Static analysis with fixed turbine: 250 seconds
- Static analysis ULS condition: 12250 seconds (FAILS)
- Static analysis no environment: 4000 seconds
- Constraints, cost function, other adjustments and creating files: -

The times for computation of constraints, cost function and the other adjustments can not be determined as the workflow has not been completed. Assuming the model is close to convergence in the static ULS condition analysis, the total simulation time for one iteration would 4.6 hours.

6 Conclusion

The single turbine mooring system has been optimized based on static time domain analysis in combination with the ULS condition to asses the potential mooring system material cost savings, in comparison to an optimized shared mooring concept, and to asses the hypothesis that the ULS condition is design driving. The optimization of a semi-taut mooring system in deep water led to a reduction of 48% in mooring system material cost. The cost reduction is driven by a reduction in weight per meter mooring line length, governed by the bottom chain segment. This is achieved by reducing the diameter of the mooring line segments. Additionally, the reduction in mooring line diameter is required to satisfy the tension related constraints of the mooring line segments. The pretension, minimum breaking load and anchor uplift constraints are critical constraints. The minimum breaking load constraint is affected by the standard deviation and mean mooring line tension relation, which is required to perform the optimization procedure outlined in Section 4. The implemented ratio of 20% is satisfied, but analysis of the optimized design showed that this relation is design dependent.

The performance, and search direction, of the gradient-based sequential quadratic programming optimization algorithm are sensitive to the number of constraints and the corresponding sum of constraint violations. Two different mooring system designs were obtained from the same starting design but with a different number of constraints. The designs had similar costs but different values for the design variables. A smaller desired final accuracy is required to determine if a local minimum has been obtained and to assess the convergence of the algorithm.

The hypothesis that the ULS condition is design driving was tested in a dynamic analysis of the optimized single turbine mooring system. The required reduction in weight and mooring line tension in the ULS condition lead to an increase in surge and sway natural periods. Additionally, the increase in mooring line weight, with respect to the mooring system at 150 meter depth, requires a reduced semi-submersible mass. This reduces the heave natural period of the system. The accumulated fatigue damage in the optimized mooring system over the life time of the structure must be smaller than 1 for ULS to be design driving. Fatigue analysis of the optimized mooring system showed that the accumulated damage in 20 years exceeds the limit of 1 for the given condition set. The initial hypothesis of this thesis that the ULS condition is design driving in the optimization of mooring line characteristics with respect to mooring system material costs is therefore incorrect, as outlined in Section 4. A fatigue limit constraint is therefore required to optimize based on static analysis. A time efficient fatigue damage estimation model in the frequency domain based on surge motion was created and assessed to further investigate the feasibility of static analysis optimization.

The created estimation model based on surge motion significantly underestimates the accumulated damage over the life time of the structure. The most severe underestimation occurs for the polyester segment and conditions with long wave periods. Long wave periods excite the natural heave frequency of the system and cause excessive heave motion. This results in high frequency oscillations in mooring line tension, which are not captured by the single degree of freedom estimation model. Heave and pitch motion must therefore be included in the fatigue damage estimation model. This can be done by adding an additional single degree of freedom heave motion frequency domain model. Additionally, the wind induced surge motion is overestimated for conditions that do not excite the natural heave period of the system. The estimation model utilizes a single stiffness value while nonlinear stiffness characteristics occur in the dynamic simulation. Besides that, the model is based on the linear damping coefficients. Therefore the total damping of the system is underestimated as aerodynamic damping is not included. This results in an overestimated motion amplitude for wind induced motion and mooring line tension. The wave induced surge motion is captured more accurately but is also affected by the underestimated damping coefficient and single stiffness value. Estimation of the accumulated damage in the frequency domain only based on surge motion is not sufficient. An improved FLS constraint must be implemented to assess the feasibility of mooring system optimization in the time domain based on static analysis. Additionally, the selected combined wind wave condition set is not desired for the used system due to long wave period and the small natural heave period of the system. A condition with wave periods shorter than the current condition set must be used to test the model or the heave natural period of the system must be increased.

The static analysis optimization does shown significant decrease in required optimization time. An estimated reduction of 40% is achieved in comparison to performing a dynamic ULS analysis optimization. This number significantly increases if an efficient and correct frequency domain fatigue damage estimation model is included, in comparison to a full dynamic fatigue damage analysis. However, the computation of gradients is governing in the optimization time. A non-gradient based optimization algorithm in combination with static analysis

optimization is likely to further reduce simulation time.

The initial goal of assessing the potential cost savings of an optimized shared mooring farm concept in comparison to individually mooring six floating wind turbine, with an optimized single turbine mooring system, at 600 meter depth has not been achieved. The focus of the thesis had been redirected once it was found that the ULS condition is not design driving.

The design of the shared mooring farm concept is challenging as the turbine is not centered on the semi-submersible. Additionally, the reduced number of anchor lines leads to a required increase in anchor line resistance. This is paired with a required weight increase, leading to large vertical forces at the anchor line fairlead. Balancing the vertical forces from the shared mooring lines and anchor lines based on the optimization procedure and FEM time domain analysis is sensitive to errors. The vertical force imbalance in combination with the off center turbine create a challenging design task. The current implement relation between shared mooring line diameter and anchor line diameter was found to be reasonable for the static analysis without environmental loading. Additionally, the column on which the turbine is positioned and the distribution of ballast in the semi-submersible may become important to implement the proposed concept.

7 Future Work Recommendations

This section provides an overview of ways to expand on the methodology and results presented in this report.

Firstly, to verify the feasibility of optimization based on static ULS analysis, the estimation model for accumulated fatigue damage should be improved by including heave and pitch motion as outlined in Section 4. Additionally, the performance of the improved model on the system should be assessed on multiple environmental condition sets, preferably ones with short wave periods. Upon verification of the estimation model, it can be included in the optimization procedure by communicating with external software and calculating the accumulated damage for the design and condition set. The optimization procedure should be expanded by including a constraint according to Equation 46. In addition, the applied 1 hour simulation for fatigue analysis only includes approximately 10 surge motion cycles which is not a representative number for damage calculation. The design standards recommend 3 hour simulations or even longer. However, due to the number of conditions and the limited storage on the computer used for simulations this was not possible. It is recommended to asses the performance using longer simulations. For improved verification of the feasibility of optimization based on static analysis, the optimization algorithm should be assessed on convergence through multiple simulations with different starting points and step sizes.

Additionally, the relation between standard deviation and mooring line tension was found to be design dependent. An exact relation between the mooring system characteristics in terms of line length and diameter is desired. The obtained percentages in Section 4 are 30% smaller than the current applied relation. A more accurate relation can improve the accuracy of the static analysis optimization model as the constraints related to mooring line tension will be accurately represented for each design evaluated by the optimization algorithm. It is therefore recommended to perform studies on the relation between standard deviation and mean mooring line tension as a function of the mooring line characteristics and static properties of the system. In addition, static current loads on the mooring lines and support structure should be included for a more accurate static position of the system under environmental loading. Besides that, the optimized system should be assessed on multiple loading directions and checked for displacement and tension constraints. If these are not satisfied the procedure should be adjusted to work for the most severe loading direction.

Lastly, the feasibility of the shared mooring farm concept should be assessed in a simplified model before comparing to the single turbine system. The design may be adjusted to a catenary anchor mooring line and designed according to the anchor line weight relation and the procedure outlined in *Comparison of pilot-scale floating offshore wind farms with shared moorings* by Connolly and Hall 2019. Research can be performed on a similar anchor line weight relation for a semi-taut or taut-leg anchor line. The anchor uplift constraint for the shared mooring farm concept may be satisfied by implementing clump weights.

8 Appendix

8.1 Simplified model

The new mass moments of inertia in the nacelle are determined using Table 56 and Equation 119. Here, j represents the axis of interest.

$$I_{jj} = I_{jj,nacelle} + I_{jj,blades} + (M_{blades} \cdot \Delta j^2) \tag{119}$$

Table 56: Mass moments of inertia and center of gravity (Table 5.3 Carlos Eduardo Silva de Souza et al. 2021)

	COGx [m]	COGy [m]	COGz [m]	Ixx [kgm^2]	Iyy [kgm^2]	Izz [kgm^2]
Blades	13.23	0	6.24	3.25e8	1.64e8	1.66e8
Nacelle	3.30	0	3.46	1.00e6	7.00e6	7.00e6

The updates mass moments of inertia in the nacelle are given in Table 57.

Table 57: Updated mass moments of inertia in nacelle

	Ixx [kgm^2]	Iyy [kgm^2]	Izz [kgm^2]
Nacelle	3.45e8	1.71e8	1.74e8

The displacement of the mass to the hub requires an additional moment applied in pitch. The mass of the blades is 189072 kg and the displacement is 2.29 meters. This leads to a moment of 4.25 MN. The moment was initially applied at the bottom of the tower, leading to a reasonable mismatch between static positions between the full model and simplified model. Finally, the moment was applied at the center of gravity leading to the results shown in Table 20, Table 19 and Table 21.

8.2 SIMA static simulation parameters

The applied static calculation parameters are given in Table 58. Running with previous defines that the load groups are applied simultaneously. The boundary change load group, freeing the system, is implemented for the static ULS simulation module and the static simulation module without environment. For the simulation module with a fixed turbine the number of steps for specified forces is set to 1 and the number of iterations to 0, as no forces are applied and to minimize required simulation time.

Table 58: Static calculation parameters for optimization

No	Load Type	Run With Previous	Steps	Iterations	Convergence Norm	Accuracy
1	Volume Forces	-	500	100	Displacement	1e-5
2	Specified Displacements	X	-	-	-	-
3	Body Forces	X	-	-	-	-
4	Marine Growth	X	-	-	-	-
5	Boundary Change	-	1	20	Displacement	1e-5
6	Specified Forces	-	500	200	Displacement	1e-5

The user specified optimization algorithm input parameters are given in Table 59.

Table 59: User specified optimization parameters

Optimization parameter	
Maximum iterations	50
Accuracy	0.001
Tolerance	1e-6
Maximum function calls	50
Minimum step length	1e-12
Automatic normalization	yes
Handling failure	yes

Normalization is applied and the desired final accuracy is set to 0.1%. The accuracy is defined as the sum of all constraint violations. The tolerance is defined as the number for which the optimization algorithm considers a value zero or not.

8.3 SIMA decay test simulation parameters

The dynamic simulation parameters in SIMA for the decay tests are given in Table 60.

Table 60: Simulation parameters for decay tests

Simulation time step	0.01 [s]
Wind speed	0.001 [m/s]
Environmental times series step	0.5 [s]
Wave condition	Hs = 0.001 [m], Tp = 20 [s]

8.4 SIMA FLS simulation parameters

The dynamic simulation parameters for FLS simulations are given in Table 61.

Table 61: Simulation parameters for FLS simulations

Simulation time step	0.01 [s]
Wind speed	condition dependent
Environmental times series step	0.5 [s]
Wave condition	condition dependent

8.5 Analysis

8.5.1 Decay test results

The natural periods for the first obtained design, defined by Table 32, are given in Table 39.

Table 62: Natural periods for design defined by Table 32

	Surge	Sway	Heave	Roll	Pitch	Yaw
Natural period [s]	430	412	15.7	30.6	30.5	270

The natural periods for the base case mooring system design, defined by Table 16, are given in Table 63.

Table 63: Natural periods for design defined by Table 16

	Surge	Sway	Heave	Roll	Pitch	Yaw
Natural period [s]	220	208	15.6	30.5	31.0	78.3

8.5.2 FLS measurements vs estimation data

Fairlead line 1

Table 64: Accumulated damage at fairlead

Design 2		Design 0
Condition	1 hour damage	1 hour damage
1	8.216e-6	3.465e-7
2	8.158e-6	3.217e-7
3	1.020e-5	4.029e-7
4	4.748e-5	1.317e-6
5	4.678e-5	1.262e-6
6	5.887e-5	1.504e-6
7	8.556e-5	2.892e-6
8	1.026e-4	2.783e-6
9	1.620e-4	3.900e-6
10	1.296e-4	3.330e-6
11	1.778e-4	7.016e-6
12	2.303e-4	5.759e-6
13	1.844e-4	7.124e-6
14	4.910e-4	2.230e-5
15	4.909e-4	1.194e-5
16	2.162e-3	1.152e-4
17	2.093e-3	6.216e-5
18	2.530e-3	4.386e-5
19	7.179e-3	4.592e-4
20	7.446e-3	3.114e-4
21	7.129e-3	1.782e-4

Table 65: Estimated damage at fairlead

Design 2		Design 0
Condition	1 hour damage	1 hour damage
1	6.330e-7	1.631e-8
2	3.048e-6	1.053e-7
3	5.331e-6	1.979e-7
4	3.308e-5	8.011e-7
5	4.635e-5	1.196e-6
6	6.548e-5	2.551e-6
7	2.066e-4	1.512e-6
8	5.245e-5	3.819e-6
9	2.783e-5	1.765e-5
10	3.765e-6	3.221e-8
11	7.431e-6	3.912e-8
12	2.505e-5	7.558e-8
13	8.611e-6	1.374e-8
14	1.485e-6	9.408e-8
15	9.093e-6	6.741e-7
16	5.106e-7	2.672e-8
17	9.110e-6	7.582e-8
18	1.032e-5	5.160e-8
19	1.519e-7	1.243e-8
20	7.813e-7	1.645e-8
21	3.830e-6	2.439e-8

Top of polyester segment line 1

Table 66: Accumulated damage at top of polyester segment

	Design 2	Design 0
Condition	1 hour damage	1 hour damage
1	1.709e-13	3.615e-15
2	1.153e-13	2.678e-15
3	2.316e-13	2.624e-15
4	1.214e-9	2.364e-12
5	1.004e-9	2.077e-12
6	2.799e-9	5.013e-12
7	2.170e-10	4.978e-13
8	2.997e-10	5.159e-13
9	2.387e-9	6.133e-12
10	6.941e-11	1.362e-13
11	1.642e-10	4.188e-12
12	4.039e-9	8.406e-12
13	1.351e-11	2.696e-13
14	2.326e-8	5.278e-9
15	6.393e-8	2.266e-10
16	1.776e-5	1.834e-5
17	9.469e-6	3.823e-7
18	5.195e-5	1.150e-7
19	1.020e-3	3.976e-3
20	1.587e-3	1.680e-3
21	3.481e-3	4.818e-5

Table 67: Estimated damage at top of polyester segment

	Design 2	Design 0
Condition	1 hour damage	1 hour damage
1	1.845e-18	2.943e-21
2	2.630e-15	6.854e-18
3	3.115e-14	1.271e-16
4	1.430e-10	4.719e-13
5	8.360e-10	1.208e-12
6	4.566e-9	1.282e-11
7	7.823e-8	3.202e-12
8	1.195e-10	8.977e-11
9	5.481e-12	1.025e-7
10	1.050e-14	1.641e-19
11	2.016e-13	3.894e-19
12	3.702e-11	3.368e-18
13	4.330e-14	1.869e-21
14	1.797e-17	4.224e-18
15	2.188e-13	3.307e-14
16	1.002e-19	4.183e-20
17	1.546e-13	1.687e-18
18	2.971e-13	2.313e-19
19	4.785e-23	8.684e-23
20	1.541e-18	5.682e-23
21	3.371e-15	1.147e-21

Top of bottom chain segment line 1

Table 68: Accumulated damage at top of bottom chain segment

Design 2		Design 0
Condition	1 hour damage	1 hour damage
1	7.982e-6	3.324e-7
2	7.829e-6	3.054e-7
3	9.638e-6	3.774e-7
4	4.709e-5	1.280e-6
5	4.559e-5	1.215e-6
6	5.684e-5	1.449e-6
7	8.290e-5	2.698e-6
8	9.665e-5	2.535e-6
9	1.499e-4	3.545e-6
10	1.172e-4	2.919e-6
11	1.524e-4	6.039e-6
12	2.059e-4	5.125e-6
13	1.504e-4	5.967e-6
14	3.921e-4	1.844e-5
15	4.247e-4	1.045e-5
16	1.585e-3	8.881e-5
17	1.741e-3	5.273e-5
18	2.160e-3	3.696e-5
19	4.965e-3	3.361e-4
20	5.903e-3	2.530e-4
21	5.959e-3	1.493e-4

Table 69: Estimated damage at top of bottom chain segment

Design 2		Design 0
Condition	1 hour damage	1 hour damage
1	6.566e-7	1.688e-8
2	3.163e-6	1.090e-7
3	5.532e-6	2.049e-7
4	3.406e-5	8.277e-7
5	4.775e-5	1.236e-6
6	6.745e-5	2.636e-6
7	2.119e-4	1.559e-6
8	5.383e-5	3.939e-6
9	2.856e-5	1.820e-5
10	3.879e-6	3.328e-8
11	7.660e-6	4.043e-8
12	2.583e-5	7.812e-8
13	8.884e-6	1.420e-8
14	1.533e-6	9.719e-8
15	9.397e-6	6.971e-7
16	5.266e-7	2.756e-8
17	9.413e-6	7.836e-8
18	1.067e-5	5.334e-8
19	1.560e-7	1.274e-8
20	8.049e-7	1.693e-8
21	3.953e-6	2.514e-8

References

[1] Audubon. *A Brief Look at Standards and Regulations Affecting Offshore Design, Development, and Operations*. 2015. URL: https://auduboncompanies.com/a-brief-look-at-standards-and-regulations-affecting-offshore-design-development-and-operations/. (accessed: 13.04.2021).

[2] Erin Bachynski. "Basic aerodynamics for wind turbines". In: (2020). (accessed: 11.04.2021).

[3] Erin Bachynski. "Integrated Dynamic Analysis of Wind Turbines course project". In: (2020). (accessed: 11.04.2021).

[4] Petter Andreas Berthelsen. *New Ocean Energy Concepts*. 2021. URL: https://www.sintef.no/en/projects/2015/new-ocean-energy-concepts/. (accessed: 11.05.2021).

[5] Pietro Bortolotti et al. "IEA Wind TCP Task 37: Systems Engineering in Wind Energy - WP2.1 Reference Wind Turbines". In: (June 2019). DOI: 10.2172/1529216.

[6] Bridon-Bekaert. *Find a rope - offshore production - mooring - permanent mooring lines*. 2021. URL: https://www.bridon-bekaert.com/en-gb/find-a-rope. (accessed: 13.04.2021).

[7] Bridon-Bekaert. *Offshore mooring lines - MoorLine Polyester*. 2021. URL: https://www.bridon-bekaert.com/en-gb/steel-and-synthetic-ropes/marine/mooring/offshore-mooring-lines. (accessed: 13.04.2021).

[8] Matthias Brommundt et al. "Mooring system optimization for floating wind turbines using frequency domain analysis". In: *Energy Procedia* 24 (2012), pp. 289–296. DOI: https://doi.org/10.1016/j.egypro.2012.06.111.

[9] Patrick Connolly and Matthew Hall. "Comparison of pilot-scale floating offshore wind farms with shared moorings". In: *Ocean Engineering* 171 (2019), pp. 172–180. DOI: https://doi.org/10.1016/j.oceaneng.2018.08.040.

[10] Damen. *Damen Anchor Chain Factory - Studless Chain Offshore*. 2016. URL: https://akfanchorchain.com/wp-content/uploads/2016/02/Product-Sheet-Chain-Studless-Offshore-may-2016.pdf. (accessed: 13.04.2021).

[11] Damen. *Damen Anchor Chain Factory - Studlink Chain Marine*. 2017. URL: https://akfanchorchain.com/wp-content/uploads/2016/02/Product-Sheet-Anchor-Chain-Studlink-Marine-July-2017.pdf. (accessed: 13.04.2021).

[12] DNVGL. *Design of Offshore Wind Turbine Structures*. 2014. URL: https://rules.dnv.com/docs/pdf/DNVPM/codes/docs/2014-05/Os-J101.pdf. (accessed: 12.05.2021).

[13] DNVGL. *Offshore standards - DNVGL-OS-E301 - Position Mooring*. 2018. URL: https://rules.dnvgl.com/docs/pdf/dnvgl/os/2018-07/dnvgl-os-e301.pdf. (accessed: 13.04.2021).

[14] DNVGL. *Standard - DNVGL-ST-0119 - Floating Wind Turbine Structures*. 2018. URL: https://rules.dnvgl.com/docs/pdf/DNVGL/ST/2018-07/DNVGL-ST-0119.pdf. (accessed: 13.04.2021).

[15] ExchangeRates.org.uk. *2015 GBP to EUR exchange rate history*. 2021. URL: https://www.exchangerates.org.uk/GBP-EUR-spot-exchange-rates-history-2015.html. (accessed: 20.04.2021).

[16] O.M. Faltinsen. *Sea Loads on Ships and Offshore Structures*. Cambridge University Press, 1999. ISBN: 0521458706.

[17] Casey M. Fontana et al. "Efficient Multiline Anchor Systems For Floating Offshore Wind Turbines". In: *ASME International Conference on Ocean, Offshore and Arctic Engineering* 35 (2016).

[18] GE. *Haliade-X offshore wind turbine - the world's most powerful offshore wind turbine in operation*. 2020. URL: https://www.ge.com/renewableenergy/wind-energy/offshore-wind/haliade-x-offshore-turbine. (accessed: 11.04.2021).

[19] Tuhfe Göçmen et al. "Wind turbine wake models developed at the technical university of Denmark: A review". In: *Renewable and Sustainable Energy Reviews* 60 (2016), pp. 752–769. ISSN: 1364-0321. DOI: https://doi.org/10.1016/j.rser.2016.01.113. URL: https://www.sciencedirect.com/science/article/pii/S136403211600143X.

[20] Marek Goldschmidt and Michael Muskulus. "Coupled mooring systems for floating wind farms". In: *Energy Procedia* 80 (2015), pp. 255–262. DOI: https://doi.org/10.1016/j.egypro.2015.11.429.

[21] Martin Hansen. *Aerodynamics of wind turbines*. Abingdon, Oxon England New York, NY: Routledge, 2015. ISBN: 9781138775077.

[22] Ole Andreas Hermundstad. *SIMA*. 2021. URL: https://www.sintef.no/en/software/sima/. (accessed: 11.05.2021).

[23] Hoff. "Estimation of linear and quadratic roll damping from free-decay tests". In: (2001).

[24] Rhodri James and Marc Costa Ros. *Floating Offshore Wind: Market and Technology Review*. 2015. URL: https://prod-drupal-files.storage.googleapis.com/documents/resource/public/Floating%20Offshore%20Wind%20Market%20Technology%20Review%20-%20REPORT.pdf. (accessed: 20.04.2021).

[25] B.J. Jonkman. *TurbSim User's Guide: Version 1.50*. 2009. URL: https://www.nrel.gov/docs/fy09osti/46198.pdf. (accessed: 10.06.2021).

[26] LIFES50+. *D1.1 Design Basis*. 2015. URL: https://lifes50plus.eu/wp-content/uploads/2015/11/D72_Design_Basis_Retyped-v1.1.pdf. (accessed: 4-12-2020).

[27] LIFES50+. *D1.1 Oceanographic and meteorological conditions for the design*. 2015. URL: https://lifes50plus.eu/wp-content/uploads/2015/12/GA_640741_LIFES50-_D1.1.pdf. (accessed: 13.04.2021).

[28] LIFES50+. *Innovative offshore floating wind energy*. 2015. URL: https://lifes50plus.eu/. (accessed: 4-12-2020).

[29] LIFES50+. *innovative Offshore Floating Wind Energy*. 2015. URL: https://lifes50plus.eu/. (accessed: 22.04.2020).

[30] Kai-Tung Ma et al. "Chapter 4 - Mooring design". In: *Mooring System Engineering for Offshore Structures*. Ed. by Kai-Tung Ma et al. Gulf Professional Publishing, 2019, pp. 63–83. ISBN: 978-0-12-818551-3. DOI: https://doi.org/10.1016/B978-0-12-818551-3.00004-1. URL: http://www.sciencedirect.com/science/article/pii/B9780128185513000041.

[31] Kai-Tung Ma et al. "Chapter 5 - Mooring analysis". In: *Mooring System Engineering for Offshore Structures*. Ed. by Kai-Tung Ma et al. Gulf Professional Publishing, 2019, pp. 85–114. ISBN: 978-0-12-818551-3. DOI: https://doi.org/10.1016/B978-0-12-818551-3.00005-3. URL: https://www.sciencedirect.com/science/article/pii/B9780128185513000053.

[32] Kai-Tung Ma et al. "Chapter 9 - Hardware—off-vessel components". In: *Mooring System Engineering for Offshore Structures*. Ed. by Kai-Tung Ma et al. Gulf Professional Publishing, 2019, pp. 175–198. ISBN: 978-0-12-818551-3. DOI: https://doi.org/10.1016/B978-0-12-818551-3.00009-0. URL: https://www.sciencedirect.com/science/article/pii/B9780128185513000090.

[33] Joaquim R. R. A. Martins and Andrew Ning. *Engineering Design Optimization*. 2020. URL: https://www.dropbox.com/s/3i1qmydet323nx5/mdobook.pdf. (accessed: 09.04.2021).

[34] Johan Meyers and Charles Meneveau. "Optimal turbine spacing in fully developed wind farm boundary layers". In: *Wind Energy* 15 (Mar. 2012), pp. 305–317. DOI: 10.1002/we.469.

[35] Mahdi Mirzaei et al. *Mooring Pattern Optimization Using A Genetic Algorithm*. 2013. URL: https://journals.utm.my/jurnalteknologi/article/view/2519/1949. (accessed: 12.04.2021).

[36] W. Musial, S. Butterfield, and A. Boone. "Feasibility of Floating Platform Systems for Wind Turbines". In: *National Renewable Energy Laboratory* (2004), p. 11. DOI: https://arc.aiaa.org/doi/10.2514/6.2004-1007.

[37] NOAA. *Bathymetric Data Viewer*. 2021. URL: https://www.ngdc.noaa.gov/maps/bathymetry/. (accessed: 13.04.2021).

[38] NREL. *TurbSim*. 2012. URL: https://www.nrel.gov/wind/nwtc/turbsim.html. (accessed: 10.06.2021).

[39] Prof. K. Schittkowski. "NLPQLP: A Fortran Implementation of a Sequential Quadratic Programming Algorithm with Distributed and Non-Monotone Line Search - User's Guide, Version 3.1 -". In: (2011). (accessed: 12.04.2021).

[40] SINTEF-Ocean. "RIFLEX 4.18.1 Theory Manual". In: (2020). (accessed: 11.04.2021).

[41] SINTEF-Ocean. "RIFLEX 4.18.1 User Guide". In: (2020). (accessed: 11.04.2021).

[42] SINTEF-Ocean. "SIMO 4.18.1 User Guide". In: (2020). (accessed: 11.04.2021).

[43] Senu Sirnivas et al. *Assessment of Offshore Wind System Design, Safety, and Operation Standards*. 2014. URL: https://www.nrel.gov/docs/fy14osti/60573.pdf. (accessed: 13.04.2021).

[44] Carlos Eduardo S Souza, John Marius Hegseth, and Erin E Bachynski. "Frequency-Dependent Aerodynamic Damping and Inertia in Linearized Dynamic Analysis of Floating Wind Turbines". In: *Journal of Physics: Conference Series* 1452 (Jan. 2020), p. 012040. DOI: 10.1088/1742-6596/1452/1/012040. URL: https://doi.org/10.1088/1742-6596/1452/1/012040.

[45] Carlos Eduardo Silva de Souza et al. "Definition of the INO WINDMOOR 12 MW base case floating wind turbine". In: (2021). DOI: http://dx.doi.org/10.13140/RG.2.2.32947.25121.

[46] WindEurope. *Economics*. 2019. URL: https://windeurope.org/policy/topics/economics/. (accessed: 09.04.2021).

[47] WindEurope. *Floating Offshore Wind Energy - A Policy Blueprint for Europe*. 2020. URL: https://windeurope.org/wp-content/uploads/files/policy/position-papers/Floating-offshore-wind-energy-a-policy-blueprint-for-Europe.pdf. (accessed: 09.04.2021).

[48] WindEurope. *Floating Offshore Wind Vision Statement - June 2017*. 2017. URL: https://windeurope.org/intelligence-platform/product/floating-offshore-wind-vision-statement/. (accessed: 09.04.2021).

[49] WindEurope. *Wind energy in Europe - 2020 Statistics and the outlook for 2021 - 2025*. 2020. URL: https://windeurope.org/intelligence-platform/product/wind-energy-in-europe-in-2020-trends-and-statistics/. (accessed: 09.04.2021).

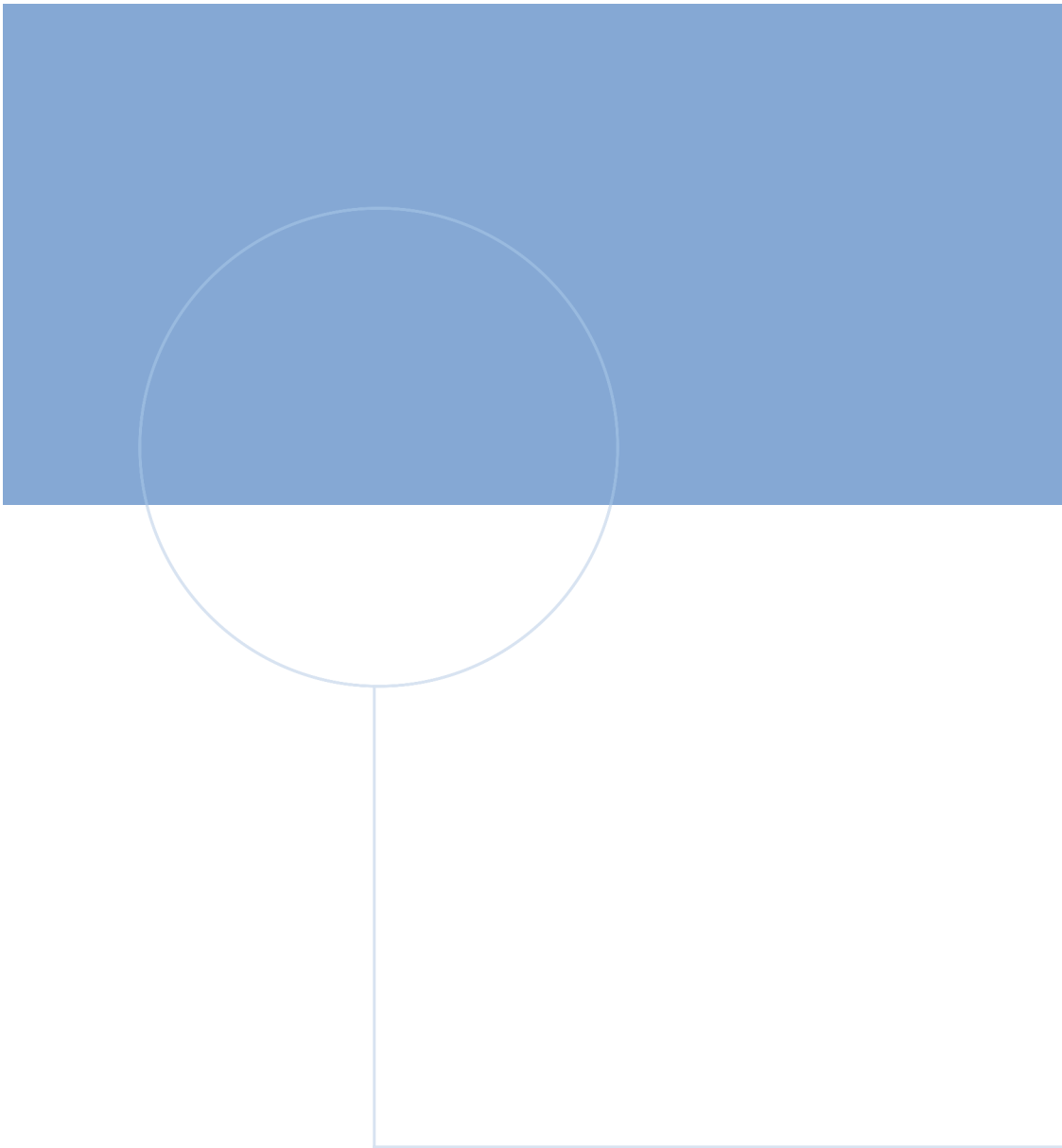

NTNU

Norwegian University of
Science and Technology